Neutrinos from Stored Muons (νSTORM): Expression of Interest [1]

D. Adey[1], S.K. Agarwalla[4], C.M. Ankenbrandt[2,1], R. Asfandiyarov[5], J.J. Back[6], G. Barker[6], E. Baussan[7], R. Bayes[8], S. Bhadra[9], V. Blackmore[11], A. Blondel[5], S.A. Bogacz[12], C. Booth[10], S.B. Boyd[6], A. Bravar[5], S.J. Brice[1], A.D. Bross[1], F. Cadoux[5], H. Cease[1], A. Cervera[13], J. Cobb[11], D. Colling[14], L. Coney[15], A. Dobbs[14], J. Dobson[14], A. Donini[13], P.J. Dornan[14], M. Dracos[7], F. Dufour[5], R. Edgecock[30], J. Evans[16], M. Geelhoed[1], M.A. George[14], T. Ghosh[13], A. de Gouvêa[17], J.J. Gomez-Cadenas[13], A. Haesler[5], G. Hanson[15], P.F. Harrison[6], M. Hartz[9,18], P. Hernandez[13], J.A. Hernando-Morata[19], P.J. Hodgson[10], P. Huber[20], A. Izmaylov[13], Y. Karadhzov[5], T. Kobilarcik[1], J. Kopp[21], L. Kormos[22], A. Korzenev[5], A. Kurup[14], Y. Kuno[23], P. Kyberd[24], J.P. Lagrange[25], A.M. Laing[13], J. Link[20], A. Liu[1,3], K.R. Long[14], N. McCauley[26], K.T. McDonald[27], K. Mahn[28], C. Martin[5], J. Martin[18], O. Mena[13], S.R. Mishra[29], N. Mokhov[1], J. Morfin[1], Y. Mori[25], W. Murray[30], D. Neuffer[1], R. Nichol[31], E. Noah[5], M.A. Palmer[1], S. Parke[1], S. Pascoli[32], J. Pasternak[14], M. Popovic[1], P. Ratoff[22], M. Ravonel[5], M. Rayner[5], S. Ricciardi[30], C. Rogers[30], P. Rubinov[1], E. Santos[14], A. Sato[23], E. Scantamburlo[5], J.K. Sedgbeer[14], D.R. Smith[24], P.J. Smith[10], J.T. Sobczyk[33], S. Soldner-Rembold[16], F.J.P. Soler[8], M. Sorel[13], A. Stahl[35], L. Stanco[34], P. Stamoulis[13], S. Striganov[1], H. Tanaka[36], I.J. Taylor[6], C. Touramanis[26], C.D. Tunnell[11], Y. Uchida[14], N. Vassilopoulos[14], M.O. Wascko[14], M.J. Wilking[28], A. Weber[11], E. Wildner[37], W. Winter[38], U.K. Yang[16]

[1] Fermilab, P.O. Box 500, Batavia, IL 60510-5011, USA
[2] Muons Inc., 552 N. Batavia Avenue, Batavia, IL 60510, USA
[3] Also at Indiana University Bloomington, 107 S Indiana Ave, Bloomington, IN 47405, USA
[4] Institute of Physics, Sachivalaya Marg, Sainik School Post, Bhubaneswar 751005, Orissa, India
[5] University de Geneve, 24, Quai Ernest-Ansermet, 1211 Geneva 4, Suisse
[6] Department of Physics, University of Warwick, Coventry, CV4 7AL, UK
[7] IPHC, Université de Strasbourg, CNRS/IN2P3, F-67037 Strasbourg, France
[8] School of Physics and Astronomy, Kelvin Building, University of Glasgow, Glasgow G12 8QQ, Scotland, UK
[9] Department of Physics and Astronomy, York University, 4700 Keele Street, Toronto, Ontario, M3J 1P3, Canada
[10] University of Sheffield, Dept. of Physics and Astronomy, Hicks Bldg., Sheffield S3 7RH, UK
[11] Particle Physics Department, The Denys Wilkinson Building, Keble Road, Oxford, OX1 3RH, UK
[12] Thomas Jefferson National Laboratory, 12000 Jefferson Avenue, Newport News, VA 23606, USA
[13] Instituto de Fisica Corpuscular (IFIC), Centro Mixto CSIC-UVEG, Edificio Institutos Investigacion, Paterna, Apartado 22085, 46071 Valencia, Spain
[14] Physics Department, Blackett Laboratory, Imperial College London, Exhibition Road, London, SW7 2AZ, UK
[15] Department of Physics and Astronomy, University of California, Riverside, CA 92521, US
[16] School of Physics and Astronomy, The University of Manchester, Oxford Road, Manchester, M13 9PL, UK
[17] Northwestern University, Dept. of Physics and Astronomy, 2145 Sheridan Road, Evanston, Illinois 60208-3112 USA
[18] Department of Physics, University of Toronto, 60 St. George Street, Toronto, Ontario, M5S 1A7, Canada
[19] Universidade de Santiago de Compostela (USC), Departamento de Fisica de Particulas, E-15706 Santiago de Compostela, Spain
[20] Virginia Polytechnic Inst. and State Univ., Physics Dept., Blacksburg, VA 24061-0435
[21] Max-Planck-Institut für Kernphysik, PO Box 103980, 69029 Heidelberg, Germany
[22] Physics Department, Lancaster University, Lancaster, LA1 4YB, UK
[23] Osaka University, Graduate School, School of Science, 1-1 Machikaneyama-cho, Toyonaka, Osaka 560-0043, Japan
[24] Brunel University West London, Uxbridge, Middlesex UB8 3PH, UK.
[25] Kyoto University, Research Reactor Institute, 2,Asashiro-Nishi, Kumatori-cho, Sennan-gun, Osaka 590-0494 Japan
[26] Department of Physics, Oliver Lodge Laboratory, University of Liverpool, Liverpool, L69 7ZE, UK
[27] Princeton University, Princeton, NJ, 08544, USA
[28] TRIUMF, 4004 Wesbrook Mall, Vancouver, B.C., V6T 2A3, Canada
[29] Department of Physics and Astronomy, University of South Carolina, Columbia SC 29208, USA
[30] STFC Rutherford Appleton Laboratory, Chilton, Didcot, Oxfordshire, OX11 0QX, UK
[31] Department of Physics and Astronomy, University College London, Gower Street, London, WC1E 6BT, UK
[32] Institute for Particle Physics Phenomenology, Department of Physics, University of Durham, Science Laboratories, South Rd, Durham, DH1 3LE, UK
[33] Institute of Theoretical Physics, University of Wroclaw, pl. M. Borna 9,50-204, Wroclaw, Poland
[34] INFN, Sezione di Padova, 35131 Padova, Italy
[35] III. Physikalisches Institut B, RWTH Aachen University, Templergraben 55, 52056 Aachen, Germany
[36] Department of Physics and Astronomy, Hennings Building, The University of British Columbia, 6224 Agricultural Road, Vancouver, B.C., V6T 1Z1, Canada
[37] CERN,CH-1211, Geneva 23, Switzerland
[38] Fakultät für Physik und Astronomie, Universität Würzburg Am Hubland, 97074 Würzburg, Germany

[1] Submitted to the SPSC at CERN on the 5^{th} April 2013 [1]

Executive summary

The νSTORM facility has been designed to deliver beams of $\overset{(-)}{\nu}_e$ and $\overset{(-)}{\nu}_\mu$ from the decay of a stored $\mu^\pm$ beam with a central momentum of 3.8 GeV/c and a momentum spread of 10% [2]. The facility is unique in that it will:

- Serve the future long- and short-baseline neutrino-oscillation programmes by providing definitive measurements of $\overset{(-)}{\nu}_e N$ and $\overset{(-)}{\nu}_\mu N$ scattering cross sections with percent-level precision;
- Allow searches for sterile neutrinos of exquisite sensitivity to be carried out; and
- Constitute the essential first step in the incremental development of muon accelerators as a powerful new technique for particle physics.

The race to discover CP-invariance violation in the lepton sector and to determine the neutrino mass-hierarchy has begun with the recent discovery that $\theta_{13} \neq 0$ [3–7]. The measured value of θ_{13} is large ($\sin^2 2\theta_{13} \sim 0.1$) so measurements of oscillation probabilities with uncertainties at the percent level are required. For the next generation of long-baseline experiments to reach the requisite precision requires that the $\overset{(-)}{\nu}_e N$ and the $\overset{(-)}{\nu}_\mu N$ cross sections are known precisely for neutrino energies (E_ν) in the range $0.5 < E_\nu < 3$ GeV. At νSTORM, the flavour composition of the beam and the neutrino-energy spectrum are both precisely known. The storage-ring instrumentation combined with measurements at a near detector will allow the neutrino flux to be determined to a precision of 1% or better. νSTORM is therefore unique as it makes it possible to measure the $\overset{(-)}{\nu}_e N$ and the $\overset{(-)}{\nu}_\mu N$ cross sections with a precision $\simeq 1\%$ over the required neutrino-energy range.

A number of results have been reported that can be interpreted as hints for oscillations involving sterile neutrinos [8–18] (for a recent review see [19]). Taken together, these hints warrant a systematically different and definitive search for sterile neutrinos. A magnetised iron neutrino detector at a distance of $\simeq$ 1 500 m from the storage ring combined with a near detector, identical but with a fiducial mass one tenth that of the far detector, placed at 20–50 m, will allow searches for active/sterile neutrino oscillations in both the appearance and disappearance channels. Simulations of the $\nu_e \rightarrow \nu_\mu$ appearance channel show that the presently allowed region can be excluded at the 10σ level while in the ν_e disappearance channel, νSTORM has the statistical power to exclude the presently allowed parameter space. Furthermore, the definitive studies of $\overset{(-)}{\nu}_e N$ ($\overset{(-)}{\nu}_\mu N$) scattering that can be done at νSTORM will allow backgrounds to be quantified precisely.

The European Strategy for Particle Physics provides for the development of a vibrant neutrino-physics programme in Europe in which CERN plays an essential enabling role [20]. νSTORM is ideally matched to the development of such a programme combining first-rate discovery potential with a unique neutrino-nucleus scattering programme. νSTORM could be developed in the North Area at CERN as part of the CERN Neutrino Facility (CENF) [21]. Furthermore, νSTORM is capable of providing the technology test-bed that is needed to prove the techniques required by the Neutrino Factory and, eventually, the Muon Collider. νSTORM is therefore the critical first step in establishing a revolutionary new technique for particle physics.

Of the world's proton-accelerator laboratories, only CERN and FNAL have the infrastructure required to mount νSTORM. In view of the fact that no siting decision has yet been taken, the purpose of this Expression of Interest (EoI) is to request the resources required to:

- Investigate in detail how νSTORM could be implemented at CERN; and
- Develop options for decisive European contributions to the νSTORM facility and experimental programme wherever the facility is sited.

The EoI defines a two-year programme culminating in the delivery of a Technical Design Report.

1 Introduction

1.1 Overview

Muon accelerators have been proposed as sources of intense, high-energy electron- and muon-neutrino beams at the Neutrino Factory [22, 23] and as the basis for multi-TeV l^+l^- collisions at the Muon Collider [24, 25]. An incremental approach to the development of the facility has been outlined in [26]. At νSTORM, a stored muon beam with a central momentum of 3.8 GeV/c and a momentum spread of 10% will:

- Serve a first-rate neutrino-physics programme will encompass:
  - Detailed and precise studies of electron- and muon-neutrino-nucleus scattering over the energy range required by the future long- and short-baseline neutrino oscillation programme; and
  - Exquisitely sensitive searches for sterile neutrinos in both appearance and disappearance modes; and
- Provide the technology test-bed required to carry-out the R&D critical to the implementation of the next increment in the muon-accelerator based particle-physics programme.

νSTORM is, therefore, the essential first step in the incremental development of muon accelerators as a new technique for particle physics.

Neutrino oscillations are readily described in terms of three neutrino-mass eigenstates and a unitary mixing matrix that relates the mass states to the flavour states (the Standard Neutrino Model, SνM) [27–30]. The three-neutrino-mixing paradigm is able to give an accurate description of the observed fluxes of neutrinos produced in the sun, by cosmic ray interactions in the atmosphere, by high-energy particle accelerators and anti-neutrinos produced by nuclear reactors [31]. However, a number of results can not be described by the SνM. First, the LSND collaboration reported evidence for $\bar{\nu}_\mu \rightarrow \bar{\nu}_e$ oscillations corresponding to a mass-squared difference of $\sim 1\,\mathrm{eV}^2$ [8]; a value which is much larger than the two mass-squared differences of the SνM. A third mass-squared difference, if confirmed, would imply a fourth neutrino-mass state and hence the existence of a sterile neutrino. The MiniBooNE experiment observed an effect consistent with the LSND result [9, 10]. A further hint for the existence of sterile neutrinos may be provided by the discrepancy between the measured reactor-neutrino flux and that obtained in calculations of the expected flux [11–13]. Finally, the GALLEX and SAGE experiments reported anomalies in the rate of neutrinos observed from the sources used to calibrate their radio-chemical detection techniques [14–18]. A detailed review of the relevant data may be found in [19].

Now that the small mixing angle θ_{13} is known [3–7], the emphasis of the study of the SνM has shifted to the determination of the mass hierarchy and the search for CP-invariance violation. In a conventional super-beam experiment, both of these objectives requires the measurement of ν_e ($\bar{\nu}_e$) appearance in a ν_μ ($\bar{\nu}_\mu$) beam. With a sufficiently large data sample, the measurement of the mass hierarchy is relatively insensitive to systematic uncertainties. By contrast, the sensitivity to CP-invariance violation depends critically on systematic effects in general and on the knowledge of the $\nu_e N$ ($\bar{\nu}_e N$) cross sections in particular [32, 33]. The νSTORM facility described in this Expression of Interest (EoI) is unique in that it is capable of serving a near detector (or suite of near detectors) that will be able to measure $\nu_e N$ ($\bar{\nu}_e N$) and $\nu_\mu N$ ($\bar{\nu}_\mu N$) cross sections at the percent level and of studying the hadronic final states.

Unambiguous evidence for the existence of one or more sterile neutrinos would revolutionise the field. νSTORM is capable of making the measurements required to confirm or refute the evidence for sterile neutrinos summarised above using a technique that is both qualitatively and quantitatively new [2]. The νSTORM facility has been designed to deliver beams of ν_e ($\bar{\nu}_e$) and $\bar{\nu}_\mu$ (ν_μ). A detector located at a distance $\sim 1\,500$ m from the end of one of the straight sections will be able to make sensitive searches for the existence of sterile neutrinos. If no appearance ($\bar{\nu}_\mu \rightarrow \bar{\nu}_e$) signal is observed, the LSND allowed region can be ruled out at the $\sim 10\sigma$ level. Instrumenting the νSTORM neutrino beam with a near detector at a distance of ~ 50 m makes it possible to search for sterile neutrinos in the disappearance $\nu_e \rightarrow \nu_X$ and $\nu_\mu \rightarrow \nu_X$ channels. In the disappearance search,

the absence of a signal would permit the presently allowed region to be excluded at the 90% confidence level [34].

By providing the ideal technology test-bed, the νSTORM facility will play a pivotal role in the development of neutrino detectors, accelerator systems and instrumentation techniques. It is capable of providing a high-intensity, high-emittance, low-energy muon beam for studies of ionisation cooling and of supporting the development of the high-resolution, totally-active, magnetised neutrino detectors. The development of the νSTORM ring, together with the instrumentation required for the νN-scattering and sterile-neutrino-search programmes will allow the next step in the development of muon accelerators for particle physics to be defined. Just as the Cambridge Electron Accelerator [35], built by Harvard and MIT at the end of the '50s, was the first in a series of electron synchrotrons that culminated in LEP, νSTORM has the potential to establish a new technique for particle physics that can be developed to deliver the high-energy ν_e ($\bar{\nu}_e$) beams required to elucidate the physics of flavour at the Neutrino Factory [23] and to provide the basis for multi-TeV lepton-antilepton collisions at the Muon Collider [25].

1.2 νSTORM and the emerging CERN neutrino programme

1.2.1 Short-baseline neutrino facility in the North Area

It has been proposed to develop the North Area at CERN to host a portfolio of neutrino experiments [21]. In the short term, it has been proposed that a search for sterile neutrinos be carried out by the ICARUS and NESSiE collaborations [36, 37]. These experiments will be served by a conventional neutrino beam generated by the fast extraction of protons from the SPS at 100 GeV. For these experiments to take sufficient data before the second long shutdown of the LHC in 2017 requires that the beam and experiments be implemented such that data taking can start early in 2016. νSTORM requires a primary proton beam similar to that which is being prepared for ICARUS/NESSiE but with a smaller transverse and longitudinal emittance. A beam with the appropriate properties will be available once LINAC4 becomes operational after the 2017 long shutdown [38]. The near and far source–detector distances required by νSTORM closely match those specified for ICARUS/NESSiE.

The concept for the implementation of the νSTORM facility at CERN presented in this EoI is self-consistent and is capable of delivering searches for sterile neutrinos with exquisite sensitivity and serving a unique and detailed $\nu_{e,\mu}N$ ($\bar{\nu}_{e,\mu}N$) scattering programme. Given the technical synergies, it is natural to consider how the νSTORM facility could be developed first to enhance and then to take forward the short-baseline neutrino programme at CERN.

1.2.2 A step on the way to the Neutrino Factory

To go beyond the sensitivity offered by the next generation super-beam experiments requires the development of novel techniques for the production of neutrino beams and novel detector systems. Pure ν_e ($\bar{\nu}_e$) beams may be generated from the decay of radioactive ions at a "beta-beam" facility [39]. The low charge-to-mass ratio of the ions places a practical limit of $\sim$ 1 GeV on the neutrino energies that can be produced in this way. Alternatively, high-energy electron- and muon-neutrino beams of precisely known flux may be generated from the decay of stored muon beams at the Neutrino Factory [23].

The Neutrino Factory has been shown to offer a sensitivity to CP-invariance violation superior to that which can be achieved at any other proposed facility [22, 23]. The EUROν consortium demonstrated that the CERN baseline ($\gamma = 100$) beta-beam becomes competitive only if it is combined with the CERN-Frejus super-beam, or a super-beam of comparable performance [40]. Detailed and precise measurements of neutrino oscillations

will be required for the physics of flavour to be elucidated. The challenge to the experimental community is to establish a programme capable of delivering measurements of the neutrino-mixing parameters with a precision approaching that with which the quark mixing parameters are known. Only the Neutrino Factory offers such precision.

It is conceivable that the Neutrino Factory can be implemented in a series of increments or stages—each increment offering a first-rate neutrino-science programme and being capable of delivering the R&D required for the development of the subsequent increment. The International Design Study for the Neutrino Factory (IDS-NF) collaboration will include a discussion of the incremental implementation of the facility in its Reference Design Report that will be published in the autumn of 2013. The νSTORM facility, by proving the feasibility of using stored muon beams to provide neutrino beams for physics, will be the essential first increment.

1.2.3 Long-baseline neutrino oscillation physics

The present generation of long-baseline neutrino-oscillation experiments (MINOS [41], T2K [42], NOνA [43]) will continue to refine the measurements of the mixing parameters. Their data, taken together with that obtained in atmospheric-neutrino experiments, may constrain the neutrino mass hierarchy at the 2σ—3σ confidence level. However, even in combination with all oscillation data, the present generation of experiments will be essentially insensitive to leptonic CP-invariance violation.

High-power conventional neutrino beams serving very large detectors have been proposed to determine the mass hierarchy. Such "super-beam" experiments fall into two broad categories: narrow-band beams, in which a low-energy ($E_\nu \leq 1$ GeV) beam is used to illuminate a detector 100 km—300 km from the source; and wide-band beams in which neutrinos with energies spanning the range ~ 1 GeV to 10 GeV illuminate a detector at a distance of between 700 km and 2 300 km.

The opportunities for CERN to host a next-generation super-beam has been studied by the EUROν Framework Programme 7 (FP7) Design Study consortium [44]. EUROν studied a narrow-band beam generated using the 5 GeV, 4 MW Superconducting Proton Linac (SPL) at CERN illuminating the MEMPHYS, 450 kT water Cherenkov detector located in the Laboratoire Souterrain de Modane (LSM) at a distance of 130 km (this option is referred to as CERN-Frejus since the LSM is located in the Frejus tunnel) [45].

The study of super-beam experiments at CERN is now being taken forward by the LAGUNA-LBNO FP7 Design Study consortium [46]. In LAGUNA-LBNO, the CERN-Frejus narrow-band beam continues to be developed and a new wide-band beam option, the Long-Baseline Neutrino Observatory (LBNO), is being considered [47]. LBNO calls for a high-energy, wide-band neutrino beam to be created using protons from the SPS. The beam would serve a suite of detectors in the Pyhäsalmi mine in Finland, at a distance of 2 300 km from CERN. The long baseline, coupled with the wide-band beam makes CERN-Pyhäsalmi a powerful option since it would allow LBNO to determine the mass hierarchy at a confidence level in excess of 5σ no matter what the value of the CP phase. Alternative proposals for next generation super-beam experiments have been brought forward in Japan (the Tokai to Hyper-Kamiokande, T2HK, experiment [48]) and in the US (the Long-Baseline Neutrino Experiment, LBNE [49]).

Each of the super-beam experiments outlined above exploits the sub-leading $\nu_\mu \to \nu_e$ ($\bar{\nu}_\mu \to \bar{\nu}_e$) oscillation to determine the mass hierarchy and to search for leptonic CP-invariance violation. At present, data on neutrino-nucleus scattering in the energy range of interest is limited to relatively sparse $\nu_\mu N$ ($\bar{\nu}_\mu N$) measurements; $\nu_e N$ ($\bar{\nu}_e N$) cross sections being inferred from the $\nu_\mu N$ ($\bar{\nu}_\mu N$) measurements. As a result, uncertainties in oscillation measurements made using conventional beams suffer from systematic uncertainties arising from the absence of reliable electron-neutrino-nucleus (and muon-neutrino-nucleus) scattering cross sections. Moreover, the lack of knowledge of the relevant cross sections gives rise to correlated uncertainties in the estimate of the neutrino-beam flux.

νSTORM will make detailed studies of both $\nu_e N$ ($\bar{\nu}_e N$) and $\nu_\mu N$ ($\bar{\nu}_\mu N$) scattering. As discussed in this EoI, an appropriately designed suite of near detectors will be able to determine the scattering cross sections and provide detailed information on the hadronic final states. The latter will be of first importance not only in the long-baseline oscillation programme, but will allow the systematic study of the sources of background that currently affect sterile-neutrino searches. The cross-section measurements that νSTORM will provide will therefore be an essential part of the emerging CERN neutrino programme.

2 Motivation

The case for the νSTORM facility rests on three themes. First, the uniquely well-known neutrino beam generated in muon decay may be exploited to make detailed studies of neutrino-nucleus scattering over the neutrino-energy range of interest to present and future long- and short-baseline neutrino oscillation experiment from In long-baseline experiments, these measurements are required to break the correlation between the cross-section and flux uncertainties and to reduce the overall systematic uncertainty to a level that justifies the investment in high-power conventional super-beam experiments such as T2HK, LBNE, LBNO and SPL-Frejus. The νSTORM $\overleftarrow{\nu}N$ scattering programme is no less important for the next generation of short-baseline experiments for which uncertainties in the magnitude and shape of backgrounds to the sterile-neutrino searches will be come critically important. Second, the νSTORM neutrino beam, instrumented with a pair of magnetised detectors near and far, will allow searches for sterile neutrinos of exquisite sensitivity to be carried out. The signal to background ratio for this combination is of order ten and is much larger than other accelerator-based projects. Thirdly, the storage ring itself, and the muon beam it contains, can be used to carry out the R&D programme required to implement the next step in the incremental development of muon accelerators for particle physics. The muon accelerator programme has the potential to elucidation of the physics of flavour at the Neutrino Factory and to provide multi-TeV l^+l^- collisions at the Muon Collider. Just as the three legs of a tripod make it a uniquely stable platform, the three individually-compelling themes that make up the case for νSTORM constitute a uniquely robust case for a facility that will be at once immensely productive scientifically and seminal in the creation of a new technique for particle physics.

2.1 Neutrino-nucleus scattering

2.1.1 Introduction

To date, neutrino oscillations [50] remain the only observed and confirmed phenomenon not described by the Standard Model (SM) of particle physics. Neutrino-oscillation data, combined with searches for kinematic effects of neutrino mass in tritium-decay experiments, very clearly indicate that, in the SνM, the mass of the heaviest neutrino must be smaller than ~ 1 eV. This mass is too small to be explained naturally by the Higgs mechanism, making it necessary to invoke physics beyond the SM to explain neutrino mass and mixing. The detailed exploration of the neutrino sector is one of the most important goals for the next decade in particle physics research. The neutrino community is converging on the conclusion that a wide-band long-baseline (LBL) accelerator-based neutrino experiment is an important part of this research programme [47–49]. The principal goals of the next-generation LBL experiments are the determination of the neutrino mass-hierarchy and the search for CP-invariance violation. Recent observations that the value of the third neutrino mixing angle, θ_{13}, is large [3, 4, 6] mean that the rates of ν_e or $\bar{\nu}_e$ appearance in a wide-band beam will be substantial and that high-statistics measurements will be dominated by systematic uncertainties, especially uncertainties in the modelling of neutrino-nucleus scattering. It is therefore crucial that these systematic uncertainties are

reduced in order for the next generation experiments to achieve the precision and sensitivity defined by the collaborations in the various proposals.

The current generation of neutrino-oscillation experiments employ neutrino-interaction models developed in the 1970's and 1980's [51–53]. In the energy region of interest to the LBL programme (0.1 GeV–10 GeV) the dominant reaction types, in order of threshold, are: quasi-elastic scattering; resonant and coherent pion-production; and deep inelastic scattering. High statistics neutrino-scattering measurements made in the past decade by K2K [54–57], MiniBooNE [58–64] and SciBooNE [65–68] indicate that the quasi-elastic scattering and pion-production models do not describe nature.

Even with this degree of activity, the precision with which the basic neutrino-nucleon cross sections are known is still not better than 20%–30%. There are two main reasons for this: the poor knowledge of neutrino fluxes and the fact that all the recent cross-section measurements have been performed on nuclear targets. It is important to recall that current neutrino experiments measure events that are a convolution of an energy-dependent neutrino flux with an energy-dependent cross section with energy-dependent nuclear effects. Experiments have, for example, measured an effective neutrino-carbon cross section. Extracting a neutrino-nucleon cross section from these measurements requires separating nuclear-physics effects that can be done only with limited precision. For many experiments, using the same nuclear targets in their near and far detectors is a good start. However, even with the same nuclear target near and far, the presence of oscillations leads to different neutrino fluxes at the near and far detectors. This means that there is a different convolution of cross section with nuclear effects near and far, so there is no automatic cancellation between the near-and-far detectors at the precision needed for the LBL programme. Furthermore, these effects are exacerbated in measurements of anti-neutrino cross sections because the event rates are significantly reduced. Finally, the intrinsic differences between ν_μ- and ν_e-interaction cross sections must be measured with a precision commensurate with the precision goals of the LBL programme (see section 2.1.4).

In summary, to ensure a successful LBL programme, a thorough comparison of measured neutrino-nucleon cross sections with theoretical models is needed so that all these convoluted effects can be understood.

2.1.2 Charged-current quasi-elastic scattering

Neutrino-nucleon charged-current quasi-elastic (CCQE) scattering, $\nu_l\, n \rightarrow l^-\, p$, is the most abundant neutrino reaction in the 1 GeV energy region and also the most important in investigations of the oscillation signal. Despite its importance and apparent simplicity, the CCQE cross section is known with limited accuracy. The main reasons for the poor understanding of this reaction [69, 70] are the large neutrino-flux uncertainties (both the overall normalisation and the energy spectrum) and the fact that all recent CCQE cross-section measurements were made on bound nucleons with many complications coming from nuclear effects.

In the standard theoretical approach to describe the CCQE cross section, a weak-current transition matrix element is expressed in terms of three independent form factors [51]. The two vector form factors are known from electron-scattering experiments, thanks to the conserved vector-current hypothesis [71–74]. Assuming the partially conserved axial-current hypothesis leaves one independent axial-vector form-factor for which one usually assumes a dipole form and this, in turn, leaves only one free parameter: the axial mass (M_A). Within this simple theoretical framework, an investigation of CCQE scattering is equivalent to an M_A measurement. Experience from electron scattering tells us that dipole expressions provide a reasonable approximation to electric and magnetic form factors, and *extrapolation* of this argument to the axial form factors seems to be a justified, though not completely obvious, assumption. M_A determines both the overall CCQE cross section and also the shape of the distribution of events in Q^2, the square of four-momentum transfer. The preferred way to measure M_A is to analyse the shape of the $d\sigma/dQ^2$ spectrum because this mitigates the dependence on the overall flux normalisation.

Another problem with measuring the CCQE cross section stems from the fact that the energy spectrum of all neutrino beams are broad making it difficult to separate the various dynamic mechanisms in neutrino-nucleon (-nucleus) interactions. The situation is much more complex than for electron scattering where good knowledge of the initial and final electron states allows a model-independent measurement of Q^2. For these reasons, neutrino cross-section measurements are always inclusive and there is even reason to consider the limitations of the commonly-assumed impulse approximation [75] in which it is assumed that the neutrino interacts with an individual bound nucleon and thus one can neglect collective effects (all the major Monte Carlo (MC) event generators do not include (continuous) random-phase approximation corrections).

Nuclear effects include Fermi motion and nucleon binding. Clearly, in investigations of CCQE, it is important to use the best Fermi motion models, which means employing the spectral-function formalism [76] that has been validated in electron scattering. Moreover, it is important to consider a two body current contribution to the cross section [77, 78]; these currents give rise to events that can be easily confused with genuine CCQE events unless one investigates final-state nucleons carefully.

Recent interest in CCQE scattering was triggered by several large M_A measurements, in particular the high-statistics muon-carbon double-differential cross sections from the MiniBooNE collaboration [59]. Here, "large" is relative to values obtained from older, mostly light nuclear target, neutrino [79] and pion electroproduction data [80]. The MiniBooNE detector is not sensitive to final-state nucleons, which are produced below Cherenkov threshold. What MiniBooNE measures can be described as CCQE-like events—defined as those with no pion in the final state—with data-driven corrections for the contribution from pion production and absorption. Several theoretical groups have attempted to explain the MiniBooNE CCQE double-differential cross-section data with models containing significant contributions from np-nh mechanisms, which allow n particles and n holes, with $n \geq 2$, in the final state (np-nh mechanisms are also called meson exchange currents (MEC), multi-nucleon knock-out, or two-body currents). The Valencia/IFIC group performed a fit with its model to the two-dimensional MiniBooNE CCQE data, obtaining $M_A = 1.077 \pm 0.027\,\text{GeV}$ [81]. Good qualitative agreement was obtained by the Lyon group [82]. These two models are shown compared to MiniBooNE double-differential muon data in figure 1. Qualitative agreement has also been obtained with an optical-potential model [83], while slightly worse agreement was found with the super-scaling approach [84] and transverse enhancement (TE) model [85, 86]. A general observation is that theoretical models are usually able to explain the normalisation effect of the large M_A value from MiniBooNE but their predictions do not agree with the full two-dimensional muon data set.

Theoretical models of the MEC contribution give quite different estimates of the significance of the effect in the case of anti-neutrino scattering. Recently, MiniBooNE showed the first high-statistics anti-neutrino CCQE cross section and in particular a ratio of neutrino and anti-neutrino CCQE-like cross sections (defined as explained above) as a function of energy. These data may allow some comparison between the models, but higher precision data on multiple nuclear targets are needed.

For CCQE events one can calculate the energy of the incoming neutrino using just the final charged-lepton three-momentum assuming the target nucleon was at rest. Clearly, the effects of Fermi motion and binding energy limit the accuracy of the neutrino-energy reconstruction and introduce some model-dependent bias. The neutrino energy is used for oscillation studies since that is the only experimental parameter which affects the oscillation probability. Additional complications come from events which mimic CCQE interactions, e.g., from real pion production and absorption. The MiniBooNE data for the muon double-differential cross section can be described using the standard CCQE model with a large value of M_A (although it is better to call this an effective parameter M_A^{eff} as proposed in [58]). However, use of the CCQE model with M_A^{eff} in the oscillation signal analysis introduces some bias since the presence of two-body current contributions changes the mapping from neutrino energy to charged-lepton momentum, as noted in several recent studies [70, 87–90].

Separation of two-body-current contributions should be possible by looking at final-state nucleons [89, 91].

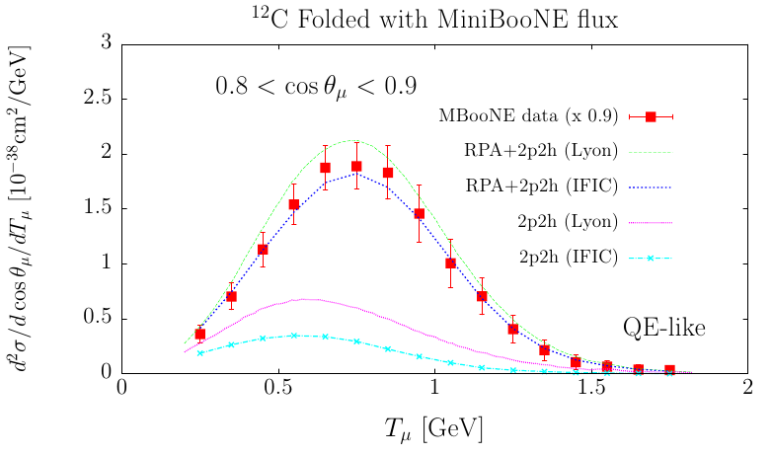

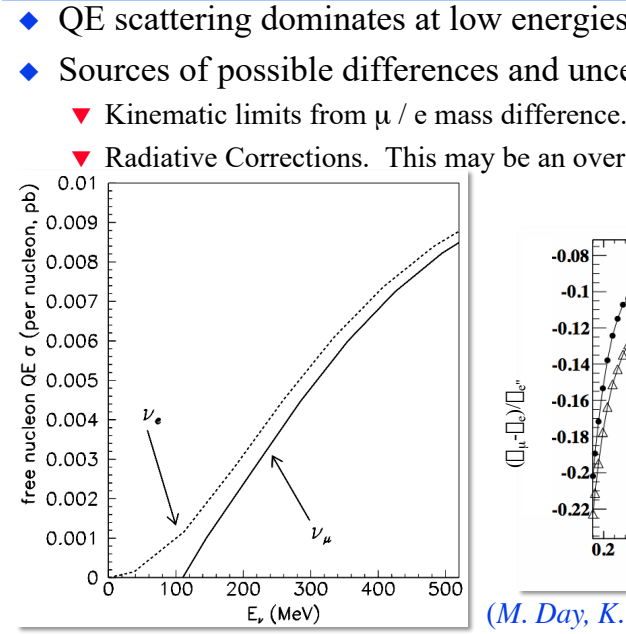

Figure 1: (left) MiniBooNE flux averaged CCQE-like cross section normalised per neutron with experimental points rescaled by 0.9. $\cos\theta_\mu \in (0.8, 0.9)$. Predictions from two theoretical models are compared and contributions from np-nh mechanism are also shown separately. (right) The total charged-current quasi-elastic cross-section for ν_μ and ν_e neutrinos.

This is, however, a very challenging goal because of nucleon final-state interactions and contamination from real-pion production and absorption events. One needs very good resolution of final-state nucleons with a low threshold for the momentum of reconstructed tracks. Liquid argon TPCs have been suggested as candidate instruments to improve MC cascade models [92].

2.1.3 Resonance Region

The neutrino-interaction landscape in the few-GeV region is a complex mix of resonance production, shallow-inelastic-scattering physics, where resonance production merges into deep-inelastic scattering, and coherent processes. The dominant production mechanism in this region is the production of a $\Delta(1232)$ baryon followed by its decay to a single pion final state. A challenging process to study experimentally, most experiments being complicated by the fact that the neutrinos interact in an extended nuclear target; the final state particles must leave the nucleus to be observed and along the way can be scattered, absorbed or undergo charge-exchange reactions. These final-state interactions must somehow be decoupled from the underlying neutrino-nucleon cross-sections—a process which is model-dependent—making interpretation of the data challenging. The resonance-production channel presents the largest background to current neutrino-oscillation experiments and it is therefore important to understand its contribution. Moreover, future experiments such as LBNE [49] and LBNO [47] are designed to operate at neutrino energies of 3 GeV–7 GeV where this transition region between quasi-elastic scattering and deep inelastic scattering is most important. For these experiments, a much better understanding of this region is required if they are to have maximum sensitivity to CP-invariance violation in the neutrino sector.

The quality of experimental data in the resonance region is varied. Whilst there has been recent work on neutrino-induced single-pion production mechanisms in experiments such as MiniBooNE, data on multi-pion and other final-state production mechanisms are sparse or non-existent. Figure 2 (left) shows, for example, the only data on the $\nu_\mu p \to \nu_\mu n\pi^+$ channel. In recent years experiments such as K2K [55, 96, 97], MiniBooNE [59–61] and SciBooNE [67, 68] have presented data on neutral-current π^0 (NC π^0) production, charged current π^+ (CC π^+) production and the charged-current π^0 (CC π^0) channel. Improved knowledge of the NC π^0 production cross section is vital as it is a dominant systematic error in $\overset{(-)}{\nu}_e$-appearance oscillation experiments.

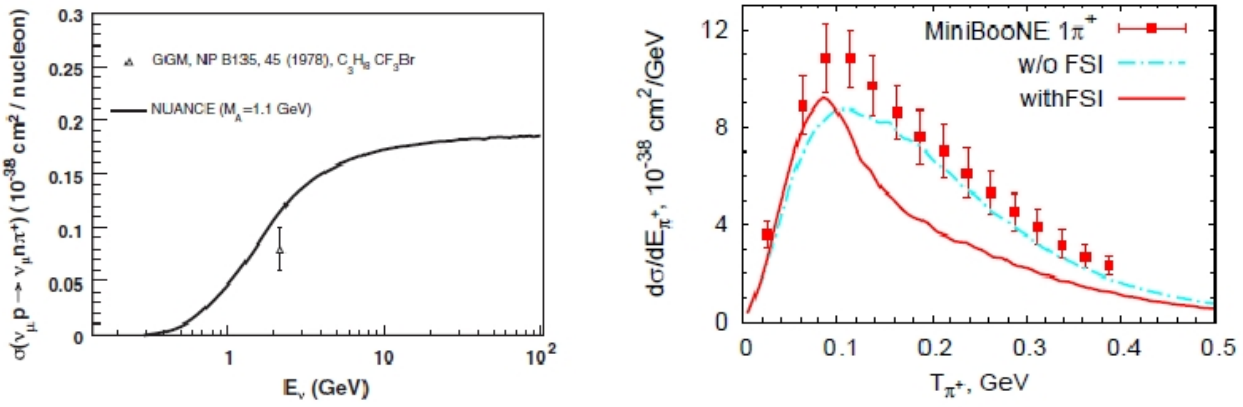

Figure 2: (left) Existing measurements of the $\nu_\mu p \to \nu_\mu n\pi^+$ cross section as a function of neutrino energy [93]. Data points come from the Gargamelle bubble chamber data [94]. The line is the prediction from the NUANCE Monte Carlo event generator. (right) Distribution of $\nu_\mu C \to \mu^-\pi^+ X$ cross section as a function of the pion momentum from the GIBBU simulation [95], compared with MiniBooNE data [62].

The CC π^+ and CC π^0 channels have been studied by MiniBooNE [61] which has produced differential cross sections in the final-state particle momenta and angles. The cross-section results differ from the current Monte Carlo models by up to 20% in the case of the charged-pion mode and by up to a factor of two for the neutral-pion mode, suggesting a discrepancy in both the understanding of the neutrino-nucleon cross section and the final state effects. Figure 2 (right) shows the differential cross section for CC π^+ production on ^{12}C as a function of pion kinetic energy from MiniBooNE compared to the sophisticated GIBUU simulation [95]. The model appears to favour no, or at least a very small, component of final-state interactions even though it is known that final-state interactions have a large effect. The solution to this puzzle lies in understanding both the neutrino-nucleon cross section and final-state effects independently. Such a program of study would involve the comparison of the final-state topologies of the CC π reaction on different nuclei. A critical element, however, is knowledge of the neutrino-nucleon cross section on an H_2 or D_2 target. This is an anchor point, allowing the analysers to tune their models to the nucleon cross section before comparison with nuclear data. Light nucleon data was last taken by the bubble-chamber experiments in the 1970's and 1980's. More complete, and better understood, data on light nuclei is now necessary to understand the resonance-production models. A dedicated light-target detector in the νSTORM facility is therefore of interest. It should be emphasised that this is the state of data from neutrino-induced interactions. Data on anti-neutrino resonance production are even more sparse and there is no data on resonance production in an electron-neutrino beam. One of the primary means of studying CP-invariance violation is to investigate differences between measurements of oscillations of neutrinos and anti-neutrinos. Poor knowledge of the cross-sections present one of the largest systematic errors limiting these analyses and so a precise determination of these cross sections is vital.

Another pion-production process is the coherent neutrino-nucleus interaction. In this process the neutrino interacts with the entire nucleus at very low momentum-transfer, resulting in a forward-going pion and leaving the nucleus in the ground state. This process can proceed via the charged and neutral currents for both neutrinos and anti-neutrinos. Neutral-current interactions which result in a π^0 in the final state are of particular interest for oscillation experiments investigating ν_e appearance as they form a large part of the background. The process has been observed at high (greater than 5 GeV) neutrino energy [98] and agrees with the standard Rein-Seghal model [99] predictions, which are based on PCAC with pion dominance. However, in the 1 GeV–3 GeV range, the landscape becomes unclear as the available data are limited. Both MiniBooNE [100] and SciBooNE [68]

have measured the neutral-current mode at an average neutrino energy of 0.8 GeV. The charged-current mode is mode is more puzzling. Isospin symmetry implies that the charged-current process should occur with twice the rate of the neutral-current process. However K2K [101] and SciBooNE [102] have reported no evidence for the charged-current coherent process. It is now becoming clear that it is not appropriate to continue the high-energy theory down to lower energies and that other models involving microscopic Δ dominance are more reliable [103, 104]. Testing these models requires data on a number of different types of target nucleus and over a range of neutrino energies. This is crucial since the contribution of this process to the ν_e backgrounds in the first oscillation maximum must be predicted accurately for the LBL experiments.

2.1.4 Differences in the energy-dependent cross sections of ν_μ- and ν_e-nucleus interactions

To determine the mass hierarchy of neutrinos and to search for CP-invariance violation in the neutrino sector, current and upcoming accelerator-based neutrino-oscillation experiments such as T2K [42] and NOvA [43] as well as future proposed experiments such as LBNE [49] and the Neutrino Factory [49] plan to make precision measurements of the neutrino flavour oscillations $\overset{(-)}{\nu}_\mu \rightarrow \overset{(-)}{\nu}_e$ or $\overset{(-)}{\nu}_e \rightarrow \overset{(-)}{\nu}_\mu$. An important factor in the ability to fit the difference in observed event rates between the near and far detectors will be an accurate understanding of the cross section of ν_μ- and ν_e-nucleus interactions. Uncertainties on differences in expected event rates due to differences between these cross-sections will contribute to experimental uncertainties in these flavour-oscillation measurements.

There are obvious differences in the cross sections due to the difference in mass of the outgoing lepton. These can be calculated by including the lepton-mass term in the cross-section expression. Figure 1 (right) [105], shows these expected differences in the cross sections as a function of neutrino energy. Another such calculable difference occurs because of radiative corrections. Radiative corrections from a particle of mass m are proportional to $\log(1/m)$, which implies a significant difference since the muon is ~ 200 times heavier than the electron [106]. This turns into a difference of $\sim 10\%$ in the cross sections. In addition to these differences, there are other more subtle differences due to the coupling of poorly-known or unknown form factors to the lepton tensor that reflect the differences in the outgoing lepton mass. These effects have been investigated in some detail [105] but must be probed experimentally.

Regarding nuclear effects, while there are no differences expected in the final-state interactions, there are expected differences in the initial reaction cross-sections between ν_μ- and ν_e-nucleus interactions. Since the lepton tensor, reflecting the mass of the outgoing lepton, couples to the hadron-response functions, there is a difference in nuclear effects at the interaction vertex due to the μ-to-e mass difference. The expected difference in the ν_μ- and ν_e-nucleus cross-section ratio is around 5% when using a spectral-function model [107] for the initial nucleon momentum compared to the relativistic Fermi gas model [52, 108]. There is another 5% difference expected for multi-nucleon (np-nh) contribution [109]. These differences in cross sections extend up into the resonance region with the low-Q^2 behaviour of Δ production exhibiting 10% differences at values of Q^2 where the cross section has levelled off.

While each of the individual effects outlined above may not be large compared to current neutrino-interaction uncertainties, they are large compared to the assumed precision of oscillation measurements in the future LBL programme. Moreover, the sum of these effects could be quite significant and the uncertainty in our knowledge of the size of these effects will contribute directly to uncertainties in the neutrino-oscillation parameters determined from these experiments—and these uncertainties can only be reduced with good quality $\overset{(-)}{\nu}_e$ scattering data. νSTORM is the only source of a well-understood and well-controlled $\overset{(-)}{\nu}_e$ neutrino beam with which these cross-section differences can be studied systematically.

2.1.5 Effects of neutrino-nucleus interaction systematics on oscillation measurements

A neutrino-oscillation experiment must compare neutrino-scattering event rates with a prediction in order to extract oscillation parameters. Many systematic errors in such analyses can be mitigated by using of a near detector with similar target nuclei, but, importantly, several systematic uncertainties still remain. Neutrino oscillation is a function of the true energy of the neutrino, but experiments must infer the energy of neutrino interactions from measurements of the outgoing charged-lepton partner (which also identifies the neutrino flavour).

As discussed in section 2.1.2, the problem we face is that the micro-physics of the nuclear environment can change the mapping between the charged-lepton momentum and the neutrino energy. This mapping is model-dependent because the form factors for axial-currents have not yet been measured precisely since the uncertainty in the reconstructed neutrino energy is inherently larger than the widths generated by nuclear effects. The model-dependence of these predictions adds a systematic uncertainty that cannot be mitigated without data sets that are fine enough in final-state-particle resolution while covering enough of the kinematic phase-space and target nuclei. The systematic uncertainty due to this model dependence cannot be mitigated by a near detector unless and until the model calculations are sufficiently detailed to allow falsification with final-state particle data. Another issue that contributes to the systematic errors is the migration of events between near (and far) detector data samples. In the main, these arise because final-state particles can scatter hadronically within the target nucleus before escaping into the detector medium. As discussed in section 2.1.3, the exact kinematics of the final-state particles in the resonance region must be predicted, and then measured, in order to reduce these uncertainties. Finally there is the very real effect of differences in the $\overset{(-)}{\nu}_{\mu}$ and $\overset{(-)}{\nu}_{e}$ interaction cross sections, which must be measured with high precision.

The stated goals for the precision of the proposed next generation long-baseline neutrino oscillation experiments such as LBNE, LBNO and T2HK cannot be reached without mitigating these systematic uncertainties, even with high precision near detectors. νSTORM is the only experimental facility with the precision and flexibility needed to tackle all of these neutrino-interaction cross-section uncertainties.

2.2 Sterile neutrino search

2.2.1 Sterile neutrinos in extensions of the Standard Model

Sterile neutrinos—fermions that are uncharged under the $SU(3) \times SU(2) \times U(1)$ gauge group—arise naturally in many extensions of the Standard Model and even where they are not an integral part of a model, they can usually be accommodated easily. A detailed overview of sterile neutrino phenomenology and related model building considerations is given in [19].

In Grand Unified Theories (GUTs), fermions are grouped into multiplets of a large gauge group, of which $SU(3) \times SU(2) \times U(1)$ is a subgroup. If these multiplets contain not only the known quarks and leptons, but also additional fermions, these new fermions will, after the breaking of the GUT symmetry, often behave like gauge singlets (see for instance [110–113] for GUT models with sterile neutrinos).

Models by which the smallness of neutrino masses are explained using a "see-saw" mechanism generically contain sterile neutrinos. While in the most generic see-saw scenarios, these sterile neutrinos are extremely heavy ($\sim 10^{14}$ GeV) and have very small mixing angles ($\sim 10^{-12}$) with the active neutrinos, slightly non-minimal see-saw models can easily feature sterile neutrinos with eV-scale masses and with per-cent level mixing with the active neutrinos. Examples for non-minimal see-saw models with relatively light sterile neutrinos include the split see-saw scenario [114], see-saw models with additional flavour symmetries (see e.g. [115]),

models with a Froggatt-Nielsen mechanism [116, 117], and extended see-saw models that augment the mechanism by introducing more than three singlet fermions as well as additional symmetries [118–120].

Finally, sterile neutrinos arise naturally in "mirror models", in which the existence of an extended "dark sector", with non-trivial dynamics of its own, is postulated. If the dark sector is similar to the visible sector—as is the case, for instance in string-inspired $E_8 \times E_8$ models—it is natural to assume that it also contains neutrinos [121–123].

2.2.2 Experimental hints for light sterile neutrinos

While the theoretical motivation for the existence of sterile neutrinos is certainly strong, what has mostly prompted the interest of the scientific community in this topic is the fact that there are several experimental results that show deviations from the Standard Neutrino Model predictions which can be interpreted as hints for oscillations involving light sterile neutrinos with masses on the order of an eV.

The first of these hints was obtained by the LSND collaboration, which carried out a search for $\bar{\nu}_\mu \to \bar{\nu}_e$ oscillations over a baseline of $\sim$ 30 m [8]. Neutrinos were produced in a stopped-pion source in the decay of pions at rest ($\pi^+ \to \mu^+ + \nu_\mu$) and the subsequent decay $\mu^+ \to e^+ \bar{\nu}_\mu \nu_e$. Electron anti-neutrinos were detected through the inverse-beta-decay reaction $\bar{\nu}_e p \to e^+ n$ in a liquid-scintillator detector. Backgrounds to this search arise from the decay chain $\pi^- \to \bar{\nu}_\mu + (\mu^- \to \nu_\mu \bar{\nu}_e e^-)$ if negative pions produced in the target decay before they are captured by a nucleus and from the reaction $\bar{\nu}_\mu p \to \mu^+ n$ which is only allowed for the small fraction of muon anti-neutrinos produced by pion decay in flight rather than stopped-pion decay. The LSND collaboration found an excess of $\bar{\nu}_e$-candidate events above this background with a significance of more than 3σ. When interpreted as $\bar{\nu}_\mu \to \bar{\nu}_e$ oscillations through an intermediate sterile state $\bar{\nu}_s$, this result is best explained by sterile neutrinos with an effective mass-squared splitting $\Delta m^2 \gtrsim 0.1$ eV^2 relative to the active neutrinos, and with an effective sterile-sector induced $\bar{\nu}_\mu$–$\bar{\nu}_e$ mixing angle $\sin^2 2\theta_{e\mu,\text{eff}} \gtrsim 2 \times 10^{-3}$, depending on Δm^2.

The MiniBooNE experiment [124] was designed to test the neutrino-oscillation interpretation of the LSND result using a different technique, namely neutrinos from a horn-focused pion beam. By focusing either positive or negative pions, MiniBooNE could run either with a beam consisting mostly of neutrinos or in a beam consisting mostly of anti-neutrinos. In both modes, the experiments observed an excess of electron-like events at sub-GeV energies. The excess has a significance above 3σ and can be interpreted in terms of $\overset{(-)}{\nu}_\mu \to \overset{(-)}{\nu}_e$ oscillations consistent with the LSND observation [124, 125].

A third hint for the possible existence of sterile neutrinos is provided by the reactor anti-neutrino anomaly. In 2011, Mueller et al. published a new ab-initio computation of the expected neutrino fluxes from nuclear reactors [11]. Their results improve upon a 1985 calculation [126] by using up-to-date nuclear databases, a careful treatment of systematic uncertainties and various other corrections and improvements that were neglected in the earlier calculation. Mueller et al. find that the predicted anti-neutrino flux from a nuclear reactor is about 3% higher than previously thought. This result, which was later confirmed by Huber [12], implies that short-baseline reactor experiments have observed a deficit of anti-neutrinos compared to the prediction [13, 19]. It needs to be emphasised that the significance of the deficit depends crucially on the systematic uncertainties associated with the theoretical prediction, some of which are difficult to estimate reliably. If the reactor anti-neutrino deficit is interpreted as $\bar{\nu}_e \to \bar{\nu}_s$ disappearance via oscillation, the required 2-flavour oscillation parameters are $\Delta m^2 \gtrsim 1$ eV^2 and $\sin^2 2\theta_{ee,\text{eff}} \sim 0.1$.

Short-baseline oscillations in this parameter range could also explain another experimental result: the gallium anomaly. The GALLEX and SAGE solar neutrino experiments used electron neutrinos from intense artificial radioactive sources to demonstrate the feasibility of their radio-chemical detection principle [14–18]. Both experiments observed fewer ν_e from the source than expected. The statistical significance of the deficit is

above the 99% confidence level and can be interpreted in terms of short-baseline $\bar{\nu}_e \to \bar{\nu}_s$ disappearance with $\Delta m^2 \gtrsim 1\ \mathrm{eV}^2$ and $\sin^2 2\theta_{ee,\mathrm{eff}} \sim 0.1$–$0.8$ [127–129].

2.2.3 Constraints and global fit

While the previous section shows that there is an intriguing accumulation of hints for the existence of new oscillation effects—possibly related to sterile neutrinos—in short-baseline experiments, these hints are not undisputed. Several short-baseline oscillation experiments (KARMEN [130], NOMAD [131], E776 [132], ICARUS [133], atmospheric neutrinos [134], solar neutrinos [135–144], MINOS [145, 146], and CDHS [147]) did not confirm the observations from LSND, MiniBooNE, reactor experiments, and gallium experiments, and place very strong limits on the relevant regions of parameter space in sterile-neutrino models. To assess the viability of these models it is necessary to carry out a global fit to all relevant experimental data sets [19, 148–152]. In figure 3, which is based on the analysis presented in [19, 148, 153], we show the current constraints on the parameter space of a $3 + 1$ model (a model with three active neutrinos and one sterile neutrino). We have projected the parameter space onto a plane spanned by the mass-squared difference, Δm^2, between the heavy, mostly sterile, mass eigenstate and the light, mostly active, ones and by the effective amplitude $\sin^2 2\theta_{e\mu,\mathrm{eff}}$ for sterile-mediated $\nu_\mu \to \nu_e$ oscillations.

We see that there is severe tension in the global data set: the parameter region flavoured by the hints from LSND, MiniBooNE, reactor neutrinos and gallium experiments is incompatible, at the 99% confidence level, with constraints from other experiments. Similarly, the parameter region flavoured by the global $\langle\bar{\nu}\rangle_e$ appearance data, has only very little overlap with the region flavoured by $\langle\bar{\nu}\rangle_\mu$ and $\langle\bar{\nu}\rangle_e$ disappearance experiments. Using a parameter goodness-of-fit test [154] to quantity this tension, p-values on the order of a few $\times\, 10^{-5}$ are found for the compatibility of appearance and disappearance data. The global fit improves somewhat in models with more than one sterile neutrino, but significant tension remains [19, 148].

One can imagine several possible resolutions to this puzzle:

1. One or several of the apparent deviations from the SνM oscillation framework discussed in section 2.2.2 have explanations not related to sterile neutrinos;
2. One or several of the null results that favour the no-oscillation hypothesis is or are in error;
3. There are more than two sterile-neutrino flavours. Note that scenarios with one sterile neutrino with an eV-scale mass are already in some tension with cosmology (see, however, [155]), but the existence of one sterile neutrino with a mass well below 1 eV is actually preferred by cosmological fits [156–159]. Cosmological bounds on sterile neutrinos can be avoided in non-standard cosmologies [160] or by invoking mechanisms that suppress sterile-neutrino production in the early universe [161, 162]; and
4. There are sterile neutrinos plus some other kind of new physics at the eV scale (see for instance [163, 164] for an attempt in this direction).

We conclude that our understanding of short-baseline neutrino oscillations is currently in a rather unsatisfactory state. Several experiments hint at deviations from the established three-neutrino framework. However, none of these hints can be considered conclusive; moreover, when interpreted in the simplest sterile neutrino models, the parameter sets favoured by the data are in severe tension with existing constraints on the parameter-space of these models. An experiment searching for short-baseline neutrino oscillations with good sensitivity and well-controlled systematic uncertainties has great potential to clarify the situation either by finding a new type of neutrino oscillation or by deriving a strong and robust constraint on any such oscillation. While the former outcome would constitute a major discovery, the latter would also receive a lot of attention since it would provide the world's strongest constraints on a large variety of theoretical models postulating "new physics" in the neutrino sector at the eV scale.

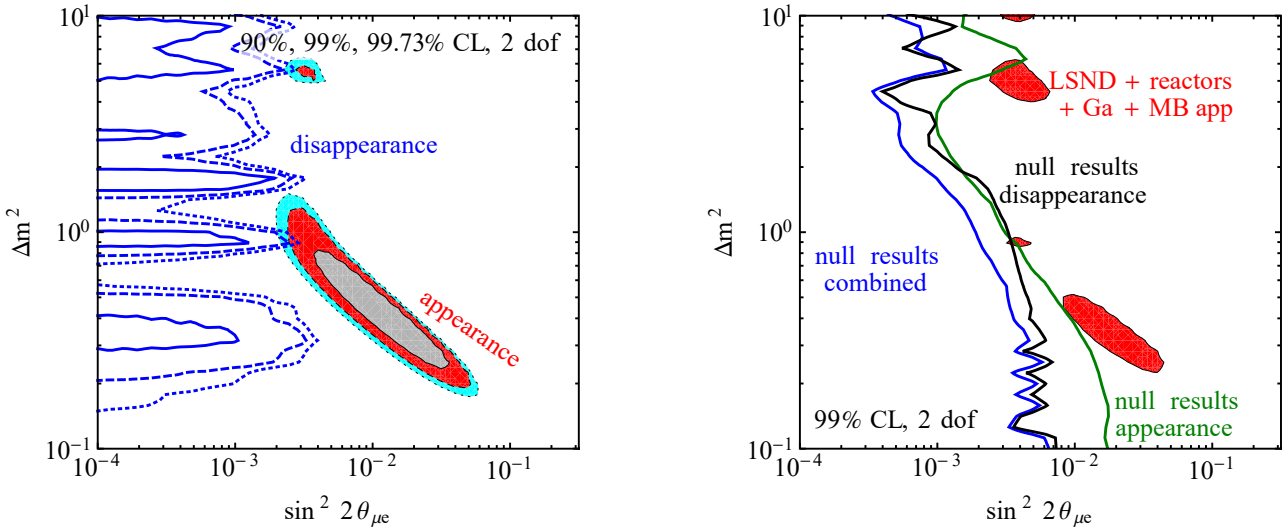

Figure 3: Global constraints on sterile neutrinos in a 3+1 model. In the left panel, we show that $\overset{(-)}{\nu}_e$ appearance data (coloured region: LSND [8], MiniBooNE [124], KARMEN [130], NOMAD [131], E776 [132], ICARUS [133]) is only marginally consistent with disappearance data (blue contours: atmospheric neutrinos [134], solar neutrinos [135–144], MiniBooNE/SciBooNE [165, 166] MINOS [145, 146], reactor experiments [4, 167–177], CDHS [147], KARMEN [178] and LSND [179] ν_e–^{12}C scattering data and gallium experiments [15, 17, 18, 136]). In the right panel, we have split the data into those experiments which see unexplained signals (LSND, MiniBooNE appearance measurements, reactor experiments, gallium experiments) and those which don't. For the analysis of reactor data, we have used the new reactor flux predictions from [11], but we have checked that the results, especially regarding consistency with LSND and MiniBooNE $\bar{\nu}$ data, are qualitatively unchanged when the old reactor fluxes are used. Fits have been carried out in the GLoBES framework [180, 181] using external modules discussed in [153, 163, 182, 183].

2.3 Technology test-bed

2.3.1 Muon beam for ionisation cooing studies

Muon ionisation cooling improves by a factor ~ 2 the stored-muon flux at the Neutrino Factory and is absolutely crucial for a Muon Collider of any centre-of-mass energy to achieve the required luminosity. The Muon Ionisation Cooling Experiment (MICE) [184] will study four-dimensional ionisation cooling and work is underway to specify the scope of a follow-on six-dimensional (6D) cooling experiment. MICE is a "single-particle" experiment; the four-momenta of single muons are measured before and after the cooling cell and then input and output beam emittances are reconstructed from an ensemble of single-muon events. A 6D cooling experiment could be done in the same fashion, but doing the experiment with a high-intensity pulsed muon beam is preferred. One feature of νSTORM is that an appropriate low-energy muon beam with these characteristics can be provided in a straightforward fashion.

Figure 4 shows a schematic of the decay ring for νSTORM. As is described in section 3.1 below, 5 GeV/c pions are injected at the end of the straight section of the ring. Given the 150 m length of the straight, only $\sim 40\%$ of the pions decay in the injection straight. Since the arcs are set for the central muon momentum of 3.8 GeV/c, the pions remaining at the end of the straight will not be transported by the arc. The power contained within the pion beam that reaches the end of the injection straight is 4 kW–5 kW making it necessary to dump the undecayed pion beam into an appropriate absorber.

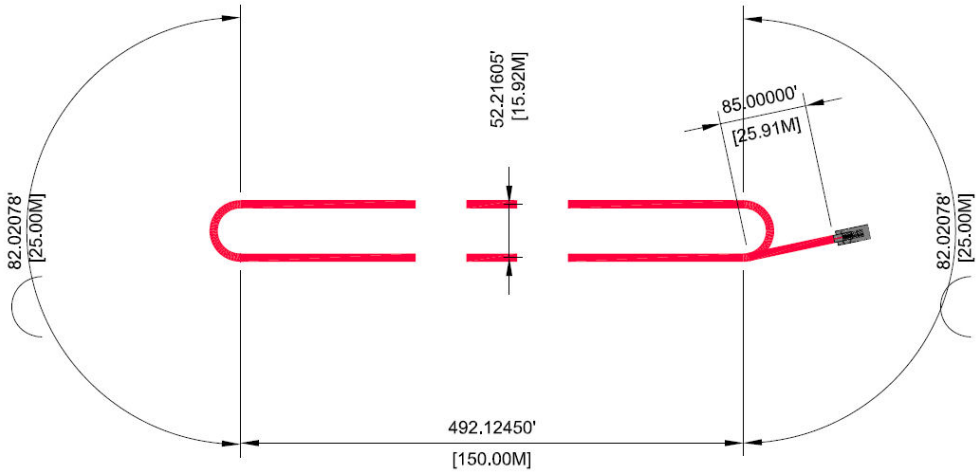

Figure 4: Schematic of the νSTORM decay ring.

The same optics that are used for injection can be used to extract the pions at the end of the straight and transport them to an absorber as shown in figure 4. However, if the absorber is "redefined" to be a "degrader" capable of stopping the pions but allowing muons above a certain energy to pass, then a low-energy muon beam appropriate for a 6D muon cooling experiment can be produced. The left panel of figure 5 shows the momentum distribution for the first pass of muons at the end of the decay-ring straight. The green band indicates the momentum acceptance of the decay ring. The red band covers the same momentum band as the input pions, these muons will be extracted along with the remaining pions. If the degrader is sized appropriately, a muon beam of the desired momentum for a 6D cooling experiment will emerge downstream of the degrader. The right panel of figure 5 shows a visualisation of a G4Beamline [185, 186] simulation of the muons in the pion momentum band ($5 \pm 10\%$ GeV/c) propagating through a 3.48 m thick iron degrader. The left panel of figure 6 shows the $x - y$ distribution of the muon beam exiting the degrader while the right panel shows the $x - x'$ distribution. Figure 7 shows the muon momentum distribution of the muons that exit the degrader. Our initial estimate is that in the momentum band of interest for a 6D cooling experiment (100–300 MeV/c), we will have approximately 10^{10} muons in the 1μsec spill.

2.3.2 Neutrino cross-section measurements for Super Beams

The neutrino spectrum produced by the νSTORM 3.8 GeV/c stored muon beam is shown in figure 8. The νSTORM flux at low neutrino energy (< 0.5 GeV) is relatively low. The neutrino energy spectrum that would be produced at a low-energy super-beam such as the SPL-based beam studied in [45] or the recent proposed super beam at the European Spallation Source (ESS) [187] is shown also shown in figure 8. Both the SPL and ESS based super beams propose to use the MEMPHYS water Cherenkov detector [188, 189]. To enhance the event rate in the low neutrino-energy region of importance to such facilities, the possibility of capturing muons

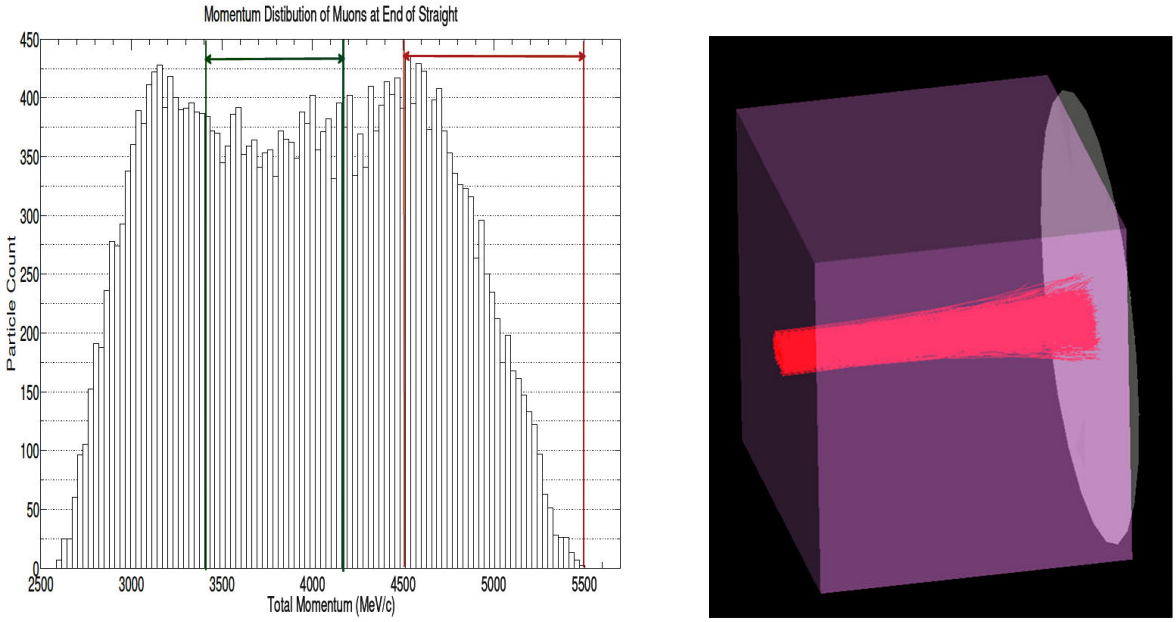

Figure 5: Left panel: Momentum distribution of muons after the first straight. Right panel: Visualisation of muons in the degrader.

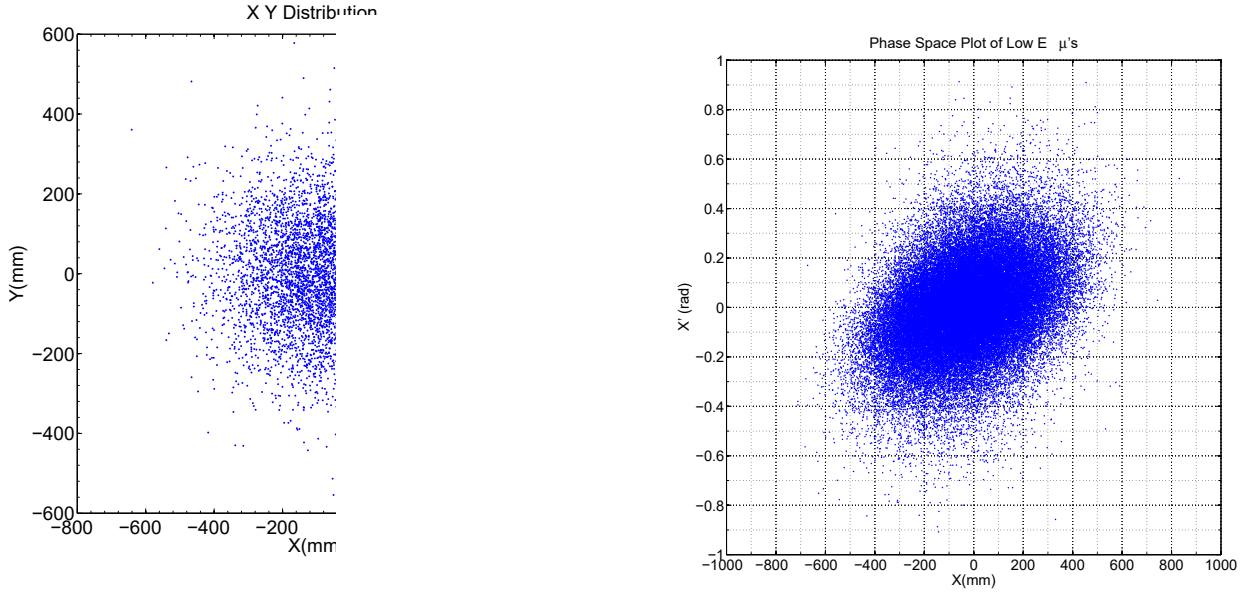

Figure 6: Phase-space of the muon beam as it leaves the degrader. Left panel: $x - y$ distribution; Right panel: $x - x'$ distribution.

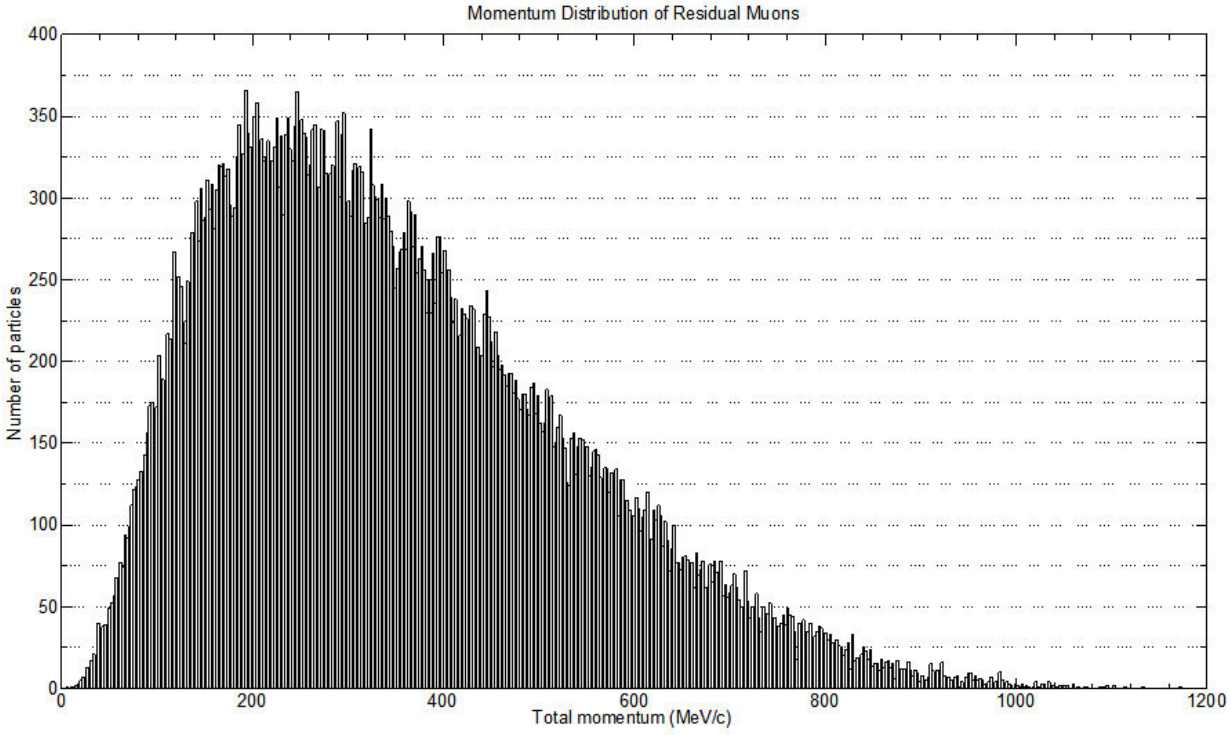

Figure 7: Muon momentum distribution after degrader.

with a central momentum below 3.8 GeV/c is being studied.

The "degrader" introduced above provides an alternative technique by which the required low-energy neutrino beam could be produced. Muons with momentum in the range 4.5 GeV/c to 5.5 GeV/c extracted and directed towards the degrader will decay to produce neutrinos with energies of around 300 MeV. A detector placed a few tens of metres behind the degrader would make it possible to measure the $\overset{(-)}{\nu}_e N$ and $\overset{(-)}{\nu}_\mu N$ cross sections required for SPL or ESS based super beams.

3 The νSTORM facility; overview

3.1 Accelerator facility

The concept for the facility proposed in [2] is shown in figure 9. The neutrino beam is generated from the decay of muons confined within a race-tracked shaped storage ring. A high-intensity proton source places beam on a target, producing a large spectrum of secondary pions. Forward pions are focused by a collection element (horn) into a transport channel. Pions decay within the first straight of the decay ring and a fraction of the resulting muons are stored in the ring. Muon decay within the straight sections will produce neutrino beams of known flux and flavour via: $\mu^+ \rightarrow e^+ \nu_e \bar{\nu}_\mu$ or $\mu^- \rightarrow e^- \bar{\nu}_e \nu_\mu$. A storage ring of 3.8 GeV/c is proposed to obtain the desired spectrum of ~ 2 GeV neutrinos; pions have then to be captured at a momentum of approximately 5 GeV/c. In table 1 the parameters for the Fermilab baseline option (60 GeV protons on target) and the proposed parameters for a CERN option (100 GeV protons on target) are shown. We assume that similar production (target and capture) and ring layout is used for the FNAL and the CERN implementations. There may be constraints for the CERN option in the North Area that can have impact on the design of the injection and of the ring itself (see section 4.1).

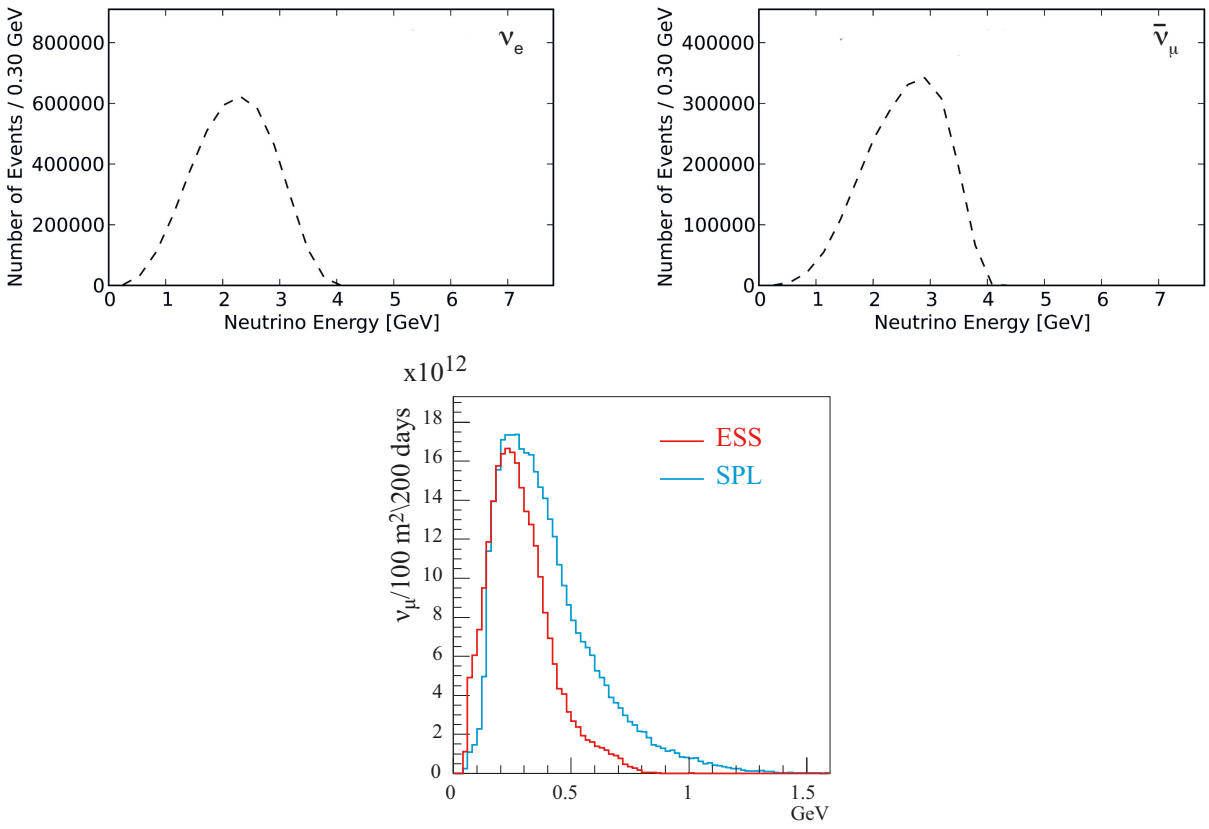

Figure 8: Top row: ν_e (left) and $\bar{\nu}$ (right) event rates per 100 T in a detector placed $\sim$ 50 m from the end of one of the straight sections (for a stored μ^+ beam). Bottom row: neutrino energy spectrum for the SPL (with proton energy of 4.5 GeV) and ESS (with proton energy of 2.5 GeV) based super beams.

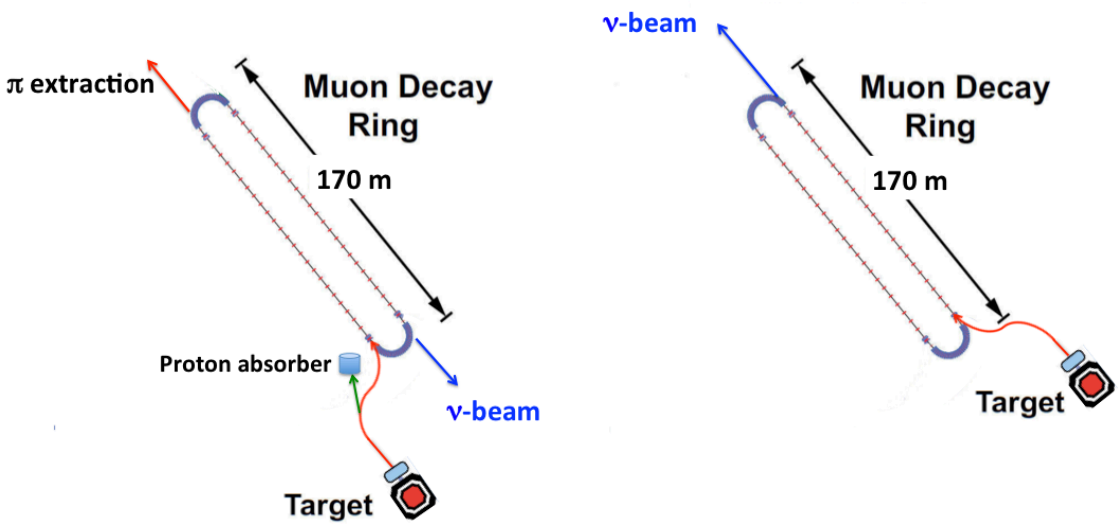

Figure 9: The νSTORM facility, with a Decay Ring having 150 m straights and 25 m, 180° arcs. The left figure shows a possible CERN layout where injection of pions produced from the full 10 μs spill of 100 GeV protons from the SPS would correspond to $\sim$ 7 turns of the muon beam in the storage ring. The FNAL option, to the right, injects pions produced during only 1 μs 60 GeV proton extraction from the Main Ring.

Table 1: Summary of parameters for νSTORM at Fermilab and at CERN. For Fermilab the performance is based on simulations with a tantalum target and a NuMI-like horn operating at 300 kA.

Neutrino characteristics	**Fermilab**	**CERN**
Aimed neutrino energy [GeV]	1.0 to 3.0	1.0 to 3.0
Flux measurement precision [%]	1.0	1.0
Protons on target (POT)	10^{21}	2.310^{20}
Useful μ decays $[10^{18}]$	1.00	$100/60 = 1.67$
Production, horn and injection		
Target (Ta) diameter/length [m], material	0.01/0.21	- / -
Pulse length [μs]	1.0	10.5
Proton energy [GeV/c]	60	100
Pion energy [GeV/c]	$5.0 \pm 10\%$	$5.0 \pm 10\%$
Horn diameter/length [m]	- / 2.0	- / -
Reflector diameter/length [m]	-	- / -
Current Horn/Reflector [kA]	300	- / -
Estimated collection efficiency	0.8	0.8
Estimated transport efficiency	0.8	0.8
Estimated injection efficiency	0.9	0.9
Acceptance [mm rad]	2.0	2.0
π/pot within momentum acceptance	0.11	$0.11 \times \frac{100}{60} = 0.187$
Length of target [m]	0.21	0.21
Distance between target and horn [m]	inside	inside
Length of horn [m]	2.0	-
Distance between horn and injection [m]	20	20
The muon storage ring		
Momentum of circulating muon beam [GeV/c]	3.8	3.8
Momentum of circulating pion beam [GeV/c]	$5.0 \pm 10\%$	$5.0 \pm 10\%$
Circumference [m]	350	350
Length of straight [m]	150	150
Ratio of Lstraight to ring circumference [Ω]	0.43	0.43
Dynamic aperture, $\mathrm{A_{dyn}}$	0.7	0.7
Acceptance [mm rad]	2.0	2.0
Decay length [m]	240	240
Fraction of π decaying in straight ($\mathrm{F_s}$)	0.41	0.41
Relative μ yield (N_μ/POT)	0.002	0.002
Detectors		
Distance from target [m]	20/1600	300/1800-2700

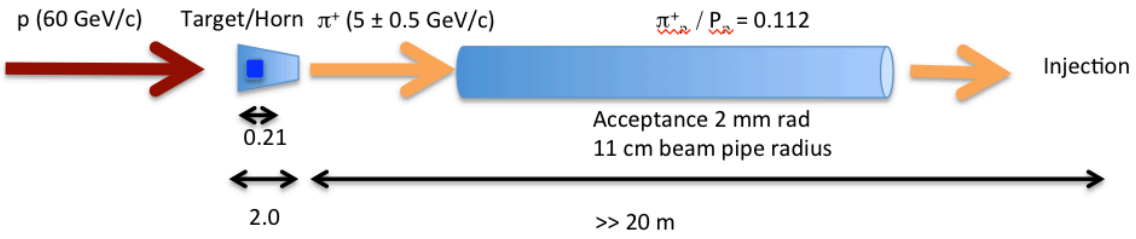

Figure 10: Block diagram of the production section of the νSTORM facility.

3.1.1 Production

The production section of the facility is sketched in figure 10. A tantalum target is being studied at FNAL, including horn collection and transport of pions up to the injection point. Different target materials, including low-Z targets such as carbon, will be considered. Assessment of the feasibility of the target design and the choice of target material will require the following studies to be made:

1. *Heat removal:*
   A significant heat load is deposited by the beam on the target and has to be removed reliably by the cooling system;
2. *Static and dynamic stresses:*
   The target must withstand thermal-mechanical stresses arising from the beam-induced heating of the target;
3. *Radiation damage:*
   Degradation of the material properties due to radiation damage must be accommodated;
4. *Geometrical constraints:* The target has to fit inside the bore of the magnetic horn whilst having an appropriate geometry for effective pion production;
5. *Remote replacement:*
   Once activated the target has to be remotely manipulated in the event of failure;
6. *Minimum expected lifetime:*
   The target is expected operate without intervention between scheduled maintenance shutdowns; and
7. *Safe operation:*
   The target design should minimise any hazard to the personnel or the environment.

Beam structure on timescales below μs will not be "seen" by the target. The beam pulse has to be fast extracted to enhance background rejection.

Simulations using a tantalum target show that, N_μ, the number of muons which decay in the production straight, would be comparable to [2]:

$$N_\mu = \mathrm{POT} \times (\pi \text{ per POT}) \times \epsilon_{\mathrm{col}} \times \epsilon_{\mathrm{trans}} \times \epsilon_{\mathrm{inj}} \times (\mu \text{ per } \pi) \times \mathrm{A}_{\mathrm{dyn}} \times \Omega\,; \tag{1}$$

where POT is the number of protons on target, ϵ_{col} is the collection efficiency, $\epsilon_{\mathrm{trans}}$ is the transport efficiency, ϵ_{inj} is the injection efficiency, μ per π is the chance that an injected pion results in a muon within the ring acceptance, $\mathrm{A}_{\mathrm{dyn}}$ is the probability that a muon within the decay ring aperture is within the dynamic aperture, and Ω is the fraction of the ring circumference that directs muons at the far detector. νSTORM assumes 10^{21} POT for a 4–5 year run using 60 GeV protons. From [2], one obtains (with horn collection) $\sim 0.1\pi/\mathrm{POT} \times \epsilon_{\mathrm{col}}$. The collection efficiency is 0.8. The transport efficiency (after collection to injection), and the injection efficiency are assumed to be 0.8 and 0.9, respectively and the probability that a π decay results in a μ within

the acceptance times A_{dyn} is estimated to be 0.08. Ω is estimated to be 0.43. With these parameters the relative muon yield, N_μ/POT, is ~ 0.002.

The number of pions produced off various targets by 60 GeV/c protons has been simulated [2]. Target optimisation based on a conservative estimate for the decay-ring acceptance of 2 mm radian corresponds to a decay ring with 11 cm internal radius and a β function of 600 cm. The optimal target length depends on the target material and the secondary pion momentum. Results of the optimisation study are included in table 1. Approximately 0.11 π^+/POT can be collected into a $\pm 10\%$ momentum acceptance off medium/heavy targets assuming ideal capture.

For the simulations, a NuMI design has been used; optimisation of the horn inner shape could increase the number of collected pions. Simulations show that μ/POT is an approximately linear function of energy for the proton energies of interest. These results are used to estimate the pion yield for the proposed SPS proton beam energy. Ultimately, the CERN implementation (100 GeV proton case) remains to be evaluated.

To determine the available number of useful muons for the CERN case, the values from the production studies in [2] have been adjusted to take into account the linear dependence of μ/POT on proton energy.

3.1.2 Injection

Pion decay within the ring, and non-Liouvillean "stochastic injection", are assumed to be optimised options. In stochastic injection, the $\simeq 5$ GeV/c pion beam is transported from the target into the storage ring and dispersion-matched into a long straight section. Circulating and injection orbits are separated by momentum. Decays within the straight section provide muons that are within the $\simeq 3.8$ GeV/c ring momentum acceptance. With stochastic injection, muons from a beam pulse as long as the FNAL Main Injector circumference (3 000 m) can be accumulated, and no injection kickers are needed, see figure 11. For 5.0 GeV/c pions, the decay length is $\simeq 280$ m; $\simeq 42\%$ decay within the 150 m decay ring straight.

3.1.3 Decay ring

The decay ring is a compact racetrack design based on separate function magnets. The design goal is to maximise the momentum acceptance (around 3.8 GeV/c central momentum), while maintaining reasonable physical apertures for the magnets in order to keep the cost down. This is accomplished by employing strongly focusing optics in the arcs (90° phase advance per FODO cell), featuring small β functions ($\simeq 3$ m average) and low dispersion ($\simeq 0.8$ m average). The linear optics for one of the 180° arcs is illustrated in figure 12.

The current lattice design incorporates a missing-magnet dispersion suppressor which will house the stochastic injection. With a dispersion of $\eta \simeq 1.2$ m at the drift, the 5 GeV/c and 3.8 GeV/c orbits are separated by $\simeq 30$ cm; an aperture of $\simeq \pm 15$ cm is available for both the 5 GeV/c π and 3.8 GeV/c μ orbits. To maintain the high compactness of the arc, while accommodating adequate drift space for the injection chicane to merge, two special "half empty" cells with only one dipole per cell were inserted at both ends of the arcs to suppress the horizontal dispersion. This solution will limit the overall arc length to about 25 m, while keeping the dipole fields below 4 T. The arc magnets assume a relatively small physical aperture of radius 15 cm, which limits the maximum field at the quadrupole magnet pole tip to less than 4 T.

On the other hand, the decay straight requires much larger values of β-functions ($\simeq 40$ m average) in order to maintain small beam divergence ($\simeq 7$ mrad). The resulting muon beam divergence is a factor of 4 smaller than the characteristic decay cone of $1/\gamma$ ($\simeq 0.028$ at 3.8 GeV/c). As illustrated in figure 13, the decay straight is configured with a much weaker focusing FODO lattice (30° phase advance per cell). It uses normal conducting large aperture (r = 30 cm) quads with a modest gradient of 1.1 T/m (0.4 T at the pole tip). Both the arc and the straight are smoothly matched via a compact telescope insert, as illustrated in figure 13.

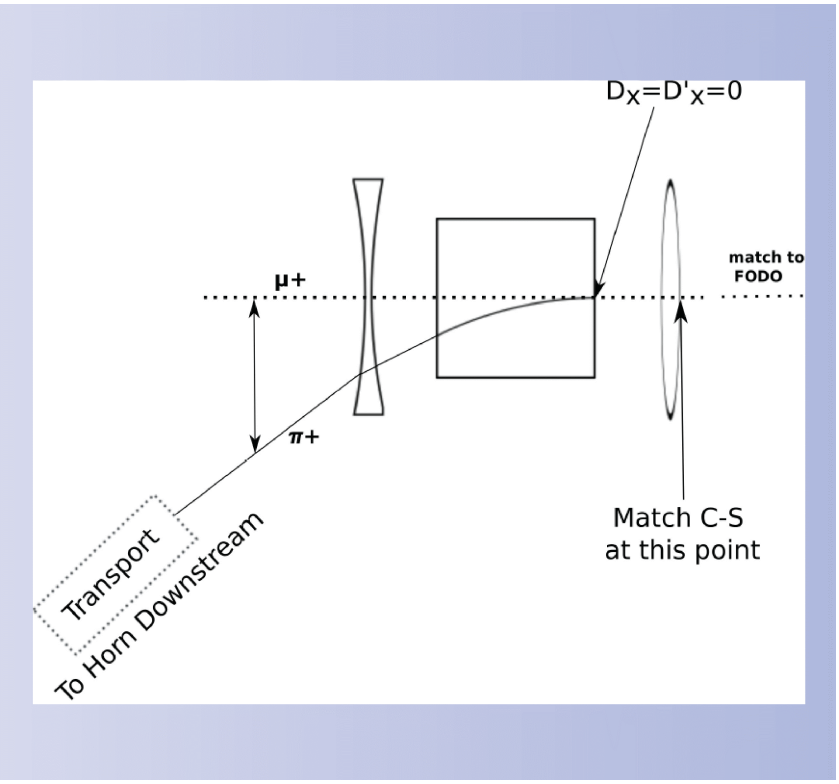

Figure 11: Schematic diagram of stochastic injection into the νSTORM ring.

The "other" 150 m straight, which is not used for neutrino production, can be designed using a much tighter FODO lattice (60° phase advance per cell), with rather small β functions comparable to those in the arc ($\simeq 5$ m average). This way one can restrict the aperture of the straight to a radius of 15 cm. The second straight uses normal conducting quads with a gradient of 11 T/m (1.6 T at the pole tip). Both the arc and the straight are smoothly matched, as illustrated in figure 14.

The complete racetrack ring architecture features the "low-β" straight matched to the 180° arc and followed by the "high-β" decay straight connected to the arc with a compact telescope insert. To summarise the magnet requirements, both 180° arcs were configured with 3.9 T dipoles and 25 T/m quads (superconducting magnets with an aperture of radius 15 cm). Both straights use normal-conducting magnets: the decay straight, 1.1 T/m quads with 30 cm radius aperture and the other straight, 11 T/m quads with 15 cm radius aperture. These magnets are challenging. The transverse normalised acceptance of the ring is 78 mm rad both in x and y (or a geometric acceptance of 2.1 mm rad) for the net momentum acceptance of $\pm 10\%$.

3.2 Detectors for sterile neutrino search

The Super B Iron Neutrino Detector (SuperBIND), an iron and scintillator sampling calorimeter similar in concept to the MINOS detector, is the baseline detector for the sterile-neutrino search focusing on muon-neutrino appearance and disappearance. Two detectors of this type would be used for short-baseline oscillation measurements; one 100 Ton detector at 50 m and a 1.6 kTon detector ~ 1.5 km from the storage ring. The near detector is required to measure the characteristics of the neutrino beam prior to oscillation for the reduction of systematic uncertainties. Simulations have been conducted for the far detector—a near detector simulation is in preparation.

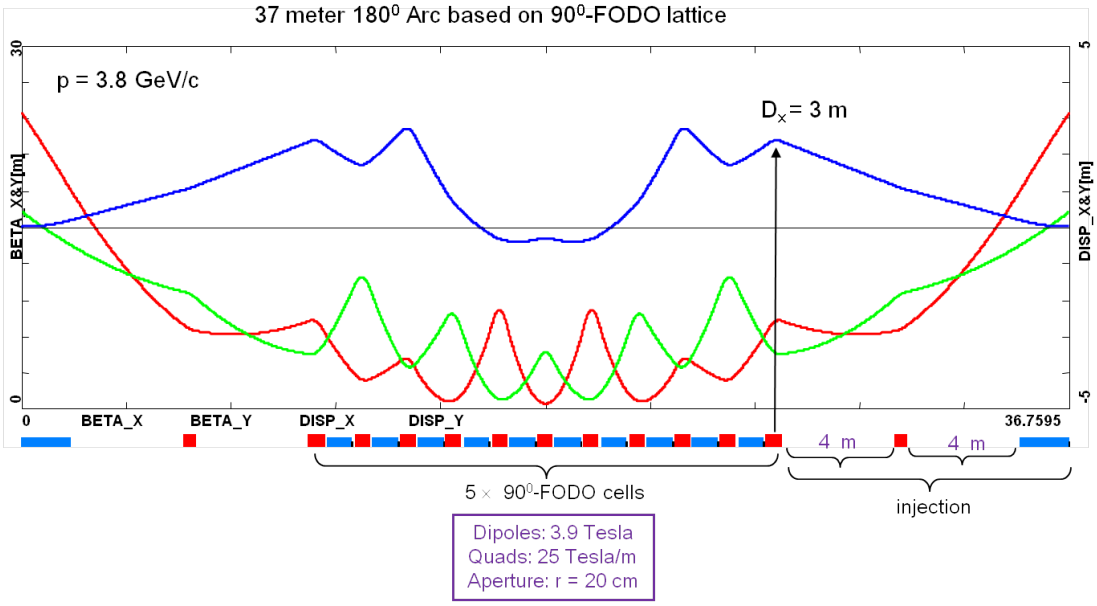

Figure 12: Schematic of the magnets that make up the lattice in the storage-ring arcs together with the optical functions as indicated in the legend.

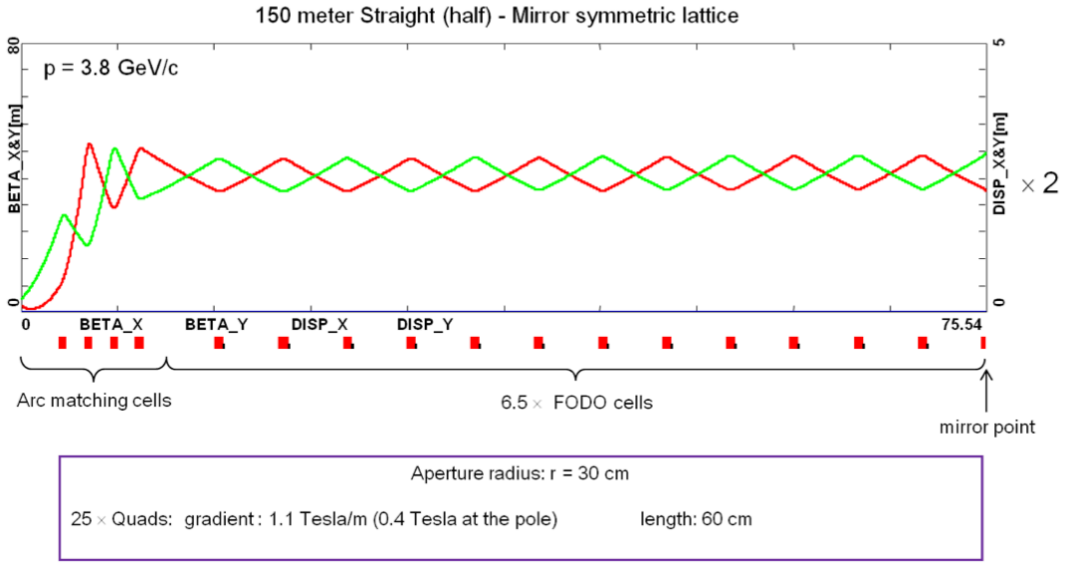

Figure 13: Magnet lattice and optical functions of the decay straight.

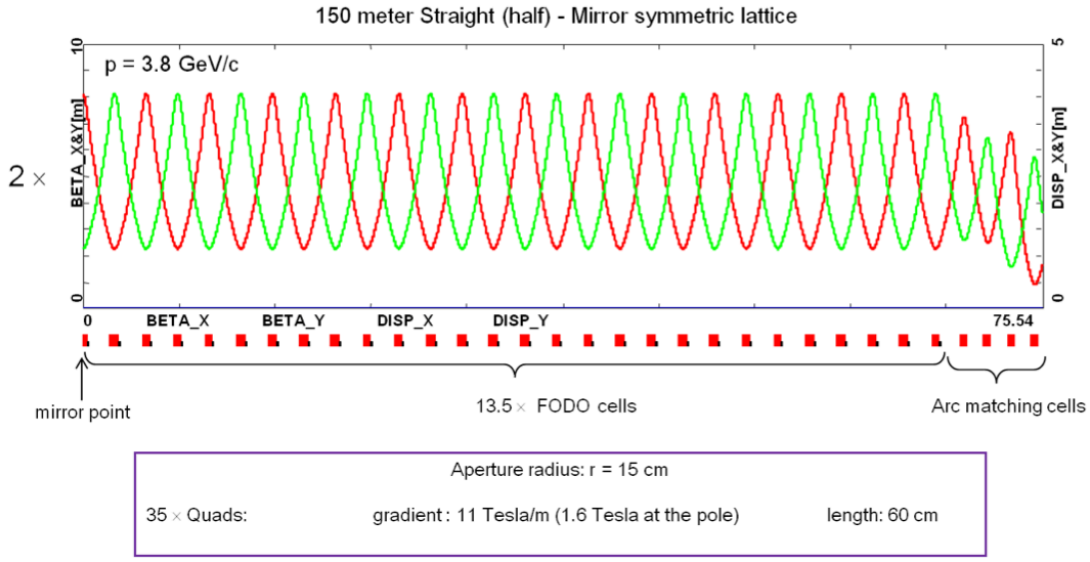

Figure 14: Magnet positions and lattice functions for the "return straight", i.e. the straight that returns the muons to the decay straight.

The far detector has a circular cross-section 5 m in diameter. The iron planes are to be 2 cm thick and constructed from two semi-circular pieces skip-welded at a central join. The detector is magnetised using multiple turns of a superconducting transmission line (STL) [190] to carry a total of 250 kA to induce a magnetic field between 1.5 T and 2.5 T within the iron plate. To accommodate the STL, a 20 cm bore runs through the centre of the detector. A 2-D finite-element magnetic-field analysis of the iron plate has been performed, with the results shown in figure 15.

The scintillator detector planes are composed of two layers of $1\times1\,\mathrm{cm}^2$ scintillating bars providing vertical and horizontal readout at each detection plane. A 1 mm bore through the centre of each bar is provided for the insertion of a wavelength shifting fibre. Each scintillator bar is read out from both ends using silicon photo-multipliers.

3.2.1 Far Detector Simulation

A detailed detector simulation and reconstruction programme has been developed for the determination of the detector response. The simulation was based on software developed for the Neutrino Factory Magnetised Iron Neutrino Detector (MIND) [191]. GENIE [192] is used to generate neutrino events. Events are passed to a GEANT4-based [193] simulation for the propagation of the final-state particles through successive steel and scintillator layers. This simulation includes hadron interactions simulated by the QGSP_BERT physics list [193]. Hits in the scintillator are grouped into clusters, smearing the detector hit position, and energy deposition of the accumulated hits is attenuated in a simple digitisation algorithm applied prior to reconstruction.

Magnetisation within the iron is introduced by reducing the model of figure 15 to a toroidal magnetic field with a radial dependence which follows the expression:

$$B_\phi(r) = B_0 + \frac{B_1}{r} + B_2 e^{-Hr}\,; \tag{2}$$

where $B_0 = 1.53\,\mathrm{T}$, $B_1 = 0.032\,\mathrm{T\,m}$, $B_2 = 0.64\,\mathrm{T}$, and $H = 0.28\,\mathrm{m}^{-1}$. This parameterisation and the field along the 45° azimuthal direction are shown in figure 16.

urrent represents approximately 80% of the critical current achieved at 6.5
st stand assembled for the VLHC proof-of-principle tests.

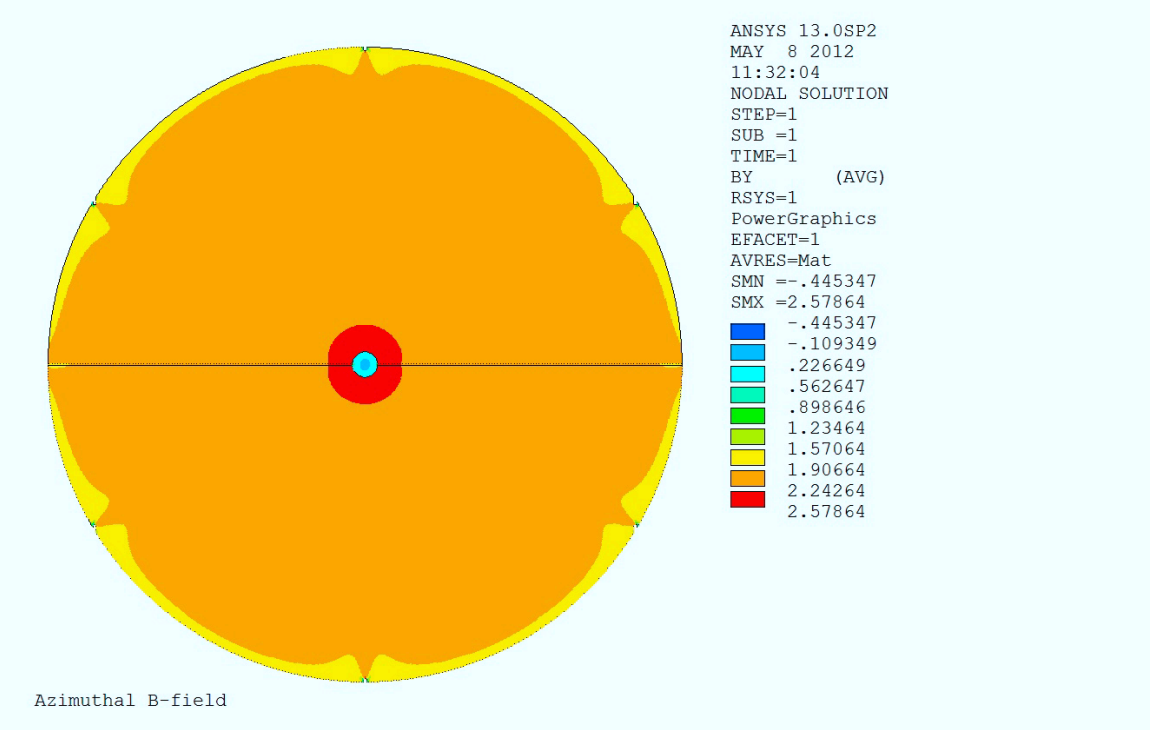

Figure 15: A 2-D finite element magnetic field simulation of the SuperBIND iron plate.

Figure 33. Toroidal Field Map

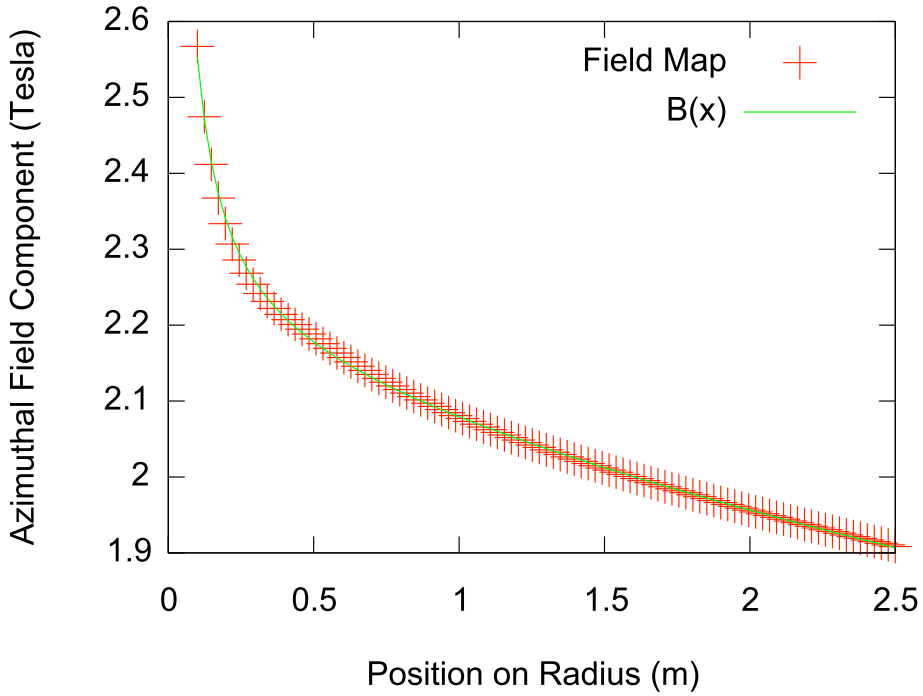

Figure 16: The magnetic field magnitude as a function of radius along the 45° azimuth with the parameterisation used in the detector simulation.

C. Detect

1. Scintill

article detectio is a mature te
OS has shown t ed wavelength s
ores and PMT ing and that it
ctured with ex dustrial setting.
nents use this s r detectors, suc
cibar [74], the [75] and the
etectors [76].

Our initial concept for the readout planes for SuperBIND is to have both
ew between each plate. The simulations done to date have assumed a scintill
rofile that is 1.0×1.0 cm^2. This gives both the required point resolution an

The reconstruction uses multiple passes of a Kalman-filter algorithm for the purposes of identifying muon trajectories within events and to determine the momentum and charge of an identified track. The algorithms are supplied by the RecPack software package [194]. Geometrical information from the track including: the length of the track; the direction of bending in the magnetic field; and the pitch of the track are used at various points in this procedure to provide information to the Kalman filter. The hadron reconstruction is not yet well developed so the neutrino energy is reconstructed either by using the quasi-elastic approximation, if no harmonisation is visible, or by smearing the true hadron energy according to MINOS CalDet test beam [195] results.

3.2.2 Event Selection

The reconstructed neutrino events are analysed to select events with well reconstructed muons rather than those where muons are mis-identified either in charge or particle identity. To achieve the target of 10σ significance the background efficiency must be reduced to less than parts in 10^4. The selection of events is accomplished with a multi-variate analysis facilitated by the ROOT based TMVA package [196]. This analysis outperforms the cuts based analysis described previously [2] by offering a lower signal-energy threshold and increasing the sensitivity of the experiment to oscillations.

Table 2: Variables used in the analysis of events in the SuperBIND simulation. Variables in (a) are used in the definition of the classifier, while the cuts in (b) are fixed.

(a) Variables used in the multivariate analysis.

Variable	Description
Track Quality	$\sigma_{q/p}/(q/p)$, the error in the trajectory curvature scaled by the curvature
Hits in Trajectory	The number of hits in the trajectory
Curvature Ratio	$(q_{init}/p_{range}) \times (p_{fit}/q_{fit})$: comparison of the initial guess of the curvature to the Kalman fit result.
Mean Energy Deposition	Mean of energy deposition of hits in fit of the trajectory
Variation in Energy	$\sum_{i=0}^{N/2} \Delta E_i / \sum_{j=N/2}^{N} \Delta E_j$ where the energy deposited per hit $\Delta E_i < \Delta E_{i+1}$.

(b) Preselection variables.

Variable	Description
Trajectory Identified	There must be at least one trajectory identified in event.
Successful Fit	The longest identified trajectory must be successfully fit.
Maximum Momentum	The momentum of the longest trajectory is less than 6 GeV/c.
Fiducial	Longest trajectory must start prior to the last 1 m of the detector.
Minimum Nodes	Fit to longest trajectory must include more than 60% of hits assigned to trajectory by filter.
Track Quality	$\sigma_{q/p}/(q/p) < 10.0$
Curvature Ratio	$(q_{init}/p_{range}) \times (p_{fit}/q_{fit}) > 0$

The analysis was trained to discriminate between the ν_μ charged current (CC) interaction signal events and $\bar{\nu}_\mu$ neutral current (NC) interaction background events using a set of five parameters to define a classifier variable. The majority of these parameters were chosen based on the experience of the MINOS experiment [197]. Table 2(a) summarises these parameters. A set of preselection cuts, detailed in Table 2(b) were applied to limit the analysis to the subset of events containing useful data. These preselection cuts were also used in the cuts based

analysis with the addition of cuts on the track quality and number of hits in a trajectory. The multi-variate analysis was trained using a variety of methods, but the best performance was achieved using Boosted Decision Trees (BDT). Based on the performance of this method, shown in figure 17, events are selected if the BDT classifier variable is greater than 0.56.

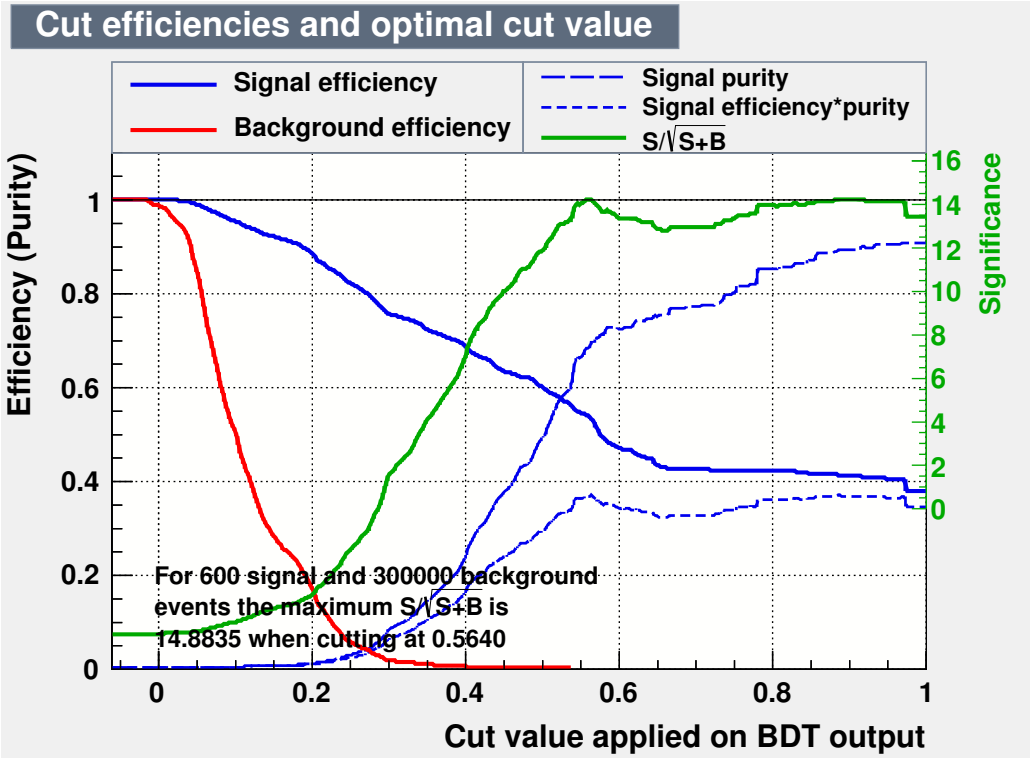

Figure 17: Results from training the BDT method to simulations of ν_μCC signal events and $\bar{\nu}_\mu$ background events, assuming a realistic number of events.

3.2.3 Sensitivities

The appearance of ν_μ, via the channel $\nu_e \rightarrow \nu_\mu$, gives νSTORM broad sensitivity to sterile neutrinos and directly tests the LSND/MiniBooNE anomaly. The oscillation probabilities for both appearance and disappearance modes are:

$$P_{\nu_e \rightarrow \nu_\mu} = 4|U_{e4}|^2|U_{\mu 4}|^2 \sin^2\left(\frac{\Delta m^2_{41} L}{4E}\right) \text{ ; and} \quad (3)$$

$$P_{\nu_\alpha \rightarrow \nu_\alpha} = 1 - [4|U_{\alpha 4}|^2(1-|U_{\alpha 4}|^2)] \sin^2\left(\frac{\Delta m^2_{41} L}{4E}\right) . \quad (4)$$

The detector is designed for the appearance signal $\nu_e \rightarrow \nu_\mu$; the CPT conjugate of the channel with which LSND observed an anomaly, $\bar{\nu}_\mu \rightarrow \bar{\nu}_e$. Although it is clear from equation 3 that the appearance channel is doubly suppressed relative to the disappearance channel, the experiment is much more sensitive to the appearance channel because the backgrounds for wrong-sign muon searches can be suppressed more readily.

The detector response derived from simulation is used to determine the sensitivity of the experiment to the presence of sterile neutrinos. The sensitivities and optimisation were computed using GLoBES [180]. Modifications were made to simulate accelerator effects such as the integration of the decay straight as outlined

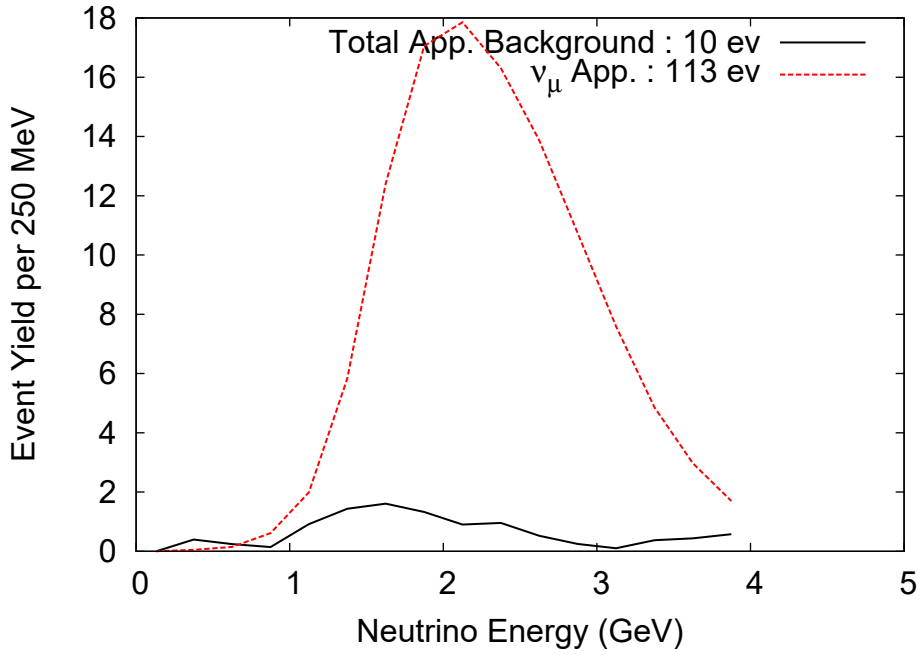

Figure 18: The neutrino spectrum measured at the SuperBIND far detector using the simulated detector response.

in [198, 199]. The detector response is summarised as a "migration" matrix of the probability that a neutrino generated in a particular energy bin i is reconstructed in energy bin j. Defined in this way, the migration matrix encapsulates both the resolution of the detector and its efficiency. Samples of all neutrino interactions that could participate in the experiment are generated to determine the response for each detection channel. The spectrum of expected signal and background for this simulation is shown in figure 18 assuming 1.8×10^{18} μ^+ decays collected over 5 years. A contour plot showing the sensitivity of the ν_μ appearance experiment to sterile neutrinos is shown in figure 19. These contours are shown with respect to the derived variable $\sin^2 2\theta_{e\mu} = |U_{e4}|^2|U_{\mu4}|^2$. Systematic uncertainties are included in the contour as stated in the legend.

The leading systematic uncertainty is expected to be related to the neutrino flux appearing within the detector fiducial volume. This systematic is anticipated to be on the order of 1% for signal events and 10% for background events. These numbers assume that the neutrino spectrum and rate will be well known from the storage ring. The experiment is robust to a five fold increase in the systematic uncertainties such that the appearance channel alone has the sensitivity to probe the LSND anomaly with a confidence level corresponding to more than 10σ.

A disappearance experiment is more sensitive to the signal normalisation than an appearance experiment. The neutrino flux is extremely well understood for νSTORM, but further understanding of the measured spectrum resulting from the combination of efficiencies and cross sections is required. To control these effects a near detector identical to the far detector is required. A study of $\bar{\nu}_\mu$ disappearance in a SuperBIND detector is in progress, but a study of ν_e disappearance using a generic detector has been completed [34]. The results are applicable to a $\bar{\nu}_\mu$ disappearance experiment. In absence of a well developed near detector simulation, a conservative approach was assumed. A 10% systematic, uncorrelated between energy bins but correlated between the near and far detector (shape error) becomes the leading systematic in this case with further details and systematics given in Ref. [34]. Geometry effects are especially important for the near detector as the beam divergence, both from the muon decay kinematics and transverse beam components will lead to a different beam spectrum for the near and far detectors [34, 200]. The oscillations will also average over the length of the

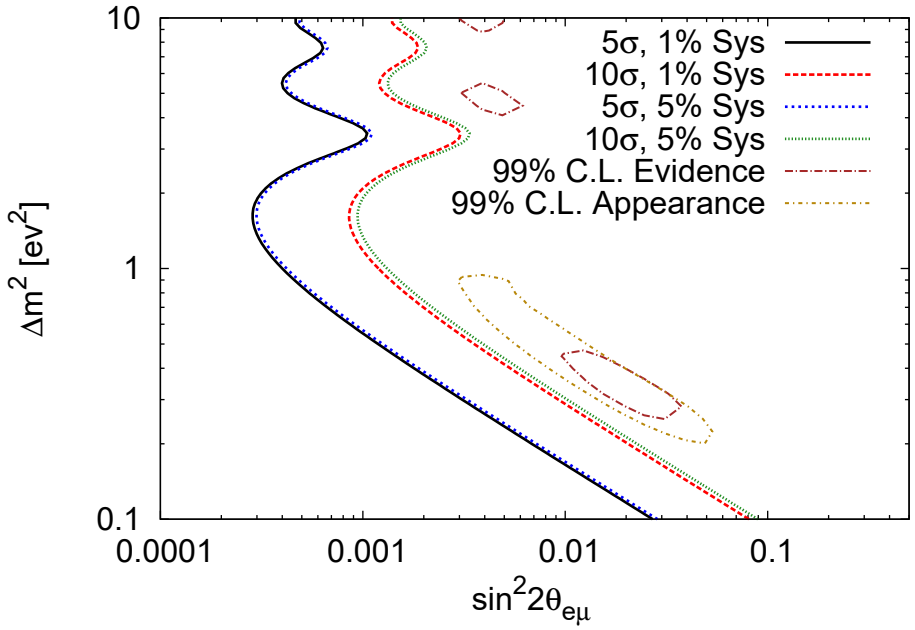

Figure 19: Contours of the χ^2 deviation from the no-sterile neutrino hypothesis corresponding to 5σ ($\chi^2 = 25$) and 10σ($\chi^2 = 100$) variations. Two different sets of systematic uncertainties are represented; the default systematics with 1% signal uncertainty and a 10% background uncertainty and a conservative set that is five times larger. The 99% confidence level contours from experiments showing evidence for unknown signals and contours derived from the accumulated data from all applicable neutrino appearance experiments, as described in figure 3.

decay straight [34, 201]. These effects are illustrated in figure 20(a). An optimisation of the baseline distances are shown in figure 20(b). The optimisation shows that all options preform equally well for $\Delta m^2 \simeq 1$ eV^2, while larger values of $\Delta m^2 \simeq 1\,\mathrm{eV}^2$ prefer shorter distances (from the end of the decay straight) for the far detector.

3.3 Detectors for neutrino scattering studies

To explore fully the broad programme of νN scattering studies described in section 2.1 will require a number of detectors optimised to address different aspects of the programme. The two detectors described below are intended to indicate possible options for further development. The development of a detailed specification for the νN-scattering detector suite is part of the programme of work we propose to carry out (see section 5.3). Physics topics offered by a high resolution detector such as the options described below in νSTORM are summarised in Appendix A.

3.3.1 HIRESMNU: A High Resolution Near Detector à la LBNE

Precision measurements of neutrino-interactions at the near-detector (ND) are necessary to ensure the highest possible sensitivity to the neutrino-oscillation studies in this proposal. Regardless of the process under study—$\nu_\mu \to \nu_e$ ($\bar{\nu}_\mu \to \bar{\nu}_e$) appearance or ν_μ ($\bar{\nu}_\mu$) disappearance—the systematic error should be less than the corresponding statistical error. The ND design must achieve the four principal goals:

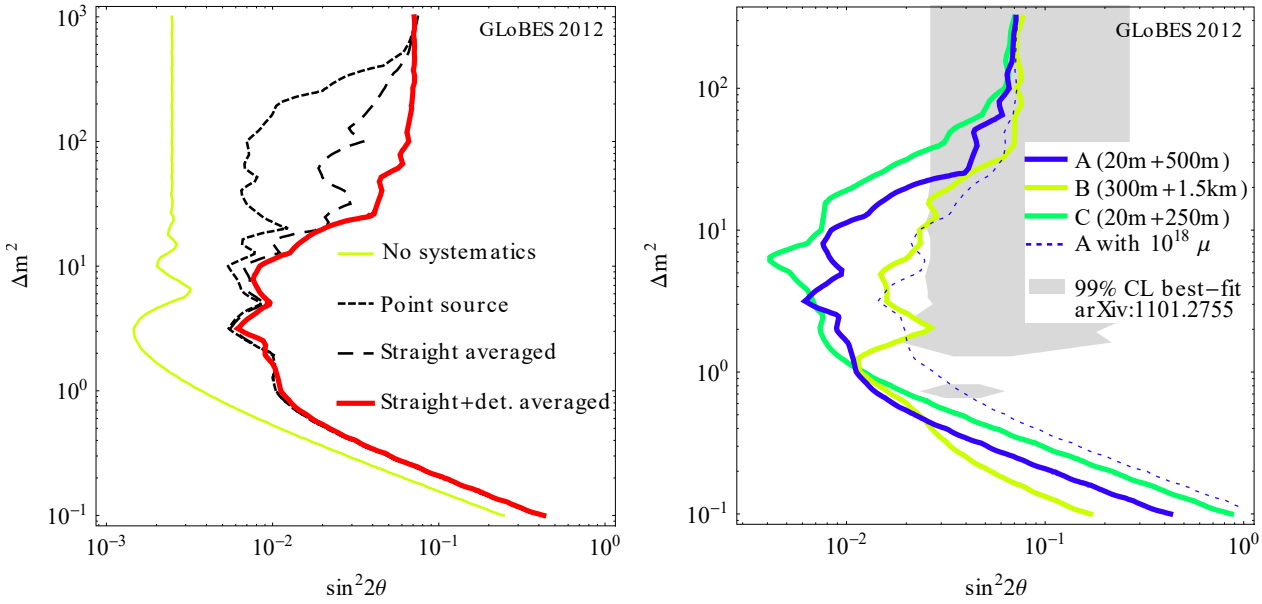

(a) Systematic effects

(b) Baseline optimisation

Figure 20: Exclusion region in $\sin^2 2\theta$-Δm^2 (right hand sides of curves) for ν_e disappearance for different geometry assumptions (left panel) and optimisation points (right panel); 90% CL, 2 d.o.f. (a): The curve "no systematics" represents a single detector at $d = 500\,\mathrm{m}$ using statistics only, whereas the other curves correspond to near-far detector setups, where the red thick curves include (conservative) full systematics, including a 10% shape error, and geometry effects. (b): Systematics are fully included, different two-distance optimisation points shown (distances to the end of the decay straight). Both panels: $E_\mu = 2\,\mathrm{GeV}$, 10^{19} useful muon decays per polarity, $d_1 = 20\,\mathrm{m}$ (200 t) and $d_2 = 500\,\mathrm{m}$ (1 kt), unless noted otherwise. Figure taken from reference [34].

- Measurement of the absolute and the relative abundance of the four species of neutrinos, ν_μ, $\bar{\nu}_\mu$, ν_e, and $\bar{\nu}_e$, as a function of energy (E_ν). Accurate determination of the angle and the momentum of the electron in neutrino-electron neutral current scattering which will provide the absolute flux;
- Determination of the absolute E_ν-scale, a factor which determines the value of the oscillation-parameter Δm^2;
- Measurement of π^0s and of π^+ and π^- produced in the NC and CC interactions. The pions are the predominant source of background for any oscillation study; and
- Measurement of ν-nucleus cross-sections. The cross-section measurements of exclusive and inclusive CC and NC processes will furnish a rich panoply of physics relevant for most neutrino research. Knowing the cross sections at the E_ν typical of the νSTORM beam is essential for predicting both the signal and the background.

A high-resolution detector, the HIRESMNU, has been proposed as the near detector for the LBNE project [202, 203]. Figure 21 shows a schematic of this the HIRESMNU design. The architecture of the detector [202, 203] builds upon the experience of NOMAD [204]. It embeds a $4 \times 4 \times 7\,\mathrm{m}^3$ Straw-tube tracker (STT), surrounded by a 4π electromagnetic calorimeter (ECAL) in a dipole magnet with $B \simeq 0.4\,\mathrm{T}$. Downstream of the magnet, and within the magnet yoke, are detectors for muon identification. The STT will have a low average density similar to liquid hydrogen, about $0.1\,\mathrm{gm/cm}^3$, which is essential for momentum determination and the identification of electrons, protons, and pions. The foil layers, up- and down-stream of the straw tubes, provide

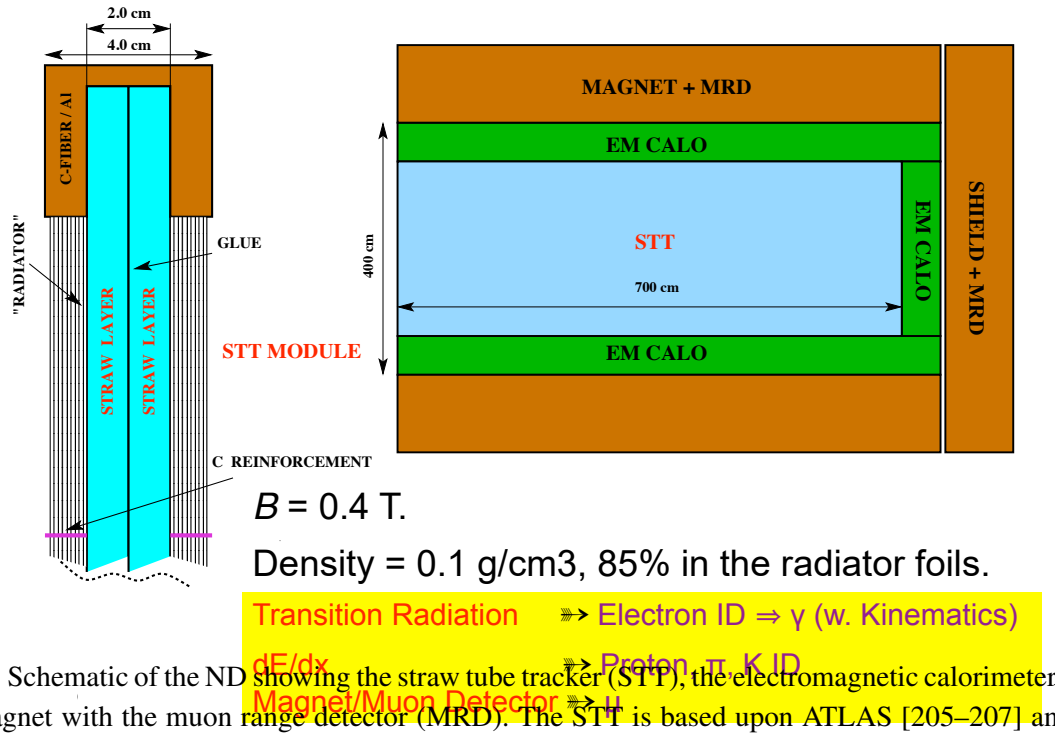

Figure 21: Schematic of the ND showing the straw tube tracker (STT), the electromagnetic calorimeter (ECAL) and the magnet with the muon range detector (MRD). The STT is based upon ATLAS [205–207] and COMPASS [208, 209] trackers. Also shown is one module of the proposed straw tube tracker (STT). Interleaved with the straw tube layers are plastic foil radiators, which provide 85% of the mass of the STT. At the upstream end of the STT are layers of nuclear-target for the measurement of cross sections and the π^0's on these materials.

the transition-radiation and constitute most of the 7 ton fiducial mass. The foil layers serve both as the mass on which the neutrinos will interact and as generators of transition radiation (TR), which provides electron identification.

Along the beam, the total depth of the detector, in radiation lengths, is sufficient for 50% of the photons, largely from π^0 decay, to be observed as e^+e^- pairs, which delivers superior resolution compared with conversions in the ECAL. Layers of nuclear-targets will be deployed at the upstream end of the STT for the determination of cross sections on these materials.

The HIRESMNU allows the cross-sections of exclusive and inclusive processes to be measured, detailed studies of the multiplicity of secondary particles to be carried out and the detailed characterisation of the neutrino source. It can identify all four neutrino species in νSTORM. Systematic studies of ν-electron scattering, quasi-elastic interactions, $\nu_e/\bar{\nu}_e$-CC, neutral-current identification, π^0 detection, etc. have been carried out in the context of LBNE. The quoted dimensions, mass, and segmentation of HIRESMNU will be further optimised for νSTORM as the proposal evolves.

3.3.2 A pressurised gas TPC option for cross section measurements

A versatile detector has been proposed as a near detector for LBNO, the Gas Argon Modular Apparatus for Neutrino Detection ($\gamma\nu$det) [210]. Based on a pressurised argon time projection chamber (TPC) located in a large 5 m diameter pressure vessel, figure 22, this proposal is well suited for the precision measurement of cross sections and detailed study of electron- and muon-neutrino interactions at a νSTORM near detector facility. A magnetic field is applied to the full volume of the pressure vessel. A magnet design similar to that of the UA1/NOMAD spectrometer dipole magnet provides a field with characteristics close to those required for this detector. The required peak field magnitude is under study. The pressure vessel can accommodate

several layers of scintillator-based calorimeter, such as the SuperBIND plastic scintillator material, between the TPC and the pressure vessel inner surface. One advantage of this design compared with a more compact pressure vessel enclosing only the TPC is that there is less redundant/passive material between the TPC and first layers of the scintillator detector and fewer blind spots. The outer layers of the embedded scintillating material can be interleaved with radiators to improve the containment within the pressure vessel of more energetic secondaries from events of interest occurring in the TPC. High energy muons of both signs > 1 GeV from neutrino events originating in the TPC would be measured downstream in a muon spectrometer similar in design to the SuperBIND but 1/10th the size.

A gas TPC provides excellent vertexing capabilities, especially relevant for the understanding of nuclear effects in neutrino interactions. Figure 23 compares a CCQE neutrino interaction in liquid argon ($\rho = 1.4\,\mathrm{g.cm^{-3}}$) with the same interaction in argon gas at 20 bar ($\rho = 0.034\,\mathrm{g.cm^{-3}}$) [211, 212]. No magnetic field is applied in this GENIE Monte Carlo simulation using the LBNO neutrino flux. With a 3 mm pitch, the three proton tracks can clearly be resolved in the argon gas but are completely undetectable in liquid argon. The liquid argon TPC (LAr TPC) would benefit from an even finer granularity and lower kinetic-energy threshold for proton detection (set to 40 MeV). Here, the pressurised argon TPC provides a compelling case for neutrino-nucleon interaction studies. By using argon as the target nucleus in the near detector, valuable data are compiled for liquid argon-based neutrino detectors such as those planned for long baseline projects. The TPC gas can be readily changed to other gases, for instance CH4 or CO2, allowing studies of interactions on different materials similar to for example the liquid scintillator of fully-active-scintillator proposals.

The ν_μ flux at the LBNO near detector location peaks around 3 GeV extending beyond 20 GeV with a mean around 5 GeV. The νSTORM near detector flux peaks at 2.5 GeV and has a cut off at 4 GeV which is set by the 3.8 GeV/c μ beam and its 10% momentum spread. Event containment is therefore less of a challenge at νSTORM i.e. the present proposal for LBNO could be applied to the νSTORM facility with little re-optimisation. Simulation work is underway to optimise the detector configuration and evaluate its physics performance.

Engineering details will be addressed by the LBNO near detector task which is due to report a conceptual design by end 2014. It will cover the dimensioning of the magnet and pressure vessel, the feasibility and cost of a large flange on the pressure vessel, the integration of TPC and scintillator calorimeter within the pressure vessel, in particular feedthroughs for the supplies and readout of those detector elements. As is mentioned in Section 2.1.3 there is a strong motivation for accurate measurements of the neutrino-nucleon interaction cross sections on an H_2 or D_2 target. The argon-filled pressure vessel would be functionally equivalent to a safety barrier, providing a second safety layer beyond the H_2 container vessel and enabling the safe operation of such an H_2 cask in this near detector proposal. The H_2 cask design could be based on the cold neutron moderators in routine operation at several neutron scattering facilities worldwide.

4 Implementing the νSTORM facility

4.1 Implementing νSTORM at CERN

The fast extraction of protons from the SPS is initiated by a kicker in LSS1. A septum in the TT20 beam line then extracts the beam from the SPS so that it can be transported to the νSTORM target. This fast-extraction scheme (see figure 24) has been demonstrated for low intensities. Several neutrino experiments are proposed for the North Area. In developing the concept for implementing νSTORM at CERN it will be important to consider exploiting the present and planned infrastructure in the North Area to the fullest extent.

To deliver the proton-beam phase space required by νSTORM requires that the LS2 upgrades to the injector systems, including the new Linac4, are complete. Figure 25 shows the timeline for these upgrades. If the

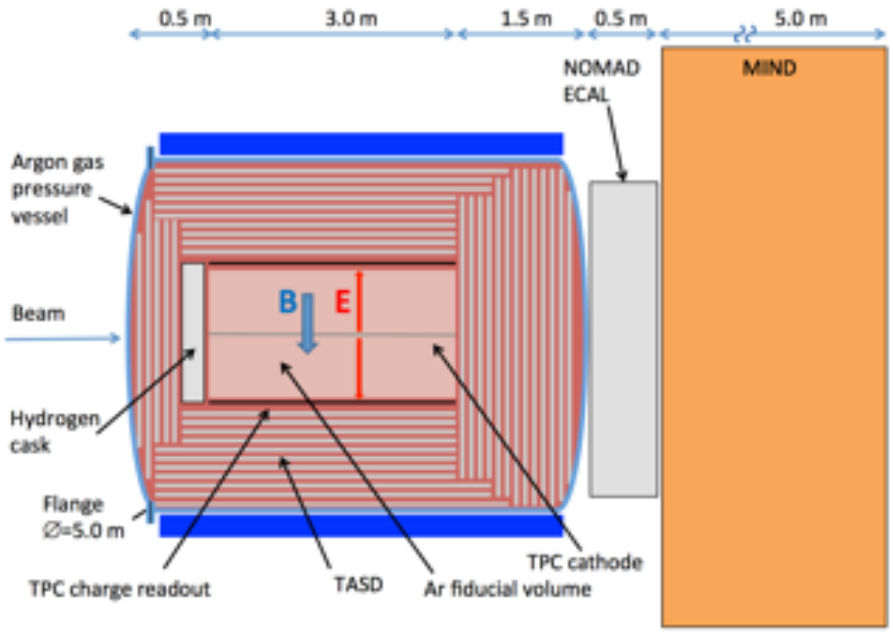

Figure 22: Schematic of the pressurised argon gas-based TPC detector. Both the TPC and scintillator calorimeter layers surrounding it are enclosed in a pressure vessel. A 0.5 T magnetic field is applied to the pressure vessel volume. Downstream of the TPC are also an electromagnetic calorimeter (ECAL) and a magnetised iron neutrino detector (MIND). The latter acts as a muon spectrometer for neutrino interactions occurring in the TPC and as an independent near detector for the sterile neutrino programme.

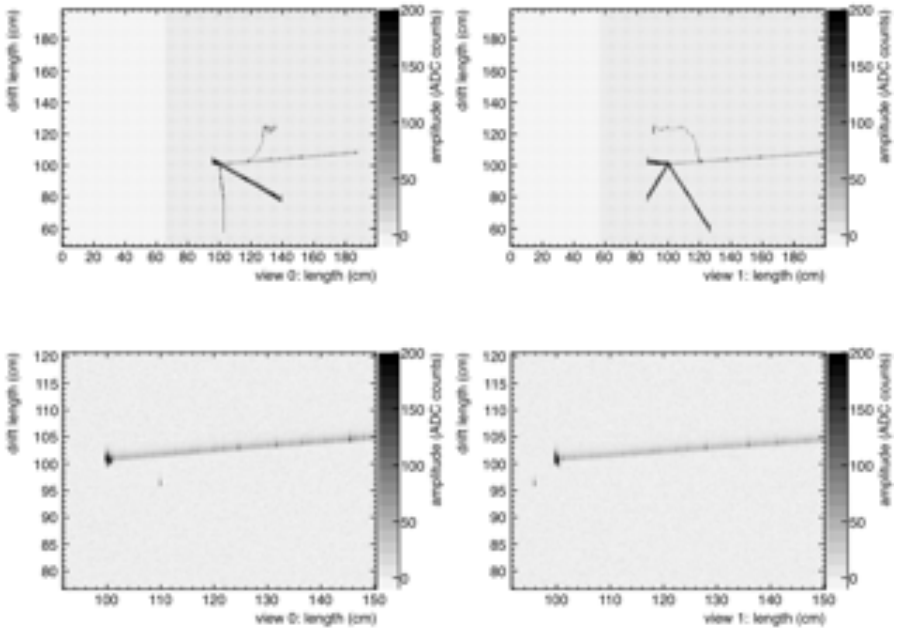

Figure 23: GENIE Monte Carlo simulations of a charged current quasi-elastic (CCQE) neutrino interaction in 20 bar pressurised argon gas (top) and liquid argon (bottom). Three proton tracks are clearly resolved in the pressurised argon and completely undetectable in the liquid argon. Of the two options, argon gas is better suited to study nuclear effects in neutrino interactions.

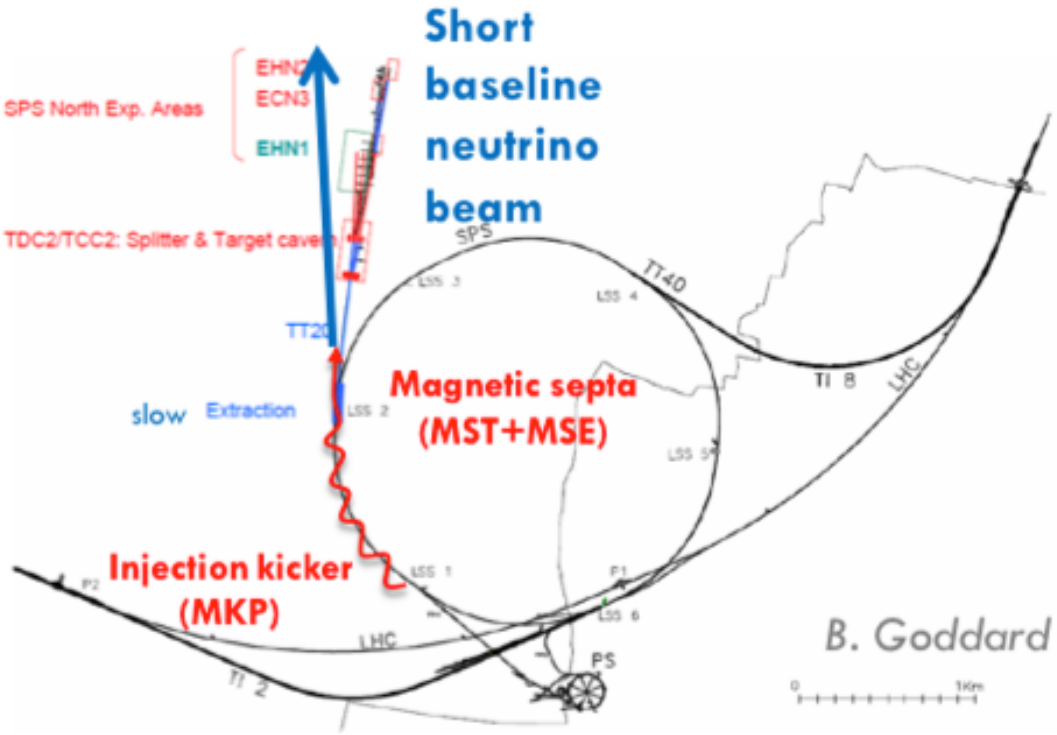

Figure 24: Extraction of the SPS beam in the North Area.

short-baseline programme proposed in [21] is executed on the timetable outlined by the proponents, νSTORM will be a highly-effective development of the short-baseline programme.

The 100 GeV beam will deliver 0.56 MJ ($100\,\mathrm{GeV} \times 3.5\,10^{13} \times 1.6\,10^{-19}$). Repeating this every 3.6 s, the ultimate repetition rate, gives 156 kW on target. The 6 s interval between pulses would reduce the beam power by roughly a factor of two compared to the FNAL option. Using fast extraction, the proton-pulse duration will be 10.5 μs which is 10 times longer than for the beam pulse from the Main Injector at FNAL. Two such pulses of 2100 bunches, spaced by 50 ms, are extracted every SPS cycle. The beam characteristics before and after the LS2 upgrades are shown in table 3 [21].

The estimations made in [21] indicate that 4.5×10^{19} POT/year may reasonably be expected. If νSTORM ran for five years with 100 GeV protons, $5 \times 4.5 \times 10^{19} = 2.3 \times 10^{20}$ POT would be delivered. With the assumption that the π/POT is proportional to the energy, a further optimisation to gain a factor of two in POT would have to be made.

The design of the target developed at FNAL has to be adapted. The differing geometry of the CERN and FNAL options is shown in figure 26. The 10.5 μs pulse of protons from the SPS means that muons will make a number of turns in the storage ring during pion injection. To ensure the neutrino beam arises solely from the decay of muons, the injection of pions and the neutrino-beam extraction are at different ends of the same arc. The pion-injection channel and the proton absorber have to be designed taking into account the proton and neutrino beam directions. The pion injection system is constrained by the limited space available for the proton absorber and by the requirement that the total length of the transport channel be minimised to limit pion decay outside the storage ring.

It is important to investigate whether existing or planned beam lines, target stations and detector caverns, or parts of them, can be re-used. The source-detector distance has to match the neutrino energy. The physics potential of the facility for varying detector positions for 3.8 GeV/c stored muons is shown in figure 27. At

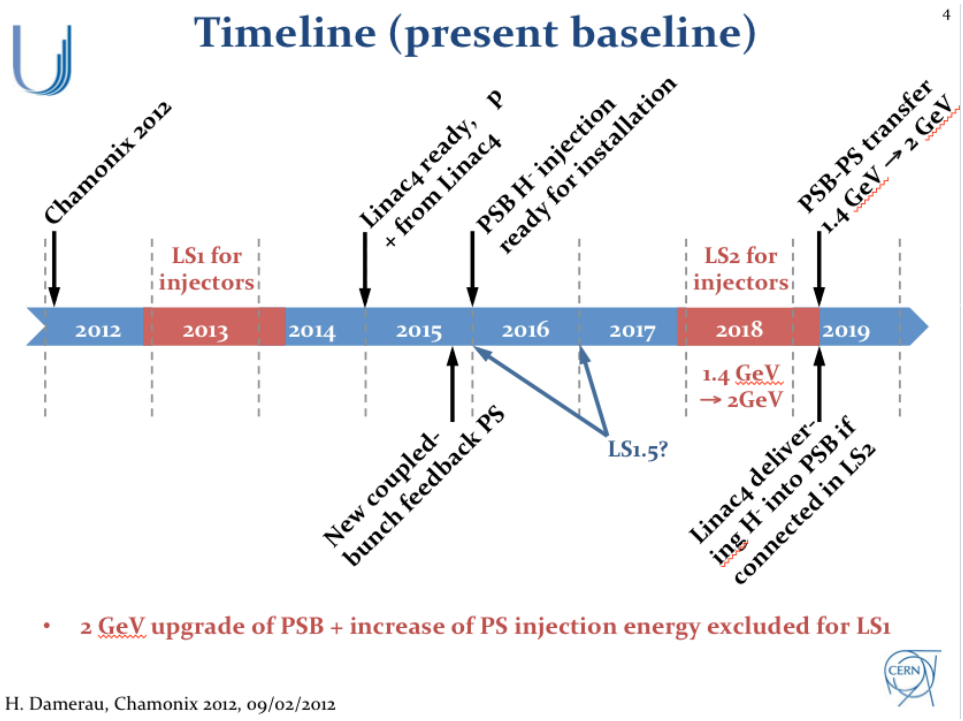

Figure 25: Timeline for the CERN injector upgrades (presented by H. Damerau at the 2012 Chamonix workshop.

Table 3: Summary of the SPS beam characteristics at present and after the LS2 upgrade.

Parameter	**SPS operation**		**SPS record**		**After LIU 2020**	
	LHC	CNGS	LHC	CNGS	LHC	νSTORM
Energy [GeV]	450	400	450	400	450	100
Bunch spacing [ns]	50	5	25	5	25	5
Bunch intensity [10^{11}]	1.6	0.105	1.3	0.13	2.2	0.17
Number of bunches	144	4200	288	4200	288	4200
SPS intensity [10^{13}]	2.3	4.4	3.75	5.3	6.35	7.0
PS intensity [10^{13}]	0.6	2.3	1.0	3.0	1.75	4.0
SPS Cycle length [s]	21.6	6.0	21.6	6.0	21.6	3.6
PS Cycle length [s]	3.6	1.2	3.6	1.2	3.6	2×1.2
PS beam mom. [GeV/c]	26	14	26	14	26	14
Beam Power [kW]	77	470	125	565	211	156

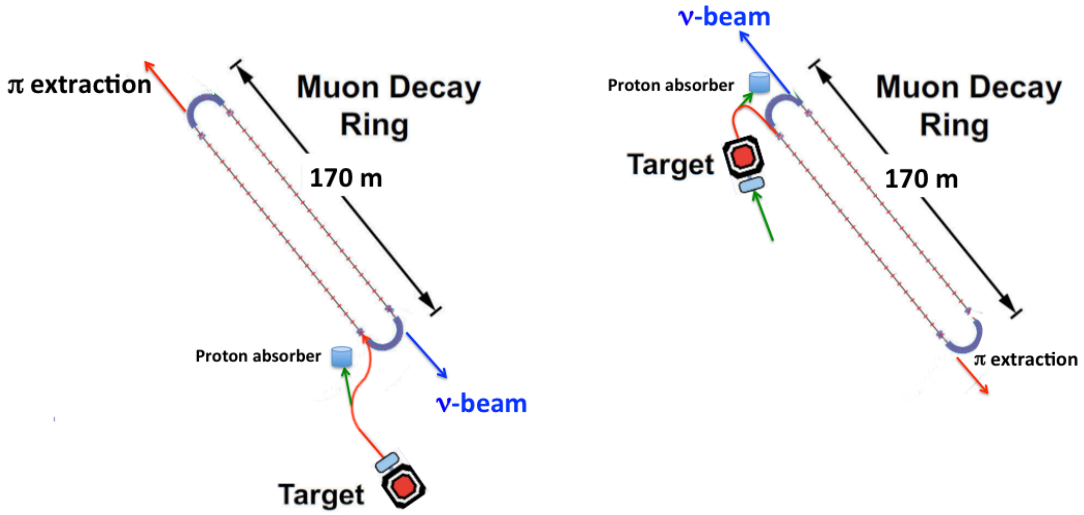

Figure 26: The proton and pion transport have to be optimised taking into account the placement of the νSTORM ring and the direction in which the beam is required. The space for the the proton absorber is constrained. The figure sketches two possible configurations: to the left where the protons and the neutrinos have similar directions and to the right when they have opposite directions.

FNAL, the position of the far detector is around 1.6 km. νSTORM also needs space for a near detector at 20 m to 50 m from the neutrino extraction point. While it is in general difficult to re-use target facilities due to the high irradiation levels, if it were possible to design a target station that could support both the CENF programme and νSTORM, it might be possible to reduce the implementation cost.

A study to lay out, in a cost effective and feasible manner, the νSTORM facility at CERN has to take into account the civil engineering constraints, re-use of existing beam lines and detector caverns etc. The facility could be placed in such a way as to exploit the CENF [21] or constructed underground at the SPS level using existing caverns, BA 1, 4 or 5. Consideration should also be given to possible use of both straight sections for physics. The pion dump could be used to produce a muon beam suitable for the implementation of a 6D ionisation cooling programme (see section 2.3.1).

Figure 28 shows νSTORM in the North Area. The design of the pion-injection section for this case may be difficult (space limitations and the requirement for high-field magnets). νSTORM could also be situated 60 m underground, at the SPS level, directed to one of the existing SPS caverns in which the detector hall would have to be built. A muon-cooling experiment could also be placed close to the decay ring after the pion extraction channel (see figure29).

Figure 30 shows an option in which the neutrino beam is sent to the Meyrin site, the far detector being placed inside the ISR ring. In this case, the design of the pion channel is similar to the FNAL option. However, the baseline is rather long (see figure 27) and, for such a long baseline, the energy of the pions and the stored muons would have to be selected higher than the present baseline.

All of the options outlined above need to be considered in more detail, in particular the proton beam lines and the pion transfer channels, including the proton absorber, must be shown to be feasible. The target station should be similar to those already developed for 100 GeV protons, however the capture system for a specific target would need to be optimised.

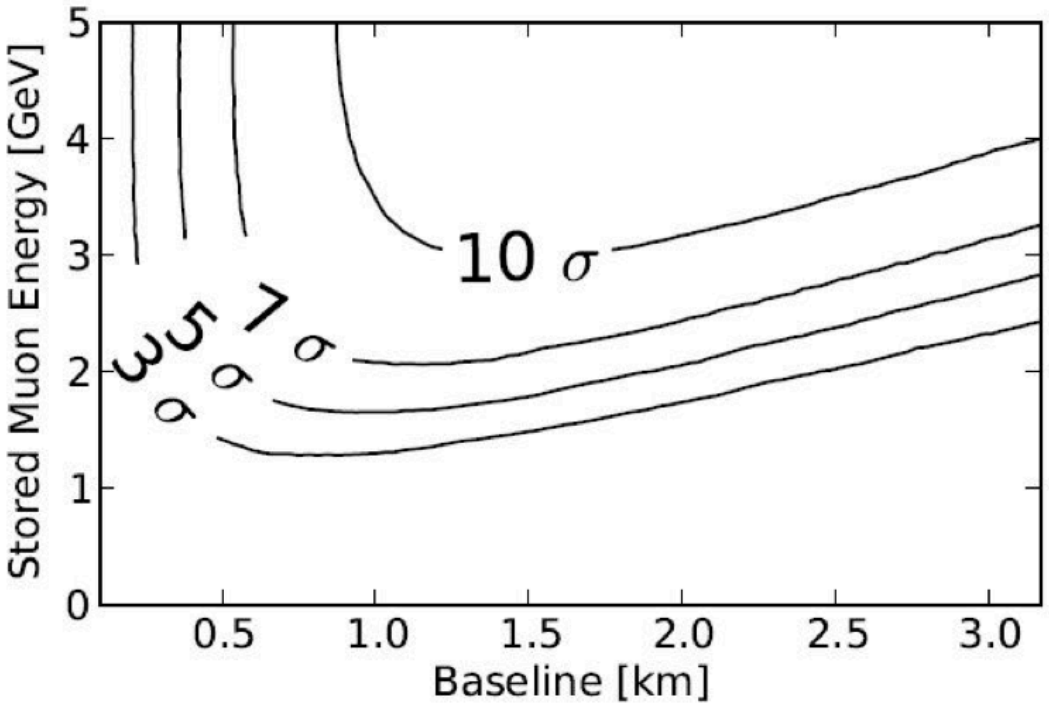

Figure 27: Physics potential for different baselines and stored muon energies (χ^2 contours were derived using the total event rate, without systematic errors, a signal efficiency of 0.5 and background rejection of charge misidentification and NCs at 10^{-3} and 10^{-2} respectively).

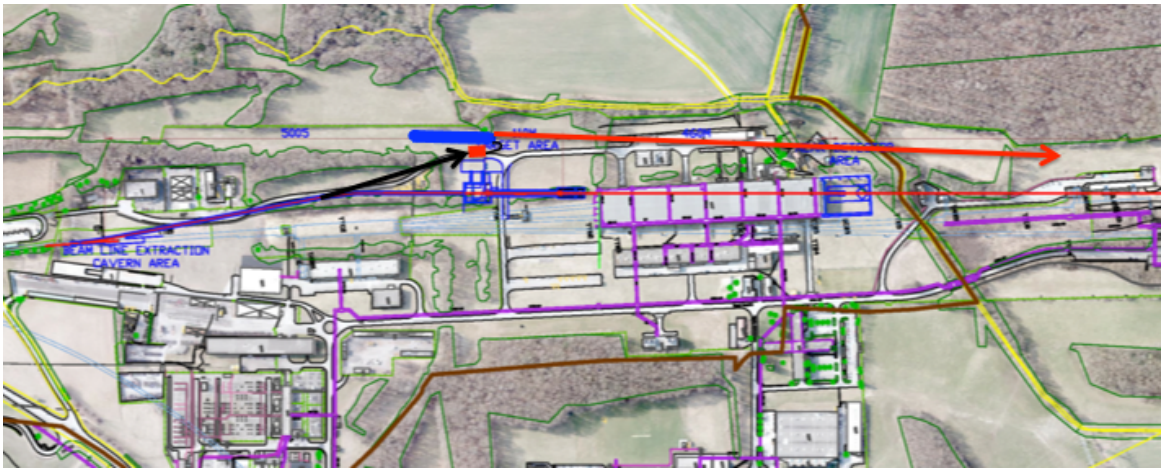

Figure 28: An option using the North Area target station for CENF (preferably prepared in advance for νSTORM) and the far detector hall.

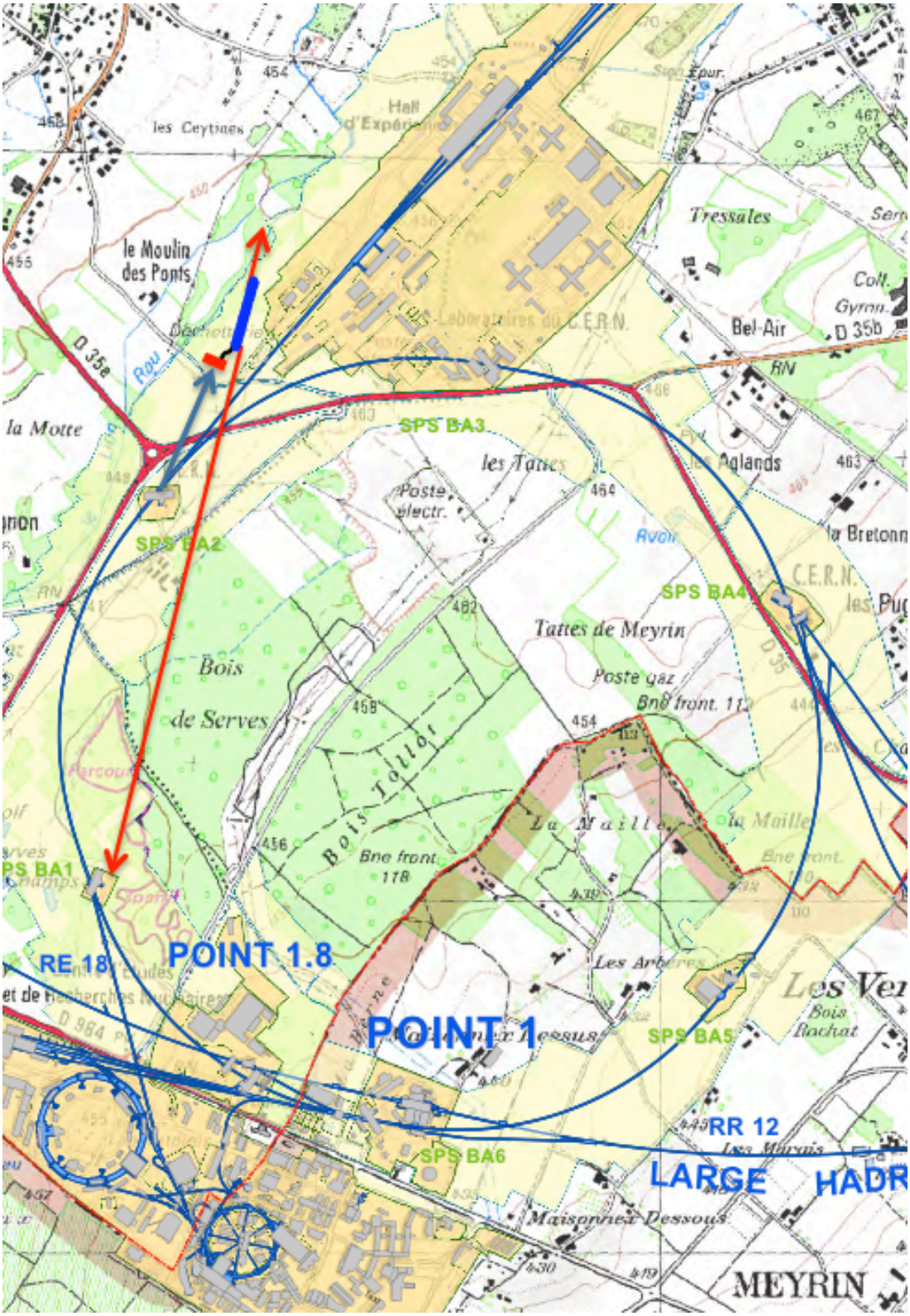

Figure 29: Extraction of the proton beam at the SPS level with a detector hall in one of the SPS caverns. The pion extraction is also shown.

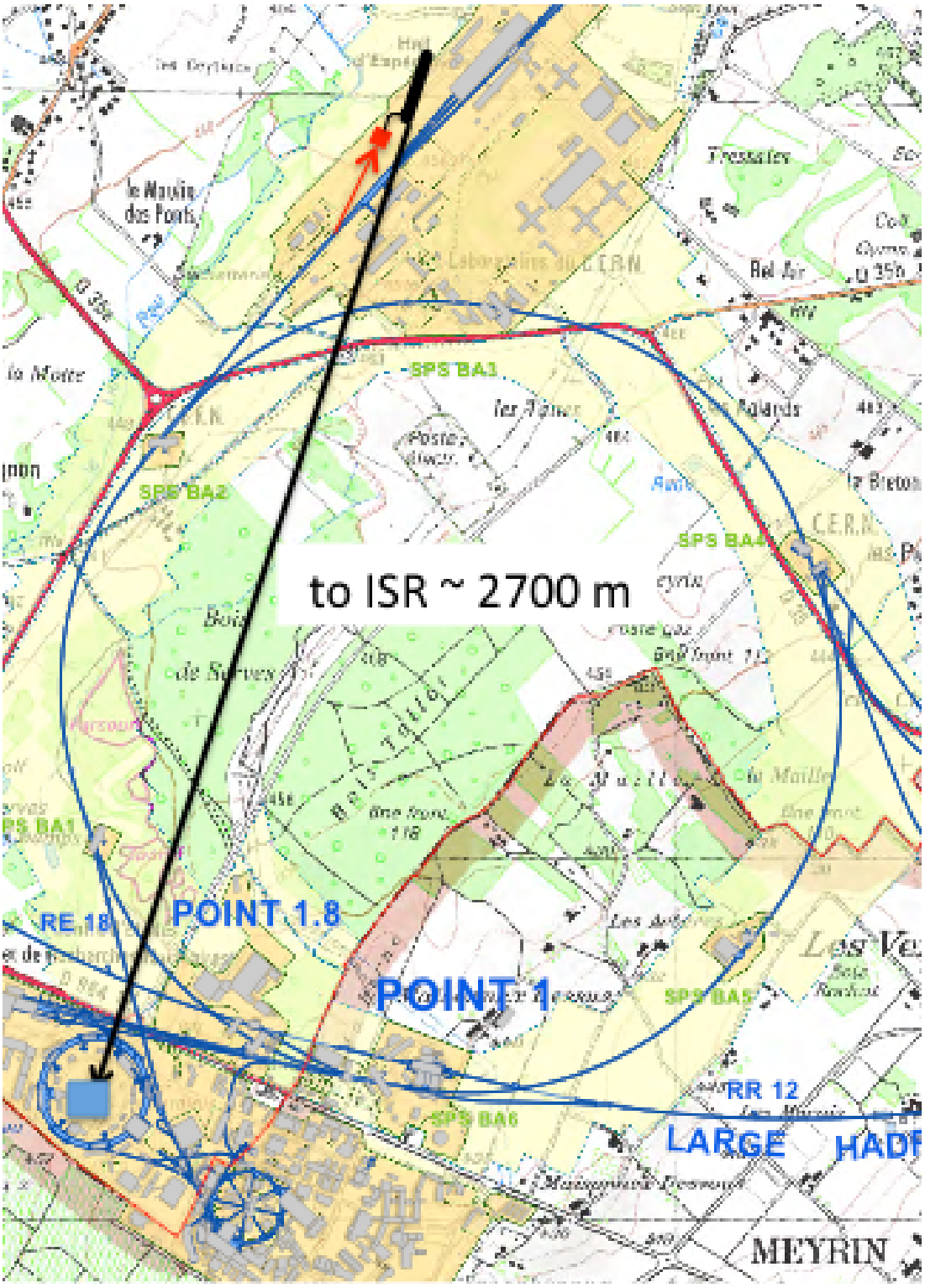

Figure 30: This layout, with a far detector at the Meyrin site, aims to use part of the proton beam line, a new target station and new detector caverns.

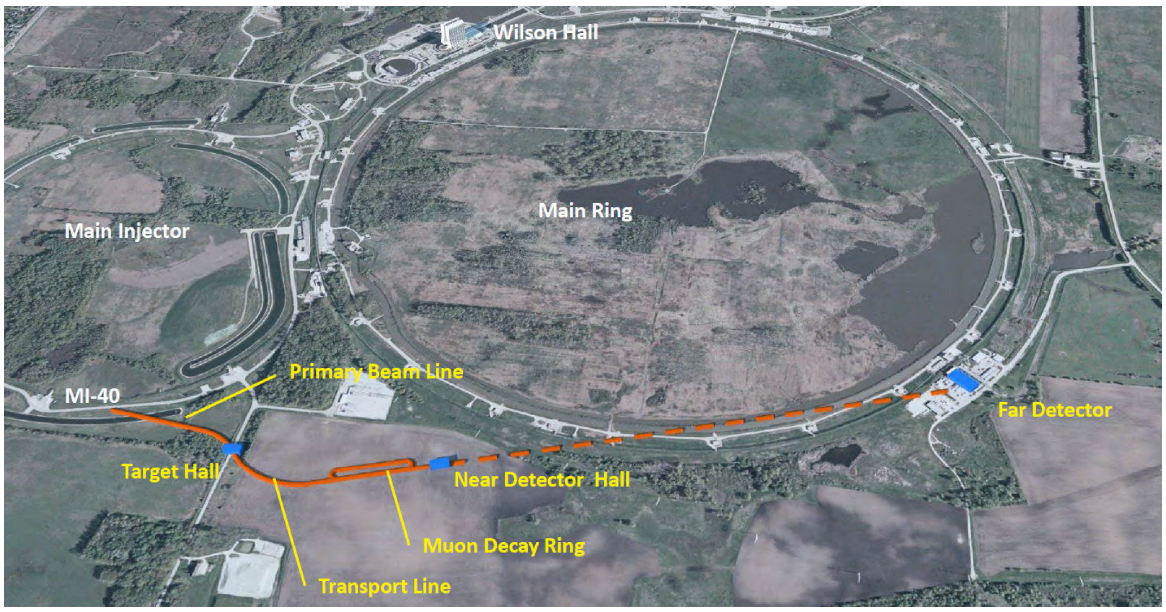

Figure 31: Schematic of the νSTORM facility on the FNAL site.

4.2 Implementing νSTORM at FNAL

The concept for siting νSTORM at Fermilab follows ideas that were developed nearly two decades ago for a short baseline $\nu_\mu \rightarrow \nu_\tau$ oscillation experiment [213, 214] that was to use protons extracted from the Fermilab Main Injector using the proton abort line of that machine. Although this experiment was never carried out, the Main Injector abort-beam absorber was assembled with the by-pass beam pipe that would have been needed for this experiment. νSTORM will use this by-pass. The basic siting concept for νSTORM at Fermilab is shown in figure 31.

Protons from the Fermilab Main Injector will be brought to a new target station located near the southern edge of the Fermilab site. The beam line will be designed for 120 GeV protons, but the beam line will be able to accommodate protons from 60 GeV to 120 GeV. Although the pion yield per proton on target increases linearly in the 60 GeV to 120 GeV range, the run conditions for νSTORM will have to take into consideration the other experiments running at the time. A detail of the currently favoured siting option for beam line, target hall, transport line and decay ring is shown in figure 32.

For νSTORM at Fermilab, the baseline is 100 kW on target which represents approximately 1/7 of the 700 kW proton power available after completion of the Fermilab Proton Improvement Plan [215]. Current simulations for νSTORM at Fermilab have assumed a tantalum target and a NuMI-like horn operating at 300 kA. A schematic of the current target station concept is given in figure 33. The pion capture and transport line starts 30 cm downstream of the horn and transports pions to the decay ring. It is tuned to collect pions in the momentum acceptance of 5 ± 0.5 GeV/c. Pions are injected into the ring on an orbit separated from the circulating muons, a process known as "stochastic injection".

The current design for the injection section is shown in figure 11. The decay ring is approximately 350 m in circumference and uses compact arcs. The ratio of the length of a single straight to the ring circumference is 0.43.

There will be a near detector hall located approximately 50 m from the end of the straight (as shown in figure 31) and νSTORM will use the existing D0 assembly building (DAB) as the far (1.5 km) detector hall. The pit area of DAB can accommodate a SuperBMIND of 1 kT to 1.5 kT plus a LAr detector with a mass in the range of 500 T to 1000 T.

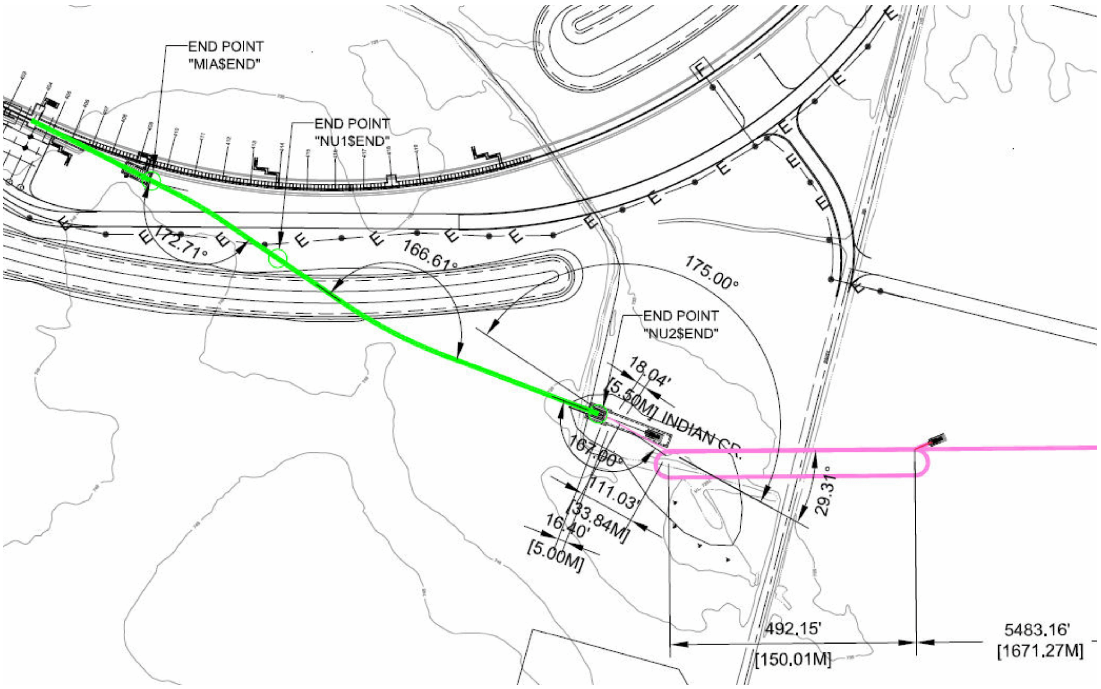

Figure 32: Site detail of extraction of the beam from the FNAL Main injector, the target hall and the decay ring.

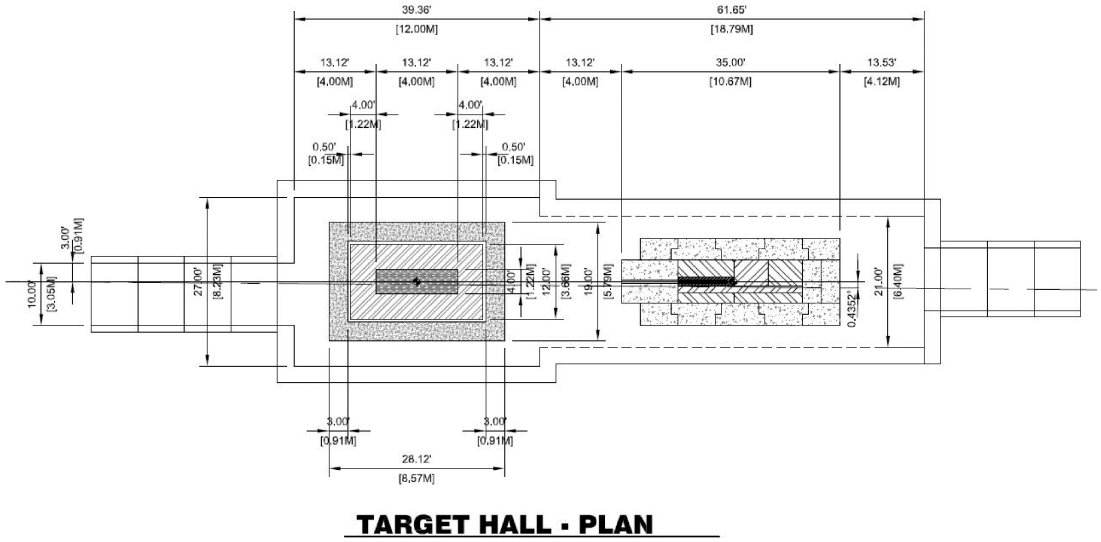

TARGET HALL - PLAN

Figure 33: Schematic of the target hall.

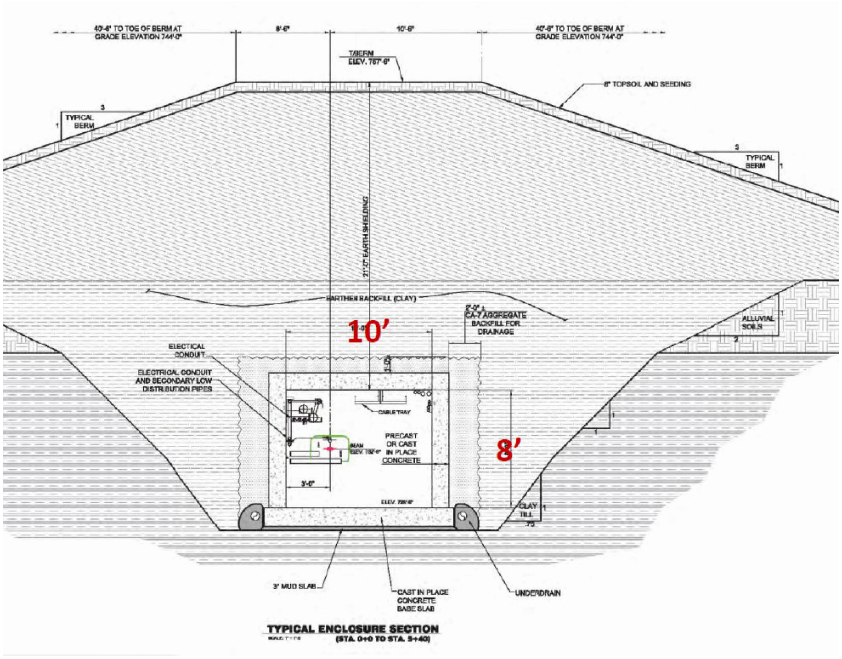

Figure 34: Schematic of tunnelling.

It is expected that all civil construction at the Fermilab site will be at the Main Injector depth of 21 ft below grade, although some additional over burden may be required for the target hall. An engineering concept for the underground tunnelling is shown in figure 34. The site location described above is ideal for νSTORM. The services (water and power) are nearby, but the area is essentially open and undeveloped so that νSTORM construction will not interfere (or have to accommodate) existing infrastructure. In addition, being able to use the D0 Assembly Building as the far detector hall represents a significant cost saving.

5 Proposed programme

5.1 Timeline

Formal consideration of νSTORM began when the collaboration submitted a Letter of Intent (LOI) to the Fermilab Physics Advisory Committee (PAC) in June 2012 [2]. The collaboration has been encouraged to submit a proposal in May 2013 [216]. Proton beams capable of serving the νSTORM facility can be provided at CERN and at FNAL. With the encouragement of the CERN management, we have made an initial investigation of the feasibility of implementing νSTORM at CERN (see section 4). In view of the fact that no siting decision has yet been taken, the purpose of this Expression of Interest (EoI) is to request the resources required to:

- Investigate in detail how νSTORM could be implemented at CERN; and
- Develop options for decisive European contributions to the νSTORM facility and experimental programme wherever the facility is sited.

The timeline presented in figure 4 identifies the principal steps along the way to the preparation of the full Technical Design Report (TDR) that is required before the project can be considered for approval. Should the collaboration's proposal to FNAL be accepted, project approval would be by the DOE "Critical Decision" process. In Europe, the usual CERN approval steps, followed by proposals to national funding agencies, would be required. In either case, the culmination of the next two years of effort will be the TDR (in the US referred to as the Conceptual Design Report) for the facility. With the exception of the site-specific elements noted

Table 4: Indicative timeline for the preparation of the νSTORM Technical Design Report.

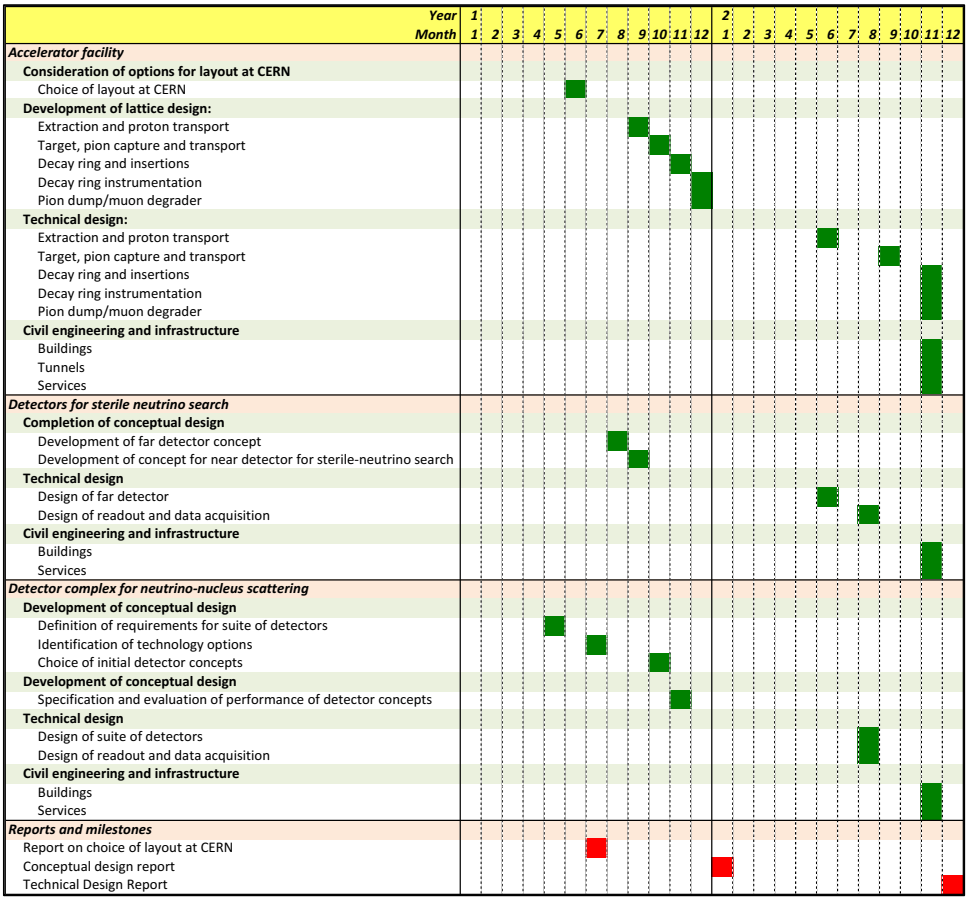

below, the work required to complete the design of the major systems is the same no matter whether νSTORM is implemented at CERN or at FNAL.

5.2 Elements of the Project Breakdown Structure

While the civil construction, the provision of the necessary services and the system integration will necessarily be the responsibility of the host laboratory, the components and systems that make up the accelerator complex, such as magnets or beam instrumentation, and the neutrino detectors could be provided as in-kind contributions by the international collaboration. The list of tasks presented in table 5 forms a rudimentary Project Breakdown Structure (PBS) for the completion of the TDR. Those tasks which must be carried out by the host laboratory, supported by the collaboration, are identified. The design of large sections of the accelerator facility, beam-line instrumentation and neutrino-detector systems are site-independent.

The optimisation and detailed design of the detectors required for the sterile-neutrino search will be the responsibility of the νSTORM collaboration. The facility will be capable of supporting the suite of near detectors necessary to carry out definitive studies of neutrino-nucleus scattering. The PBS therefore identifies the need to develop the specification of the neutrino-scattering programme and the development of designs for the suite of detectors required to carry them out.

Table 5: Elements of the project breakdown structure that must be developed to determine the work required to deliver the Technical Design Report.

Id	*System, subsystem or component*	*Site specific item*
1	nuSTORM	
1.1	The accelerator facility	
1.1.2	*Proton beam*	
1.1.2.1	Extraction	Yes
1.1.2.2	Septum	Yes
1.1.2.3	Transport line	Yes
1.1.2.4	Tunnels, surface buildings and infrastructure	Yes
1.1.3	*Target and pion capture*	
1.1.3.1	Target assembly	No
1.1.3.2	Horn	No
1.1.3.3	Transport channel	Yes
1.1.2.4	Tunnels, surface buildings and infrastructure	Yes
1.1.3	*Decay ring*	
1.1.3.1	Injection and extraction	No
1.1.3.2	Injection straight	No
1.1.3.3	Return straight	No
1.1.3.4	Arcs	No
1.1.3.5	Pion dump/muon degrader	No
1.1.2.4	Tunnels, surface buildings and infrastructure	Yes
1.2	Neutrino detectors for sterile neutrino search	
1.2.1	*Far detector*	
1.2.1.1	Iron/scintillator tracking calorimeter	No
1.2.1.2	Superconducting transmission line	No
1.2.1.3	Readout and data acquisition	No
1.2.1.4	Tunnels, surface buildings and infrastructure	Yes
1.2.2	*Near detector*	
1.2.2.1	Iron/scintillator tracking calorimeter	No
1.2.2.2	Excitation current loop	No
1.2.2.3	Readout and data acquisition	No
1.2.2.4	Tunnels, surface buildings and infrastructure	Yes
1.2.3	*Neutrino detectors for neutrino-nucleus scattering studies*	
1.2.3.1	Detector specification, design and fabrication	
1.2.3.2	Magnet	
1.2.3.3	Readout and data acquisition	No
1.2.3.4	Tunnels, surface buildings and infrastructure	Yes

5.3 Request for support

We request CERN support to participate in the development of the νSTORM facility and experimental programme. In addition, we request CERN support for those tasks where CERN's particular expertise may be brought to bear to make decisive contributions to the detailed design of the νSTORM facility. A number pf work-packages containing evaluations and technical studies have been defined and are outlined below. In each case, the evaluation of the necessary manpower needed to execute the work is an essential early part of the work. Over the period between April 2013 and June 2013, we request CERN support to carry out the necessary evaluation so that a more detailed evaluation of the resources required to carry out the proposed programme can be presented to the SPSC at its meeting in June 2013.

- **Proton beam: SPS extraction, beam lines up to target:**
  The νSTORM facility should take advantage of work already invested in the CERN North Area "neutrino hub", this means the technical evaluations and implementations already performed for the CENF and LBNO. Both the 100 GeV and the 400 GeV beams extracted from the SPS are acceptable for νSTORM. νSTORM would need an additional transport line should a new target station be needed;
- **Pion-production target:**
  It is likely that an existing target area will need substantial investment if it is to be re-used, it would be of interest to study a generic, re-usable target station at an early stage in the development of the North Area as a neutrino hub. If this is not possible, νSTORM would need to study a new target station, however, it would be largely similar to the target stations proposed for the CENF and LBNO experiments;
- **Pion transport:**
  Pion transport may be different in the CERN implementation to that already designed done for FNAL

due to site constraints on the the topology of νSTORM at CERN. Significant parts of the work that has already done at FNAL can be re-used;

- **Engineering study of pion-capture magnets:**
  The large aperture magnets will have to be studied in detail, including the effects of radiation. Superconducting magnets in the arcs also need cryogenic evaluation and radiation studies;
- **Contributions to the design of the muon storage ring:**
  The work on a storage ring is ongoing within the νSTORM collaboration;
- **Contributions to design of storage ring diagnostics:**
  Detailed studies of the storage ring are are required to specify the instrumentation that is needed. Studies of the possibility to use the beam structure from SPS for beam instrumentation (how fast is the beam de-grouping) must be carried out. The influence of electron production from the decay has to be studied;
- **Evaluation of a possible muon cooling experiment:**
  A muon cooling experiment could be set up after the straight section that is not used for for neutrino production. A muon cooling ring could be studied;
- **Contributions to the design of the neutrino-scattering programme:**
  The European Strategy for Particle Physics [20] has emphasised the importance of studying the physics of the neutrino. The next generation of long- and short-baseline, conventional neutrino-oscillation experiments rely on the observation of electron-neutrino appearance in a muon-neutrino beam. To allow such experiments to reach their full potential requires that the systematic error related to the neutrino-scattering cross sections and modelling of the hadronic final states be minimised. As described above, νSTORM is unique in that it is capable of delivering the programme that is required. CERN has the opportunity to serve the European neutrino community which seeks to establish a first-class neutrino programme at CERN by contributing to the development of the neutrino-nucleus scattering programme at νSTORM. We request support from PH Division to provide supervision for a CERN Fellow and a research student. The latter would be jointly supervised by one of the institutes within the European collaboration.

References

[1] D. Adey, C. Ankenbrandt, S. Agarwalla, R. Asfandiyarov, J. Back, G. Barker, E. Baussan, R. Bayes, S. Bhadra, C. Booth, V. Blackmore, A. Blondel, S. Bogacz, S. Boyd, A. Bravar, S. Brice, A. Bross, F. Cadoux, H. Cease, A. Cervera, J. Cobb, D. Colling, L. Coney, A. Dobbs, J. Dobson, A. Donini, P. Dornan, M. Dracos, F. Dufour, R. Edgecock, J. Evans, M. George, T. Ghosh, A. deGouvea, J. Gomez-Cadenas, A. Haesler, G. Hanson, P. Harrison, M. Hartz, P. Hernandez, J. Hernando-Morata, P. Hodgson, P. Huber, A. Izmaylov, Y. Karadhzov, J. Kopp, L. Kormos, A. Korzenev, A. Kurup, Y. Kuno, P. Kyberd, J. Lagrange, A. Laing, J. Link, A. Liu, K. Long, N. McCauley, K. McDonald, K. Mahn, C. Martin, J. Martin, O. Mena, S. Mishra, N. Mokhov, J. Morfin, Y. Mori, W. Murray, D. Neuffer, R. Nichol, E. Noah, S. Parke, S. Pascoli, J. Pasternak, M. Popovic, P. Ratoff, M. Ravonel, M. Rayner, S. Ricciardi, C. Rogers, P. Rubinov, E. Santos, A. Sato, E. Scantamburlo, J. Sedgbeer, P. Smith, J. Smith, J. Sobczyk, S. Soldner-Rembold, F. Soler, M. Sorel, P. Stamoulis, S. Striganov, H. Tanaka, I. Taylor, C. Touramanis, C. Tunnel, Y. Uchida, M. Wascko, N. Vassilopoulos, A. Weber, E. Wildner, W. Winter, and U. Yang, "Neutrinos from stored muons (storm): Expression of interest," Tech. Rep. CERN-SPSC-2013-015. SPSC-EOI-009, CERN, Geneva, Apr, 2013.

[2] **nuSTORM Collaboration** Collaboration, P. Kyberd *et al.*, "nuSTORM - Neutrinos from STORed Muons: Letter of Intent to the Fermilab Physics Advisory Committee," arXiv:1206.0294 [hep-ex].

[3] **DAYA-BAY Collaboration** Collaboration, F. An *et al.*, "Observation of electron-antineutrino disappearance at Daya Bay," *Phys.Rev.Lett.* **108** (2012) 171803, arXiv:1203.1669 [hep-ex].

[4] **RENO collaboration** Collaboration, J. Ahn *et al.*, "Observation of Reactor Electron Antineutrino Disappearance in the RENO Experiment," *Phys.Rev.Lett.* **108** (2012) 191802, arXiv:1204.0626 [hep-ex].

[5] **DOUBLE-CHOOZ Collaboration** Collaboration, Y. Abe *et al.*, "Indication for the reactor anti-neutrino disappearance in the Double Chooz experiment," *Phys.Rev.Lett.* **108** (2012) 131801, arXiv:1112.6353 [hep-ex].

[6] **T2K Collaboration** Collaboration, K. Abe *et al.*, "Indication of Electron Neutrino Appearance from an Accelerator-produced Off-axis Muon Neutrino Beam," *Phys.Rev.Lett.* **107** (2011) 041801, arXiv:1106.2822 [hep-ex].

[7] **MINOS Collaboration** Collaboration, P. Adamson *et al.*, "Improved search for muon-neutrino to electron-neutrino oscillations in MINOS," *Phys.Rev.Lett.* **107** (2011) 181802, arXiv:1108.0015 [hep-ex].

[8] **LSND** Collaboration, A. Aguilar *et al.*, "Evidence for neutrino oscillations from the observation of $\bar{\nu}_e$ appearance in a $\bar{\nu}_\mu$ beam," *Phys. Rev. D* **64** (2001) 112007, arXiv:0104049 [hep-ex].

[9] **MiniBooNE** Collaboration, A. A. Aguilar-Arevalo *et al.*, "A search for electron neutrino appearance at the $\Delta m^2 \sim 1$ eV^2 scale," *Phys. Rev. Lett.* **98** (2007) 231801, arXiv:0704.1500 [hep-ex].

[10] **MiniBooNE Collaboration** Collaboration, A. Aguilar-Arevalo *et al.*, "Event Excess in the MiniBooNE Search for $\bar{\nu}_\mu \to \bar{\nu}_e$ Oscillations," *Phys.Rev.Lett.* **105** (2010) 181801, arXiv:1007.1150 [hep-ex].

[11] T. Mueller, D. Lhuillier, M. Fallot, A. Letourneau, S. Cormon, *et al.*, "Improved Predictions of Reactor Antineutrino Spectra," *Phys.Rev.* **C83** (2011) 054615, arXiv:1101.2663 [hep-ex].

[12] P. Huber, "Determination of anti-neutrino spectra from nuclear reactors," *Phys.Rev.* **C84** (2011) 024617, arXiv:1106.0687 [hep-ph].

[13] G. Mention, M. Fechner, T. Lasserre, T. Mueller, D. Lhuillier, *et al.*, "The Reactor Antineutrino Anomaly," *Phys.Rev.* **D83** (2011) 073006, arXiv:1101.2755 [hep-ex].

[14] **GALLEX Collaboration.** Collaboration, P. Anselmann *et al.*, "First results from the Cr-51 neutrino source experiment with the GALLEX detector," *Phys.Lett.* **B342** (1995) 440–450.

[15] **GALLEX Collaboration** Collaboration, W. Hampel *et al.*, "Final results of the Cr-51 neutrino source experiments in GALLEX," *Phys.Lett.* **B420** (1998) 114–126.

[16] J. Abdurashitov, V. Gavrin, S. Girin, V. Gorbachev, T. V. Ibragimova, *et al.*, "The Russian-American gallium experiment (SAGE) Cr neutrino source measurement," *Phys.Rev.Lett.* **77** (1996) 4708–4711.

[17] **SAGE Collaboration** Collaboration, J. Abdurashitov *et al.*, "Measurement of the response of the Russian-American gallium experiment to neutrinos from a Cr-51 source," *Phys.Rev.* **C59** (1999) 2246–2263, arXiv:hep-ph/9803418 [hep-ph].

[18] **SAGE Collaboration** Collaboration, J. Abdurashitov, V. Gavrin, S. Girin, V. Gorbachev, P. Gurkina, *et al.*, "Measurement of the response of a Ga solar neutrino experiment to neutrinos from an Ar-37 source," *Phys.Rev.* **C73** (2006) 045805, arXiv:nucl-ex/0512041 [nucl-ex].

[19] K. Abazajian, M. Acero, S. Agarwalla, A. Aguilar-Arevalo, C. Albright, *et al.*, "Light Sterile Neutrinos: A White Paper," arXiv:1204.5379 [hep-ph].

[20] **The European Strategy Group** Collaboration, T. Nakada *et al.*, "Proposed Update of the European Strategy for Particle Physics."
Https://indico.cern.ch/getfile.py/access?resid=0&materialid=0&confid=217656, 2013.

[21] CERN Neutrinos study group, ICARUS-NESSiE Collaborations, LAGUNA-LBNO Consortium , " Letter of Intent for the new CERN Neutrino Facility (CENF) ," 2013.
https://edms.cern.ch/nav/P:CERN-0000096725:V0/P:CERN-0000096728:V0/TAB3 .

[22] **ISS Physics Working Group** Collaboration, A. Bandyopadhyay *et al.*, "Physics at a future Neutrino Factory and super-beam facility," *Rept. Prog. Phys.* **72** (2009) 106201, arXiv:0710.4947 [hep-ph].

[23] **IDS-NF Collaboration** Collaboration, S. Choubey *et al.*, "International Design Study for the Neutrino Factory, Interim Design Report," arXiv:1112.2853 [hep-ex].

[24] J. C. Gallardo *et al.*, "Muon Collider: Feasibility Study," 1996.
http://www.cap.bnl.gov/mumu/pubs/snowmass96/part6.pdf. Prepared for 1996 DPF / DPB Summer Study on New Directions for High Energy Physics (Snowmass 96), Snowmass, Colorado, 25 Jun - 12 Jul 1996.

[25] S. D. Holmes and V. D. Shiltsev, "Muon Collider," arXiv:1202.3803 [physics.acc-ph].

[26] **MAP Collaboration** Collaboration, D. M. Kaplan, "A Staged Muon-Based Neutrino and Collider Physics Program," arXiv:1212.4214 [physics.acc-ph].

[27] B. Pontecorvo, "Mesonium and antimesonium," *Sov. Phys. JETP* **6** (1957) 429.

[28] B. Pontecorvo, "Inverse beta processes and nonconservation of lepton charge," *Sov. Phys. JETP* **7** (1958) 172–173.

[29] Z. Maki, M. Nakagawa, and S. Sakata, "Remarks on the unified model of elementary particles," *Prog. Theor. Phys.* **28** (1962) 870–880.

[30] S. M. Bilenky, S. Pascoli, and S. T. Petcov, "Majorana neutrinos, neutrino mass spectrum, CP-violation and neutrinoless double beta-decay. I: The three-neutrino mixing case," *Phys. Rev. D* **64** (2001) 053010, arXiv:0102265 [hep-ph].

[31] C. Amsler *et al.*, "Review of particle physics," *Physics Letters B* **667** no. 1-5, (2008) 1–6. http://pdg.lbl.gov. and 2009 partial update for 2010 edition.

[32] P. Huber, M. Mezzetto, and T. Schwetz, "On the impact of systematical uncertainties for the CP violation measurement in superbeam experiments," *JHEP* **03** (2008) 021, arXiv:0711.2950 [hep-ph].

[33] P. Coloma, P. Huber, J. Kopp, and W. Winter, "Systematic uncertainties in long-baseline neutrino oscillations for large θ_{13}," arXiv:1209.5973 [hep-ph].

[34] W. Winter, "Optimization of a Very Low Energy Neutrino Factory for the Disappearance Into Sterile Neutrinos," *Phys.Rev.* **D85** (2012) 113005, arXiv:1204.2671 [hep-ph].

[35] Harvard University, "Cambridge Electron Accelerator (Cambridge, Mass.) Records of the Cambridge Electron Accelerator : an inventory," 2006. Records of the Cambridge Electron Accelerator, 1952-1974; http://oasis.lib.harvard.edu/oasis/deliver/ hua11001 .

[36] M. Antonello, D. Bagliani, B. Baibussinov, H. Bilokon, F. Boffelli, *et al.*, "Search for 'anomalies' from neutrino and anti-neutrino oscillations at $\Delta^2_m \sim 1\mathrm{eV}^2$ with muon spectrometers and large LAr-TPC imaging detectors," arXiv:1203.3432 [physics.ins-det].

[37] A. Antonello, D. Bagliani, B. Baibussinov, H. Bilokon, F. Boffelli, *et al.*, "Search for anomalies in the neutrino sector with muon spectrometers and large LArTPC imaging detectors at CERN," arXiv:1208.0862 [physics.ins-det].

[38] L. Arnaudon *et al.*, "Linac4 technical design report," Tech. Rep. CERN-AB-2006-084 ABP/RF and CARE-Note-2006-022-HIPPI, CERN, Geneva, Switzerland, December, 2006.

[39] M. Benedikt, A. Bechtold, F. Borgnolutti, E. Bouquerel, L. Bozyk, *et al.*, "Conceptual design report for a Beta-Beam facility," *Eur.Phys.J.* **A47** (2011) 24.

[40] R. Edgecock *et al.*, "Input to the European Strategy for Particle Physics from the EUROnu FP7 Design Study of a High Intensity Neutrino Oscillation Facility in Europe," 2012. EUROnu input to the update of the European Strategy for Particle Physics, https://indico.cern.ch/contributionDisplay.py?contribId=35&confId=175067.

[41] **MINOS** Collaboration, E. Ables *et al.*, "P-875: A long baseline neutrino oscillation experiment at fermilab,". FERMILAB-PROPOSAL-P-875.

[42] **T2K Collaboration** Collaboration, K. Abe *et al.*, "The T2K Experiment," *Nucl.Instrum.Meth.* **A659** (2011) 106–135, arXiv:1106.1238 [physics.ins-det].

[43] **NOvA Collaboration** Collaboration, D. Ayres *et al.*, "NOvA: Proposal to build a 30 kiloton off-axis detector to study nu(mu) –¿ nu(e) oscillations in the NuMI beamline," arXiv:hep-ex/0503053 [hep-ex].

[44] "EUROnu: A High Intensity Neutrino Oscillation Facility in Europe." http://www.euronu.org/.

[45] **EUROnu Super Beam Collaboration** Collaboration, E. Baussan *et al.*, "The SPL-based Neutrino Super Beam," arXiv:1212.0732 [physics.acc-ph].

[46] " LAGUNA - Large Apparatus studying Grand Unification and Neutrino Astrophysics." http://www.laguna-science.eu.

[47] A. Rubbia *et al.*, "Expression of Interest for a very long baseline neutrino oscillation experiment (LBNO)." Https://cdsweb.cern.ch/record/1457543/files/spsc-eoi-007.pd, 2012.

[48] K. Abe, T. Abe, H. Aihara, Y. Fukuda, Y. Hayato, *et al.*, "Letter of Intent: The Hyper-Kamiokande Experiment — Detector Design and Physics Potential —," arXiv:1109.3262 [hep-ex].

[49] **LBNE Collaboration** Collaboration, T. Akiri *et al.*, "The 2010 Interim Report of the Long-Baseline Neutrino Experiment Collaboration Physics Working Groups," arXiv:1110.6249 [hep-ex].

[50] **Particle Data Group** Collaboration, J. Beringer *et al.*, "Review of Particle Physics (RPP)," *Phys.Rev.* **D86** (2012) 010001.

[51] C. Llewellyn Smith, "Neutrino Reactions at Accelerator Energies," *Phys.Rept.* **3** (1972) 261–379.

[52] R. Smith and E. Moniz, "NEUTRINO REACTIONS ON NUCLEAR TARGETS," *Nucl.Phys.* **B43** (1972) 605.

[53] D. Rein and L. M. Sehgal, "Neutrino Excitation of Baryon Resonances and Single Pion Production," *Annals Phys.* **133** (1981) 79–153.

[54] **K2K Collaboration** Collaboration, R. Gran *et al.*, "Measurement of the quasi-elastic axial vector mass in neutrino-oxygen interactions," *Phys.Rev.* **D74** (2006) 052002, arXiv:hep-ex/0603034 [hep-ex].

[55] **K2K Collaboration** Collaboration, A. Rodriguez *et al.*, "Measurement of single charged pion production in the charged-current interactions of neutrinos in a 1.3-GeV wide band beam," *Phys.Rev.* **D78** (2008) 032003, arXiv:0805.0186 [hep-ex].

[56] **K2K Collaboration** Collaboration, C. Mariani, "Charged current neutral pion cross section measurement at K2K," *AIP Conf.Proc.* **1189** (2009) 339–342.

[57] **K2K Collaboration** Collaboration, S. Nakayama *et al.*, "Measurement of single pi0 production in neutral current neutrino interactions with water by a 1.3-GeV wide band muon neutrino beam," *Phys.Lett.* **B619** (2005) 255–262, arXiv:hep-ex/0408134 [hep-ex].

[58] **MiniBooNE Collaboration** Collaboration, A. Aguilar-Arevalo *et al.*, "Measurement of muon neutrino quasi-elastic scattering on carbon," *Phys.Rev.Lett.* **100** (2008) 032301, arXiv:0706.0926 [hep-ex].

[59] **MiniBooNE Collaboration** Collaboration, A. Aguilar-Arevalo *et al.*, "First Measurement of the Muon Neutrino Charged Current Quasielastic Double Differential Cross Section," *Phys.Rev.* **D81** (2010) 092005, arXiv:1002.2680 [hep-ex].

[60] **MiniBooNE Collaboration** Collaboration, A. Aguilar-Arevalo *et al.*, "Measurement of the ν_μ charged current π^+ to quasi-elastic cross section ratio on mineral oil in a 0.8-GeV neutrino beam," *Phys.Rev.Lett.* **103** (2009) 081801, arXiv:0904.3159 [hep-ex].

[61] **MiniBooNE Collaboration** Collaboration, A. Aguilar-Arevalo *et al.*, "Measurement of Neutrino-Induced Charged-Current Charged Pion Production Cross Sections on Mineral Oil at $E_\nu \sim 1$ GeV," *Phys.Rev.* **D83** (2011) 052007, arXiv:1011.3572 [hep-ex].

[62] **MiniBooNE Collaboration** Collaboration, A. Aguilar-Arevalo *et al.*, "Measurement of ν_μ-induced charged-current neutral pion production cross sections on mineral oil at $E_\nu \in 0.5 - 2.0$ GeV," *Phys.Rev.* **D83** (2011) 052009, arXiv:1010.3264 [hep-ex].

[63] **MiniBooNE Collaboration** Collaboration, A. A. Aguilar-Arevalo *et al.*, "Measurement of nu(mu) and anti-nu(mu) induced neutral current single pi0 production cross sections on mineral oil at E(nu) O(1-GeV)," *Phys.Rev.* **D81** (2010) 013005, arXiv:0911.2063 [hep-ex].

[64] **MiniBooNE Collaboration** Collaboration, A. Aguilar-Arevalo *et al.*, "Measurement of the Neutrino Neutral-Current Elastic Differential Cross Section on Mineral Oil at $E_\nu \sim 1$ GeV," *Phys.Rev.* **D82** (2010) 092005, arXiv:1007.4730 [hep-ex].

[65] **SciBooNE Collaboration** Collaboration, J. L. Alcaraz-Aunion and J. Walding, "Measurement of the nu(mu)-CCQE cross-section in the SciBooNE experiment," *AIP Conf.Proc.* **1189** (2009) 145–150, arXiv:0909.5647 [hep-ex].

[66] **SciBooNE Collaboration** Collaboration, Y. Nakajima *et al.*, "Measurement of inclusive charged current interactions on carbon in a few-GeV neutrino beam," *Phys.Rev.* **D83** (2011) 012005, arXiv:1011.2131 [hep-ex].

[67] **SciBooNE Collaboration** Collaboration, Y. Kurimoto *et al.*, "Measurement of Inclusive Neutral Current Neutral pi0 Production on Carbon in a Few-GeV Neutrino Beam," *Phys.Rev.* **D81** (2010) 033004, arXiv:0910.5768 [hep-ex].

[68] **SciBooNE Collaboration** Collaboration, Y. Kurimoto *et al.*, "Improved measurement of neutral current coherent π^0 production on carbon in a few-GeV neutrino beam," *Phys.Rev.* **D81** (2010) 111102, arXiv:1005.0059 [hep-ex].

[69] H. Gallagher, G. Garvey, and G. Zeller, "Neutrino-nucleus interactions," *Ann.Rev.Nucl.Part.Sci.* **61** (2011) 355–378.

[70] J. G. Morfin, J. Nieves, and J. T. Sobczyk, "Recent Developments in Neutrino/Antineutrino - Nucleus Interactions," arXiv:1209.6586 [hep-ex].

[71] R. Bradford, A. Bodek, H. S. Budd, and J. Arrington, "A New parameterization of the nucleon elastic form-factors," *Nucl.Phys.Proc.Suppl.* **159** (2006) 127–132, arXiv:hep-ex/0602017 [hep-ex].

[72] H. S. Budd, A. Bodek, and J. Arrington, "Vector and axial form-factors applied to neutrino quasielastic scattering," *Nucl.Phys.Proc.Suppl.* **139** (2005) 90–95, arXiv:hep-ex/0410055 [hep-ex].

[73] A. Bodek, H. S. Budd, and J. Arrington, "Modeling neutrino quasielastic cross-sections on nucleons and nuclei," *AIP Conf.Proc.* **698** (2004) 148–152, arXiv:hep-ex/0309024 [hep-ex].

[74] H. S. Budd, A. Bodek, and J. Arrington, "Modeling quasielastic form-factors for electron and neutrino scattering," arXiv:hep-ex/0308005 [hep-ex].

[75] A. M. Ankowski, "Breakdown of the impulse approximation and its consequences: The Low-Q**2 problem," *PoS* **NUFACT08** (2008) 118, arXiv:0810.1167 [nucl-th].

[76] O. Benhar, N. Farina, H. Nakamura, M. Sakuda, and R. Seki, "Lepton-nucleus scattering in the impulse approximation regime," *Nucl.Phys.Proc.Suppl.* **155** (2006) 254–256, arXiv:hep-ph/0510259 [hep-ph].

[77] M. Martini, M. Ericson, G. Chanfray, and J. Marteau, "A Unified approach for nucleon knock-out, coherent and incoherent pion production in neutrino interactions with nuclei," *Phys.Rev.* **C80** (2009) 065501, arXiv:0910.2622 [nucl-th].

[78] J. Nieves, I. Ruiz Simo, and M. Vicente Vacas, "Inclusive Charged–Current Neutrino–Nucleus Reactions," *Phys.Rev.* **C83** (2011) 045501, arXiv:1102.2777 [hep-ph].

[79] A. Bodek, S. Avvakumov, R. Bradford, and H. S. Budd, "Vector and Axial Nucleon Form Factors:A Duality Constrained Parameterization," *Eur.Phys.J.* **C53** (2008) 349–354, arXiv:0708.1946 [hep-ex].

[80] V. Bernard, L. Elouadrhiri, and U.-G. Meissner, "Axial structure of the nucleon," *Journal of Physics G: Nuclear and Particle Physics* **28** no. 1, (2002) R1. http://stacks.iop.org/0954-3899/28/i=1/a=201.

[81] J. Nieves, I. Ruiz Simo, and M. Vicente Vacas, "The nucleon axial mass and the MiniBooNE Quasielastic Neutrino-Nucleus Scattering problem," *Phys.Lett.* **B707** (2012) 72–75, arXiv:1106.5374 [hep-ph].

[82] M. Martini, M. Ericson, and G. Chanfray, "Neutrino quasielastic interaction and nuclear dynamics," *Phys.Rev.* **C84** (2011) 055502, arXiv:1110.0221 [nucl-th].

[83] A. Meucci and C. Giusti, "Relativistic descriptions of final-state interactions in charged-current quasielastic antineutrino-nucleus scattering at MiniBooNE kinematics," *Phys.Rev.* **D85** (2012) 093002, arXiv:1202.4312 [nucl-th].

[84] J. Amaro, M. Barbaro, J. Caballero, T. Donnelly, and J. Udias, "Relativistic analyses of quasielastic neutrino cross sections at MiniBooNE kinematics," *Phys.Rev.* **D84** (2011) 033004, arXiv:1104.5446 [nucl-th].

[85] A. Bodek, H. Budd, and M. Christy, "Neutrino Quasielastic Scattering on Nuclear Targets: Parametrizing Transverse Enhancement (Meson Exchange Currents)," *Eur.Phys.J.* **C71** (2011) 1726, arXiv:1106.0340 [hep-ph].

[86] J. T. Sobczyk, "Transverse Enhancement Model and MiniBooNE Charge Current Quasi-Elastic Neutrino Scattering Data," *Eur.Phys.J.* **C72** (2012) 1850, arXiv:1109.1081 [hep-ex].

[87] J. Nieves, F. Sanchez, I. Ruiz Simo, and M. Vicente Vacas, "Neutrino Energy Reconstruction and the Shape of the CCQE-like Total Cross Section," *Phys.Rev.* **D85** (2012) 113008, arXiv:1204.5404 [hep-ph].

[88] O. Lalakulich and U. Mosel, "Energy reconstruction in quasielastic scattering in the MiniBooNE and T2K experiments," *Phys.Rev.* **C86** (2012) 054606, arXiv:1208.3678 [nucl-th].

[89] O. Lalakulich, K. Gallmeister, and U. Mosel, "Neutrino- and antineutrino-induced reactions with nuclei between 1 and 50 GeV," *Phys.Rev.* **C86** (2012) 014607, arXiv:1205.1061 [nucl-th].

[90] M. Martini, M. Ericson, and G. Chanfray, "Neutrino energy reconstruction problems and neutrino oscillations," *Phys.Rev.* **D85** (2012) 093012, arXiv:1202.4745 [hep-ph].

[91] J. T. Sobczyk, "Multinucleon Ejection Model for Two Body Current Neutrino Interactions,".

[92] K. Partyka, "Exclusive CCQE topologies in ArgoNeuT," 2012. Talk at NuInt12, Rio de Janeiro (2012) .

[93] J. A. Formaggio and G. P. Zeller, "From ev to eev: Neutrino cross sections across energy scales," *Rev. Mod. Phys.* **84** (Sep, 2012) 1307–1341. http://link.aps.org/doi/10.1103/RevModPhys.84.1307.

[94] **Gargamelle Neutrino Propane Collaboration, Aachen-Brussels-CERN-Ecole Poly-Orsay-Padua Collaboration** Collaboration, W. Krenz *et al.*, "Experimental Study of Exclusive One Pion Production in All Neutrino Induced Neutral Current Channels," *Nucl.Phys.* **B135** (1978) 45–65.

[95] O. Lalakulich, K. Gallmeister, T. Leitner, and U. Mosel, "Pion production in the MiniBooNE," *AIP Conf.Proc.* **1405** (2011) 127–133, arXiv:1107.5947 [nucl-th].

[96] **K2K Collaboration** Collaboration, C. Mariani *et al.*, "Measurement of inclusive π^0 production in the Charged-Current Interactions of Neutrinos in a 1.3-GeV wide band beam," *Phys.Rev.* **D83** (2011) 054023, arXiv:1012.1794 [hep-ex].

[97] **K2K Collaboration** Collaboration, H. Tanaka, "K2K coherent pion production in SciBar," *Nucl.Phys.Proc.Suppl.* **159** (2006) 38–43.

[98] **NOMAD Collaboration** Collaboration, C. Kullenberg *et al.*, "A Measurement of Coherent Neutral Pion Production in Neutrino Neutral Current Interactions in NOMAD," *Phys.Lett.* **B682** (2009) 177–184, arXiv:0910.0062 [hep-ex].

[99] D. Rein and L. Sehgal, "COHERENT PRODUCTION OF PHOTONS BY NEUTRINOS," *Phys.Lett.* **B104** (1981) 394–398.

[100] **MiniBooNE Collaboration** Collaboration, A. Aguilar-Arevalo *et al.*, "First Observation of Coherent π^0 Production in Neutrino Nucleus Interactions with $E_\nu < 2$ GeV," *Phys.Lett.* **B664** (2008) 41–46, arXiv:0803.3423 [hep-ex].

[101] **K2K Collaboration** Collaboration, M. Hasegawa *et al.*, "Search for coherent charged pion production in neutrino-carbon interactions," *Phys.Rev.Lett.* **95** (2005) 252301, arXiv:hep-ex/0506008 [hep-ex].

[102] **SciBooNE Collaboration** Collaboration, K. Hiraide, "Search for neutrino charged current coherent pion production in SciBooNE," *Nuovo Cim.* **C32N5-6** (2009) 75–82.

[103] J. Amaro, E. Hernandez, J. Nieves, and M. Valverde, "Theoretical study of neutrino-induced coherent pion production off nuclei at T2K and MiniBooNE energies," *Phys.Rev.* **D79** (2009) 013002, arXiv:0811.1421 [hep-ph].

[104] S. Nakamura, T. Sato, T.-S. Lee, B. Szczerbinska, and K. Kubodera, "Dynamical Model of Coherent Pion Production in Neutrino-Nucleus Scattering," *Phys.Rev.* **C81** (2010) 035502, arXiv:0910.1057 [nucl-th].

[105] M. Day and K. S. McFarland, "Differences in Quasi-Elastic Cross-Sections of Muon and Electron Neutrinos," *Phys.Rev.* **D86** (2012) 053003, arXiv:1206.6745 [hep-ph].

[106] A. De Rujula, R. Petronzio, and A. Savoy-Navarro, "Radiative Corrections to High-Energy Neutrino Scattering," *Nucl.Phys.* **B154** (1979) 394.

[107] O. Benhar, A. Fabrocini, S. Fantoni, and I. Sick, "Spectral function of finite nuclei and scattering of GeV electrons," *Nucl.Phys.* **A579** (1994) 493–517.

[108] A. Bodek and J. Ritchie, "Fermi Motion Effects in Deep Inelastic Lepton Scattering from Nuclear Targets," *Phys.Rev.* **D23** (1981) 1070.

[109] M. Martini. Private communication via G. Zeller.

[110] M. Bando and K. Yoshioka, "Sterile neutrinos in a grand unified model," *Prog.Theor.Phys.* **100** (1998) 1239–1250, arXiv:hep-ph/9806400 [hep-ph].

[111] E. Ma, "Neutrino masses in an extended gauge model with E(6) particle content," *Phys.Lett.* **B380** (1996) 286–290, arXiv:hep-ph/9507348 [hep-ph].

[112] Q. Shafi and Z. Tavartkiladze, "Neutrino mixings and fermion masses in supersymmetric SU(5)," *Phys.Lett.* **B451** (1999) 129–135, arXiv:hep-ph/9901243 [hep-ph].

[113] K. Babu and G. Seidl, "Chiral gauge models for light sterile neutrinos," *Phys.Rev.* **D70** (2004) 113014, arXiv:hep-ph/0405197 [hep-ph].

[114] A. Kusenko, F. Takahashi, and T. T. Yanagida, "Dark Matter from Split Seesaw," *Phys.Lett.* **B693** (2010) 144–148, arXiv:1006.1731 [hep-ph].

[115] R. Mohapatra, "Connecting bimaximal neutrino mixing to a light sterile neutrino," *Phys.Rev.* **D64** (2001) 091301, arXiv:hep-ph/0107264 [hep-ph].

[116] C. D. Froggatt and H. B. Nielsen, "Hierarchy of quark masses, cabibbo angles and cp violation," *Nucl. Phys.* **B147** (1979) 277.

[117] J. Barry, W. Rodejohann, and H. Zhang, "Sterile Neutrinos for Warm Dark Matter and the Reactor Anomaly in Flavor Symmetry Models," *JCAP* **1201** (2012) 052, arXiv:1110.6382 [hep-ph].

[118] R. Mohapatra, S. Nasri, and H.-B. Yu, "Seesaw right handed neutrino as the sterile neutrino for LSND," *Phys.Rev.* **D72** (2005) 033007, arXiv:hep-ph/0505021 [hep-ph].

[119] C. S. Fong, R. N. Mohapatra, and I. Sung, "Majorana Neutrinos from Inverse Seesaw in Warped Extra Dimension," *Phys.Lett.* **B704** (2011) 171–178, arXiv:1107.4086 [hep-ph].

[120] H. Zhang, "Light Sterile Neutrino in the Minimal Extended Seesaw," *Phys.Lett.* **B714** (2012) 262–266, arXiv:1110.6838 [hep-ph].

[121] Z. G. Berezhiani and R. N. Mohapatra, "Reconciling present neutrino puzzles: Sterile neutrinos as mirror neutrinos," *Phys. Rev.* **D52** (1995) 6607–6611, hep-ph/9505385.

[122] R. Foot and R. R. Volkas, "Neutrino physics and the mirror world: How exact parity symmetry explains the solar neutrino deficit, the atmospheric neutrino anomaly and the lsnd experiment," *Phys. Rev.* **D52** (1995) 6595–6606, hep-ph/9505359.

[123] V. Berezinsky, M. Narayan, and F. Vissani, "Mirror model for sterile neutrinos," *Nucl.Phys.* **B658** (2003) 254–280, arXiv:hep-ph/0210204 [hep-ph].

[124] **MiniBooNE Collaboration** Collaboration, A. Aguilar-Arevalo *et al.*, "A Combined $\nu_\mu \to \nu_e$ and $\bar{\nu}_\mu \to \bar{\nu}_e$ Oscillation Analysis of the MiniBooNE Excesses," arXiv:1207.4809 [hep-ex].

[125] **MiniBooNE Collaboration** Collaboration, A. Aguilar-Arevalo *et al.*, "Improved Search for $\bar{\nu}_\mu \to \bar{\nu}_e$ Oscillations in the MiniBooNE Experiment," arXiv:1303.2588 [hep-ex].

[126] K. Schreckenbach, G. Colvin, W. Gelletly, and F. Von Feilitzsch, "DETERMINATION OF THE ANTI-NEUTRINO SPECTRUM FROM U-235 THERMAL NEUTRON FISSION PRODUCTS UP TO 9.5-MEV," *Phys.Lett.* **B160** (1985) 325–330.

[127] M. A. Acero, C. Giunti, and M. Laveder, "Limits on nu(e) and anti-nu(e) disappearance from Gallium and reactor experiments," *Phys.Rev.* **D78** (2008) 073009, arXiv:0711.4222 [hep-ph].

[128] C. Giunti and M. Laveder, "Short-Baseline Electron Neutrino Disappearance, Tritium Beta Decay and Neutrinoless Double-Beta Decay," arXiv:1005.4599 [hep-ph].

[129] C. Giunti and M. Laveder, "Statistical Significance of the Gallium Anomaly," *Phys.Rev.* **C83** (2011) 065504, arXiv:1006.3244 [hep-ph].

[130] **KARMEN** Collaboration, B. Armbruster *et al.*, "Upper limits for neutrino oscillations anti-nu/mu $\to$ anti- nu/e from muon decay at rest," *Phys. Rev.* **D65** (2002) 112001, hep-ex/0203021.

[131] **NOMAD** Collaboration, P. Astier *et al.*, "Final NOMAD results on $\nu_\mu \to \nu_\tau$ and $\nu_e \to \nu_\tau$ oscillations including a new search for ν_τ appearance using hadronic τ decays," *Nucl. Phys. B* **611** (2001) 3–39, arXiv:0106102 [hep-ex].

[132] L. Borodovsky, C. Chi, Y. Ho, N. Kondakis, W.-Y. Lee, *et al.*, "Search for muon-neutrino oscillations $\nu_\mu \to \nu_e$ ($\bar{\nu}_\mu \to \bar{\nu}_e$) in a wide band neutrino beam," *Phys.Rev.Lett.* **68** (1992) 274–277.

[133] M. Antonello, B. Baibussinov, P. Benetti, E. Calligarich, N. Canci, *et al.*, "Experimental search for the LSND anomaly with the ICARUS LAr TPC detector in the CNGS beam," arXiv:1209.0122 [hep-ex].

[134] **Super-Kamiokande** Collaboration, Y. Ashie *et al.*, "A measurement of atmospheric neutrino oscillation parameters by super-kamiokande i," *Phys. Rev.* **D71** (2005) 112005, hep-ex/0501064.

[135] B. T. Cleveland *et al.*, "Measurement of the solar electron neutrino flux with the Homestake chlorine detector," *Astrophys. J.* **496** (1998) 505–526.

[136] F. Kaether, W. Hampel, G. Heusser, J. Kiko, and T. Kirsten, "Reanalysis of the GALLEX solar neutrino flux and source experiments," *Phys. Lett. B* **685** (2010) 47–54, arXiv:1001.2731 [hep-ex].

[137] **SAGE** Collaboration, J. N. Abdurashitov *et al.*, "Measurement of the solar neutrino capture rate with gallium metal. III: Results for the 2002–2007 data-taking period," *Phys. Rev. C* **80** (2009) 015807, arXiv:0901.2200 [nucl-ex].

[138] **Super-Kamkiokande** Collaboration, J. Hosaka *et al.*, "Solar neutrino measurements in Super-Kamiokande-I," *Phys. Rev. D* **73** (2006) 112001, arXiv:0508053 [hep-ex].

[139] **SNO** Collaboration, B. Aharmim *et al.*, "Measurement of the ν_e and total B-8 solar neutrino fluxes with the Sudbury Neutrino Observatory phase I data set," *Phys. Rev.* **C75** (2007) 045502, arXiv:nucl-ex/0610020.

[140] **SNO** Collaboration, B. Aharmim *et al.*, "Electron energy spectra, fluxes, and day-night asymmetries of b-8 solar neutrinos from the 391-day salt phase sno data set," *Phys. Rev.* **C72** (2005) 055502, nucl-ex/0502021.

[141] **SNO** Collaboration, B. Aharmim *et al.*, "An Independent Measurement of the Total Active ^{8}B Solar Neutrino Flux Using an Array of ^{3}He Proportional Counters at the Sudbury Neutrino Observatory," *Phys. Rev. Lett.* **101** (2008) 111301, arXiv:0806.0989 [nucl-ex].

[142] **SNO** Collaboration, B. Aharmim *et al.*, "Combined Analysis of all Three Phases of Solar Neutrino Data from the Sudbury Neutrino Observatory," arXiv:1109.0763 [nucl-ex].

[143] **Borexino** Collaboration, G. Bellini *et al.*, "Precision measurement of the 7Be solar neutrino interaction rate in Borexino," *Phys.Rev.Lett.* **107** (2011) 141302, arXiv:1104.1816 [hep-ex].

[144] **Borexino Collaboration** Collaboration, G. Bellini *et al.*, "Measurement of the solar 8B neutrino rate with a liquid scintillator target and 3 MeV energy threshold in the Borexino detector," *Phys.Rev.* **D82** (2010) 033006, arXiv:0808.2868 [astro-ph].

[145] **MINOS** Collaboration, P. Adamson *et al.*, "Search for sterile neutrino mixing in the MINOS long-baseline experiment," (2010) , arXiv:1001.0336 [hep-ex].

[146] **MINOS Collaboration** Collaboration, P. Adamson *et al.*, "Active to sterile neutrino mixing limits from neutral-current interactions in MINOS," *Phys.Rev.Lett.* (2011) , arXiv:1104.3922 [hep-ex].

[147] F. Dydak *et al.*, "A Search for Muon-neutrino Oscillations in the Δm^2 Range 0.3-eV^2 to 90-eV^2," *Phys. Lett. B* **134** (1984) 281.

[148] J. Kopp, M. Maltoni, and T. Schwetz, "Are there sterile neutrinos at the eV scale?," *Phys.Rev.Lett.* **107** (2011) 091801, arXiv:1103.4570 [hep-ph].

[149] C. Giunti and M. Laveder, "Implications of 3+1 Short-Baseline Neutrino Oscillations," *Phys.Lett.* **B706** (2011) 200–207, arXiv:1111.1069 [hep-ph].

[150] G. Karagiorgi, "Confronting Recent Neutrino Oscillation Data with Sterile Neutrinos," arXiv:1110.3735 [hep-ph].

[151] C. Giunti and M. Laveder, "Status of 3+1 Neutrino Mixing," *Phys.Rev.* **D84** (2011) 093006, arXiv:1109.4033 [hep-ph].

[152] C. Giunti and M. Laveder, "3+1 and 3+2 Sterile Neutrino Fits," *Phys.Rev.* **D84** (2011) 073008, arXiv:1107.1452 [hep-ph].

[153] J. Kopp, P. A. N. Machado, M. Maltoni, and T. Schwetz, "Sterile Neutrino Oscillations: The Global Picture," arXiv:1303.3011 [hep-ph].

[154] M. Maltoni and T. Schwetz, "Testing the statistical compatibility of independent data sets," *Phys. Rev. D* **68** (2003) 033020, arXiv:0304176 [hep-ph].

[155] S. Joudaki, K. N. Abazajian, and M. Kaplinghat, "Are Light Sterile Neutrinos Preferred or Disfavored by Cosmology?," arXiv:1208.4354 [astro-ph.CO].

[156] M. Gonzalez-Garcia, M. Maltoni, and J. Salvado, "Robust Cosmological Bounds on Neutrinos and their Combination with Oscillation Results," *JHEP* **1008** (2010) 117, arXiv:1006.3795 [hep-ph].

[157] J. Hamann, S. Hannestad, G. G. Raffelt, I. Tamborra, and Y. Y. Y. Wong, "Cosmology seeking friendship with sterile neutrinos," arXiv:1006.5276 [hep-ph].

[158] E. Giusarma, M. Corsi, M. Archidiacono, R. de Putter, A. Melchiorri, *et al.*, "Constraints on massive sterile neutrino species from current and future cosmological data," *Phys.Rev.* **D83** (2011) 115023, arXiv:1102.4774 [astro-ph.CO].

[159] G. Mangano and P. D. Serpico, "A robust upper limit on $N_{\rm eff}$ from BBN, circa 2011," *Phys.Lett.* **B701** (2011) 296–299, arXiv:1103.1261 [astro-ph.CO].

[160] J. Hamann, S. Hannestad, G. G. Raffelt, and Y. Y. Wong, "Sterile neutrinos with eV masses in cosmology: How disfavoured exactly?," *JCAP* **1109** (2011) 034, arXiv:1108.4136 [astro-ph.CO].

[161] L. Bento and Z. Berezhiani, "Blocking active sterile neutrino oscillations in the early universe with a Majoron field," *Phys.Rev.* **D64** (2001) 115015, arXiv:hep-ph/0108064 [hep-ph].

[162] A. Dolgov and F. Takahashi, "Do neutrino flavor oscillations forbid large lepton asymmetry of the universe?," *Nucl.Phys.* **B688** (2004) 189–213, arXiv:hep-ph/0402066 [hep-ph].

[163] E. Akhmedov and T. Schwetz, "MiniBooNE and LSND data: non-standard neutrino interactions in a (3+1) scheme versus (3+2) oscillations," arXiv:1007.4171 [hep-ph].

[164] G. Karagiorgi, M. Shaevitz, and J. Conrad, "Confronting the short-baseline oscillation anomalies with a single sterile neutrino and non-standard matter effects," arXiv:1202.1024 [hep-ph].

[165] **MiniBooNE** Collaboration, A. A. Aguilar-Arevalo *et al.*, "A search for muon neutrino and antineutrino disappearance in MiniBooNE," *Phys. Rev. Lett.* **103** (2009) 061802, arXiv:0903.2465 [hep-ex].

[166] **MiniBooNE Collaboration, SciBooNE Collaboration** Collaboration, G. Cheng *et al.*, "Dual baseline search for muon antineutrino disappearance at $0.1\mathrm{eV}^2 < \Delta m^2 < 100\mathrm{eV}^2$," arXiv:1208.0322 [hep-ex]. Data and analysis instructions available at http://www-sciboone.fnal.gov/data_release/joint_numubar_disap/.

[167] Y. Declais *et al.*, "Search for neutrino oscillations at 15-meters, 40-meters, and 95-meters from a nuclear power reactor at bugey," *Nucl. Phys. B* **434** (1995) 503–534.

[168] Y. Declais, H. de Kerret, B. Lefievre, M. Obolensky, A. Etenko, *et al.*, "Study of reactor anti-neutrino interaction with proton at Bugey nuclear power plant," *Phys.Lett.* **B338** (1994) 383–389.

[169] A. Kuvshinnikov, L. Mikaelyan, S. Nikolaev, M. Skorokhvatov, and A. Etenko, "Measuring the anti-electron-neutrino + p -¿ n + e+ cross-section and beta decay axial constant in a new experiment at Rovno NPP reactor. (In Russian)," *JETP Lett.* **54** (1991) 253–257.

[170] G. Vidyakin, V. Vyrodov, I. Gurevich, Y. Kozlov, V. Martemyanov, *et al.*, "DETECTION OF ANTI-NEUTRINOS IN THE FLUX FROM TWO REACTORS," *Sov.Phys.JETP* **66** (1987) 243–247.

[171] H. Kwon, F. Boehm, A. Hahn, H. Henrikson, J. Vuilleumier, *et al.*, "Search for neutrino oscillations at a fission reactor," *Phys.Rev.* **D24** (1981) 1097–1111.

[172] **CALTECH-SIN-TUM** Collaboration, G. Zacek *et al.*, "Neutrino oscillation experiments at the gosgen nuclear power reactor," *Phys. Rev.* **D34** (1986) 2621–2636.

[173] **CHOOZ** Collaboration, M. Apollonio *et al.*, "Search for neutrino oscillations on a long base-line at the CHOOZ nuclear power station," *Eur. Phys. J. C* **27** (2003) 331–374, arXiv:0301017 [hep-ex].

[174] F. Boehm *et al.*, "Final results from the palo verde neutrino oscillation experiment," *Phys. Rev.* **D64** (2001) 112001, hep-ex/0107009.

[175] D. Dwyer, "Daya Bay results." Talk at Neutrino2012, 3–9 June 2012, Kyoto, Japan, 2012.

[176] **Double Chooz Collaboration** Collaboration, Y. Abe *et al.*, "Reactor electron antineutrino disappearance in the Double Chooz experiment," *Phys.Rev.* **D86** (2012) 052008, arXiv:1207.6632 [hep-ex].

[177] **KamLAND** Collaboration, A. Gando *et al.*, "Constraints on θ_{13} from A Three-Flavor Oscillation Analysis of Reactor Antineutrinos at KamLAND," arXiv:1009.4771 [hep-ex].

[178] J. Reichenbacher, "Final KARMEN results on neutrino oscillations and neutrino nucleus interactions in the energy regime of supernovae,". PhD thesis, Univ. Karlsruhe.

[179] **LSND Collaboration** Collaboration, L. Auerbach *et al.*, "Measurements of charged current reactions of nu(e) on 12-C," *Phys.Rev.* **C64** (2001) 065501, arXiv:hep-ex/0105068 [hep-ex].

[180] P. Huber, M. Lindner, and W. Winter, "Simulation of long-baseline neutrino oscillation experiments with GLoBES," *Comput. Phys. Commun.* **167** (2005) 195, hep-ph/0407333. http://www.mpi-hd.mpg.de/~globes.

[181] P. Huber, J. Kopp, M. Lindner, M. Rolinec, and W. Winter, "New features in the simulation of neutrino oscillation experiments with GLoBES 3.0," *Comput. Phys. Commun.* **177** (2007) 432–438, hep-ph/0701187. http://www.mpi-hd.mpg.de/~globes.

[182] M. C. Gonzalez-Garcia and M. Maltoni, "Phenomenology with Massive Neutrinos," *Phys. Rept.* **460** (2008) 1–129, arXiv:0704.1800 [hep-ph].

[183] M. Maltoni and T. Schwetz, "Sterile neutrino oscillations after first MiniBooNE results," *Phys. Rev. D* **76** (2007) 093005, arXiv:0705.0107 [hep-ph].

[184] The MICE collaboration, "MICE: An International Muon Ionization Cooling Experiment,Technical Reference Document." MICE-TRD-2005, 2005.

[185] T. Roberts *et al.* G4beamline; a "Swiss Army Knife" for Geant4, optimized for simulating beamlines; http://www.muonsinc.com/muons3/tiki-index.php?page=G4beamline.

[186] T. J. Roberts *et al.*, "G4Beamline particle tracking in matter-dominated beam lines,".

[187] E. Baussan, M. Dracos, T. Ekelof, E. F. Martinez, H. Ohman, *et al.*, "The use the a high intensity neutrino beam from the ESS proton linac for measurement of neutrino CP violation and mass hierarchy," arXiv:1212.5048 [hep-ex].

[188] A. de Bellefon *et al.*, "MEMPHYS: A large scale water Cerenkov detector at Frejus," arXiv:hep-ex/0607026.

[189] **MEMPHYS Collaboration** Collaboration, L. Agostino *et al.*, "Study of the performance of a large scale water-Cherenkov detector (MEMPHYS)," *JCAP* **1301** (2013) 024, arXiv:1206.6665 [hep-ex].

[190] **VLHC Design Study Group** Collaboration, G. Ambrosio *et al.*, "Design study for a staged very large hadron collider,". SLAC-R-591; FERMILAB-TM-2149.

[191] R. Bayes, A. Laing, F. Soler, A. Cervera Villanueva, J. Gomez Cadenas, *et al.*, "The Golden Channel at a Neutrino Factory revisited: improved sensitivities from a Magnetised Iron Neutrino Detector," *Phys.Rev.* **D86** (2012) 093015, arXiv:1208.2735 [hep-ex].

[192] C. Andreopoulos *et al.*, "The GENIE Neutrino Monte Carlo Generator," *Nucl. Instrum. Meth. A* **614** (2010) 87–104, arXiv:0905.2517 [hep-ph].

[193] **Geant4** Collaboration, J. Apostolakis and D. H. Wright, "An overview of the GEANT4 toolkit," *AIP Conf. Proc.* **896** (2007) 1–10.

[194] A. Cervera-Villanueva, J. J. Gomez-Cadenas, and J. A. Hernando, "'RecPack' a reconstruction toolkit," *Nucl. Instrum. Meth.* **A534** (2004) 180–183.

[195] **MINOS** Collaboration, D. G. Michael *et al.*, "The Magnetized steel and scintillator calorimeters of the MINOS experiment," *Nucl. Instrum. Meth.* **A596** (2008) 190–228, arXiv:0805.3170 [physics.ins-det].

[196] A. Hocker, J. Stelzer, F. Tegenfeldt, H. Voss, K. Voss, *et al.*, "TMVA - Toolkit for Multivariate Data Analysis," *PoS* **ACAT** (2007) 040, arXiv:physics/0703039 [PHYSICS].

[197] **MINOS** Collaboration, P. Adamson *et al.*, "New constraints on muon-neutrino to electron-neutrino transitions in MINOS," *Phys. Rev. D* **82** (2010) 051102, arXiv:1006.0996 [hep-ex].

[198] C. Tunnell, *Sensitivity to electronvolt-scale sterile neutrinos at a 3.8-GeV/c muon decay ring*. PhD thesis, University of Oxford, 2013.

[199] C. Tunnell, "Sterile Neutrino Sensitivity with Wrong-Sign Muon Appearance at nuSTORM," arXiv:1205.6338 [hep-ph].

[200] J. Tang and W. Winter, "Physics with near detectors at a neutrino factory," *Phys. Rev. D* **80** (2009) 053001, arXiv:0903.3039 [hep-ph].

[201] C. Giunti, M. Laveder, and W. Winter, "Short-Baseline Electron Neutrino Disappearance at a Neutrino Factory," *Phys. Rev.* **D80** (2009) 073005, arXiv:0907.5487 [hep-ph].

[202] S. Mishra, 2010.

[203] S. Mishra *et al.*, 2008. Letter of Intent submitted to Fermilab .

[204] **NOMAD collaboration** Collaboration, J. Altegoer *et al. Nucl. Instrum. Meth.* **A404** (1998) 96–128.

[205] **ATLAS collaboratian** Collaboration, T. Akesson *et al. Nucl. Instrum. Meth.* **A522** (2004) 50–55.

[206] **ATLAS collaboratian** Collaboration, T. Akesson *et al. Nucl. Instrum. Meth.* **A522** (2004) 131–145.

[207] **ATLAS collaboratian** Collaboration, T. Akesson *et al. IEEE Nucl.Sci.Symp.Conf.Rec.* **2** (2005) 1185–1190.

[208] **COMPASS collaboratian** Collaboration, V. Bychkov *et al. Particles and Nuclei Letters* **2** (2002) 111.

[209] **COMPASS collaboratian** Collaboration, K. Platzer *et al. IEEE Transactions on Nuclear Science* **52(3)** (2005) .

[210] A. Stahl *et al.*, "Expression of Interest for a very long baseline neutrino oscillation experiment (LBNO)," 2012. CERN-SPSC-2012-021, SPSC-EOI-007; http://cds.cern.ch/record/1457543.

[211] A. Curioni, "Hpartpc as a near detector for lnbo for the precise study of neutrino cross sections," 2012. Presented at the LAGUNA-LBNO general meeting, CERN, 1–3 October 2013. http://laguna.ethz.ch/indico/getFile.py/access?contribId=39&sessionId=7&resId=0&materialId=slides&confId=6 .

[212] A. Curioni and D. Lussi, 2013. Private communication.

[213] K. Kodama, N. Ushida, G. Tzanakos, P. Yager, V. Paolone, *et al.*, "Muon-neutrino to tau-neutrino oscillations: Proposal,".

[214] S. Dixon *et al.*, "NuMI Project (SBL MI-40)," 1994. Project Definition Report No. 6-7-1, April 1994.

[215] S. Henderson, R. Dixon, and W. Pellico, "Fermilab Proton Improvement Plan Design Handbook," 2012. Beams Document 4053-v3.

[216] P. Oddone, "Untitled." Https://indico.fnal.gov/getfile.py/access?resid=0&materialid=0&confid=5710, 2012.

A Physics Potential of near-detector suite at νSTORM

We enumerate physics papers that will be engendered with the a suite of near detectors proposed for the νSTORM facility. The topics/papers are motivated by the published results by NOMAD, CCFR, NuTeV, MiniBOONE, etc. experiments. Criteria for choosing the topics are as follows:

1. Best Measurement: If the topic deals with a Standard Model measurement then it should be most precise;
2. Most Sensitive Search: If the topic involves a search then it should be the most sensitive search; and
3. New Method: Where 1 and 2 abive are not applicable then the topic should include a novel measurement technique.

In all, we have identified over 80 topics. The list is not complete. For example, it does not include topics involving detector development, R&D measurements, or engineering research that typically are published in journals like NIM, IEEE, etc. The list comprising absolute cross-section measurements, exclusive and semi-exclusive channels, electroweak physics, perturbative and non-perturbative QCD, and searches for new physics illustrates the power of a high resolution, fine-grain-tracker based on the past experiments. Over the duration of the project, ~ 10 years, the number of theses/paper will be more than twice as many as the number of topics.

Below we present a salient subset of physics topics.

1. Measurement of the absolute neutrino/anti-neutrino flux using neutrino-electron neutral current scattering;
2. Measurement of the difference in the energy-scale of $\overline{\nu}_\mu$- versus ν_e-induced charged-current (CC) events;
3. Exclusive and quasi-exclusive single Pi0 production in neutrino- and anti-neutrino-induced neutral current interactions;
4. Coherent and quasi-exclusive single Pi+ production in neutrino-induced charged current interactions;
5. Coherent and quasi-exclusive single Pi- production in antineutrino-induced charged current interactions;
6. Proton (neutron) yield in inclusive neutrino and anti-neutrino charged current interactions;
7. The ν_e-e^- and $\overline{\nu}_\mu$-e^- interactions and search for lepton number violating process;
8. Measurement of neutrino and antineutrino quasi-elastic (QE) and resonance charged current interactions;
9. Measurement of prompt radiative photon in muon- and electron-neutrino quasi-elastic interactions;
10. Constraints on the Fermi-motion of the nucleons using the 2-track topology of neutrino quasi-elastic interactions;
11. Measurement of the hadronic content of the weak current in neutrino- and anti-neutrino CC and NC interactions;
12. Neutral Current elastic scattering on proton, nu(bar) + p $\rightarrow$ nu(bar) + p and measurement of the strange quark contribution to the nucleon spin, Delta-S;
13. Tests of sum-rules in QPM/QCD;
14. Measurement of nuclear effects on F_2 and on xF_3 in (anti)neutrino scattering from ratios of Ar, Pb, Fe and C targets;
15. Measurement of strange mesons and hyperon production in (anti-)neutrino charged and neutral current;
16. Measurement of the Λ and $\overline{\Lambda}$ polarisation in (anti-)neutrino neutral current interactions;
17. Measurement of backward going protons and pions in neutrino CC interactions and constraints on nuclear processes;
18. Search for muon-neutrino to electron-neutrino transition and the LSND/MiniBOONE anomaly;
19. Search for muon-antineutrino to electron-antineutrino transition and the LSND/MiniBOONE anomaly; and
20. Search for heavy neutrinos using its electronic, muonic and hadronic decays.